Impact of material properties, process parameters and roll compactor design on roll compaction

Inaugural-Dissertation

zur Erlangung des Doktorgrades
der Mathematisch-Naturwissenschaftlichen Fakultät
der Heinrich-Heine-Universität Düsseldorf

vorgelegt von

Kitti Szappanos-Csordás

aus Hódmezővásárhely

Düsseldorf, 2018

aus dem Institut für Pharmazeutische Technologie und Biopharmazie
der Heinrich-Heine-Universität Düsseldorf

Gedruckt mit der Genehmigung der
Mathematisch-Naturwissenschaftlichen Fakultät der
Heinrich-Heine-Universität Düsseldorf

Berichterstatter

1. Prof. Dr. Dr. h.c. Peter Kleinebudde
2. Prof. Dr. Jörg Breitkreutz

Tag der mündlichen Prüfung: 30.01.2019

„I am among those who think that science has great beauty. A scientist in his laboratory is not only a technician: he is also a child placed before natural phenomena which impress him like a fairy tale. We should not allow it to be believed that all scientific progress can be reduced to mechanisms, machines, gearings, even though such machinery has its own beauty.“

Marie Curie

7th November 1867 – 4th July 1934

Table of Contents

List of Abbreviations

α	nip angle
a	constant
b	mean grey value
c	standard deviation of grey value
CCD	charge-coupled device
CF	compaction force [kN]
c_f	conversion factor
CI	confidence interval
CV	coefficient of variation [%]
D / d	roll diameter
d50	median particle size
DF	densification factor
DoE	design of experiment
DW	drawn-in width
ESR	early stage researcher
GSD	granule size distribution
GV	grey value
GW	gap width [mm]
HP	hydraulic pressure [bar]
k	slope coefficient
kn	knurled roll surface
μ	mean
μCT	microcomputational tomography
man	spray-dried mannitol
Mater/mater	type of material
MCC/MCC 101	microcrystalline cellulose
mix	1:1 mixture of microcrystalline cellulose and spray-dried mannitol
n	number of samples
NIR	near infra-red

p	p-value, probability value
PID	Proportional Integral Derivative
Q^2	estimation of future prediction
Q3	cumulative distribution
q3	density distribution
ρ_{env}	envelope density
ρ_{He}	Helium density
R^2	model fit
RD	relative density
ROTHIST	software for evaluation of grey values in a cross section
RR	rim-rolls
RS	roll speed [rpm]
rss	residual sum of square
RW	roll width
σ / s / SD	standard deviation
SCF	specific compaction force [kN/cm]
seal	type of sealing system
SEM	scanning electron microscopy
sm	smooth roll surface
SS	side-sealing
surf	type of roll surface
UHIST	software for evaluation of grey values in a whole piece of ribbon
φ	entry angle
x_{c_min}	shortest chord of a particle
X-ray µCT	X-ray microcomputational tomography

Foreword

IPROCOM was a multidisciplinary consortium targeting the development of in silico process models and the understanding of the fundamental mechanisms of particulate manufacturing processes involving roll compaction. The development of the in silico process was based on the properties of individual particles (intermediate products, ribbons or granules and final products, e.g. tablets) with identified process conditions and formulations. This was carried forward collaborating with academic and industrial partners that were involved in the IPROCOM project. The focus of the project was divided in 3 work packages and in 4 strands, in which 12 early stage researchers (ESR) and 3 experienced researchers were active. Work package 1 worked on process understanding that fulfilled the experimental part of the project investigating the different powder, particle, ribbon and granule properties, roll compactor designs, scale-up rules in roll compaction. Its main aim was to fill the current knowledge gap on how material properties of single particles and process conditions govern the product properties. Work package 2 was multi-scale modelling using different model techniques: discrete element method and finite element method to predict the properties of final products based on the individual particle properties. The experimental data of work package 1 was used as input and as far as possible for validation for work package 2. Work package 3 was intelligent modelling, that main objective was to develop computational intelligence models for particulate product manufacturing and the establishment of a robust bio-inspired computational intelligence platform using novel adaptive algorithms and data structures to predict the product quality. The 4 strands dealt with the subjects mixing, roll compaction, milling and die compaction. Each strand included researchers working on experimental, numerical and computational intelligence modelling [1].

The present thesis is a part of work package 2 and strand 2, which introduces the investigation results of ESR2, how the behavior of different model materials, roll compaction process parameters and designs influence the roll compaction process. The impact of the aforementioned variables is presented through the evaluated ribbon and granule characteristics.

1 Introduction

1.1 Granulation

The word „*granulation*" comes from the Latin phrase "*granulatum*", which means grained or grain. Granulation is defined as a process, whereby primary particles are bonded into larger secondary particles by compression or by using a binding agent or both, in which the primary particles can be identified [2]. Different types of binding mechanisms are known that can lead to agglomeration of primary particles; solid bridges, adhesion and cohesion forces, surface tension and capillary pressure, interlocking bonds and attraction forces between solids [3]. The obtained particle is called agglomerate. Although granulation itself has been existed since several decades, the scientific interest in granulation began in the 1950s years, as the recovery of fine coal and the manufacturing of pharmaceutical solids arose [4]. Agglomeration is commonly used in various industrial fields, for instance in the fertilizer industry, in the food industry, in the coal and mineral industry, in the agrochemical industry and in the pharmaceutical industry [2, 3]. In the pharmaceutical industry, granules are used as final dosage form filled into sachets or in some cases into multidose containers, but usually granules are processed further into tablets or filled into capsule shells.

In drug manufacturing, the importance of granulation processes has been increased, as the most used excipients and the recently developed active pharmaceutical ingredients have low bulk density and inappropriate flowability, due to cohesive appearance and small particle size. Applying a suitable granulation process results in the increase of the particle mass, which leads to the increase of the weight force and thus to the decrease of the adhesive force between the particles, which redounds the flowability of the bulk [5]. This is important, as the appropriate flowability of granules into capsules, sachets or in the tableting die is inevitable to achieve constant mass and homogeneous distribution of the active substance in the final dosage form [6]. Nevertheless, also the processing of free-flowing materials has been found to be a demanding task, as segregation in the powder mixture can take place easily. A further advantage of granulation is the increased bulk density of granules [7], which allows on the one hand the manufacturing of high-dosage

preparations and on the other hand the processing of high potent drugs. When high potent drugs need to be processed, both, person and environment have to be protected, thus granulation, as manufacturing process, is an advisable choice due to the reduction of dust while production [8]. Also the reduction of the storage volume is a benefit of increased bulk density [2]. The subsequent compression process can be improved through the increased bulk density, as less air is present in the granules, which has to entrap during tableting [9]. Disintegration time, dissolution time and wettability of tablets can be improved, if the powder blend has been granulated previously [10, 11].

Various granulation techniques can ensure the improvement of the physical characteristics of the bulk material. In general, wet granulation, dry granulation and melt granulation methods are distinguished, when agglomeration processes are categorized. Liquid binders are used to gather small particles into larger during wet granulation, while no liquid is necessary, when granulation is accomplished by dry or melt granulation methods [2]. A number of wet granulation technologies are available. High shear granulation, spray drying, fluidized bed granulation and extrusion are well-known wet granulation methods [12]. Melt granulation, high shear granulation [13] and hot melt extrusion [14] can be accomplished without the application of any liquid binder using excipients that melt at higher temperature.

Since 1940s, dry granulation processes are used in the pharmaceutical industry. In the last 30 years, the frequency of choosing a dry granulation method has arisen as it offers a cost-effective and delicate handling for heat and or moisture sensitive materials since no liquid binder is needed. During dry granulation, the powder particles are compressed under high pressure, which brings the particles close to each other, increasing the direct contact between the particle surfaces developing van der Waals bonding forces between the individual powder particles. Due to the high compression pressure, the contact area between the particles is increased which improves the bonding strength [2].

There are two dry granulation processes: slugging and roll compaction. Between the 1950s-1970s slugging was the more preferred method. Slugs are produced, when the powder is fed into a large compression machine and compressed by tableting punches having large diameter. The slugs are milled into granules after the compression step. As slugging is a single batch processing method using no process control, showing poor economies of scale and low manufacturing throughput, roll compaction became a more frequently used dry granulation method improving all the drawbacks that slugging possessed [2, 7].

1.2 Roll compaction/dry granulation

1.2.1 Roll compactor design

Roll compaction is a continuous dry granulation method, which first pharmaceutical application was published in 1966 by Jaminet and Hess [15]. Roll compactors usually consist of three main process units; feeding unit (a), compaction unit (b) and milling unit (c). In case of some suppliers, the milling unit is a part of the roll compactor. A schematic illustration of a roll compactor showing the aforementioned units is depicted in Figure 1.

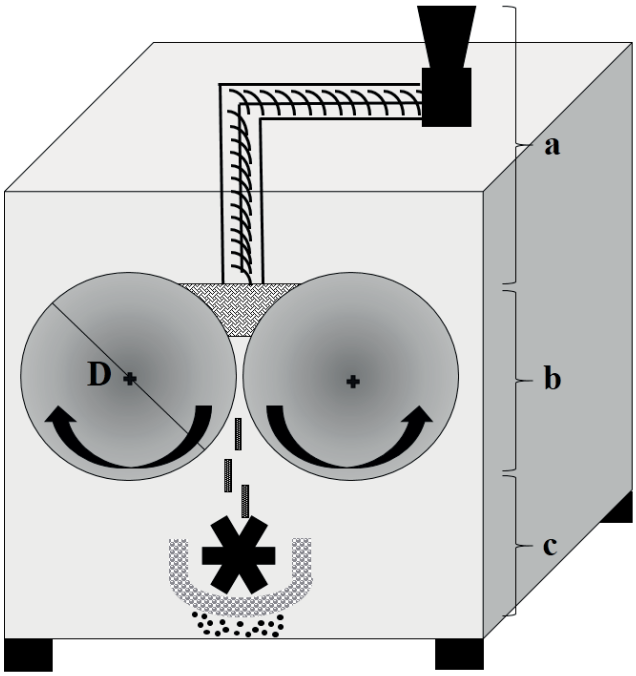

Figure 1. Schematic illustration of a roll compactor ,presenting the feeding unit (a), compaction unit (b) and milling unit (c).

The powder is transported from the hopper in between two counter-rotating rolls by force feeder or by gravity. Then the powder is densified on the roll surface at the smallest gap, forming the intermediate product, called ribbon. After compaction, the ribbon is ejected and is milled into granules. The most important process variables are the compaction pressure or specific compaction force (SCF), gap width (GW), screw speed, roll speed (RS) and the speed and angle of milling. The feeding unit consists of a hopper, usually equipped with an agitator to break powder bridges, and of one or more screws. In case of elder equipment, the feeding takes place by gravity solely. When two screws are used for

conveying the powder, the ratio between the speed of the feeding and tamping screws is a critical parameter of the process. The geometry of the feeding screw plays an important role in the predensification of the powder (de-aeration) and defines the amount of powder that can be transported into the compaction zone. Conical, cylindrical screws, single or twin screws can be assembled in the feeding system [16]. The type of screw that should be used in the feeding unit to obtain an efficient powder transport and de-aeration mechanism, is selected according to the powder blend properties. The usage of two screws can improve the density homogeneity in the ribbons [17]. Some roll compactors apply vacuum system to support the de-aeration removing the air through a porous metal plate and decreasing "fluidization" of fine particles in the feeding chamber [16].

In regards to the design of the roll compactor itself, further design variables have to be considered. In the compaction area, the rolls can be mounted in horizontal (A), inclined (B) and vertical (C) positions [18], which determines the position of the feeding unit [9]. The various configurations are exhibited in Figure 2.

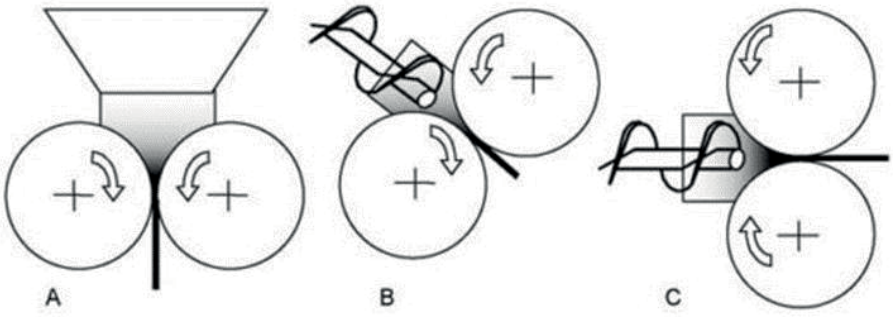

Figure 2. Horizontal (A), inclined (B) and vertical (C) position of rolls [18].

The first invented design was the horizontal positioned rolls with vertical feeding. One of the drawbacks of this design is that powders having excellent flow properties might exit the compaction area being uncompacted till roll compaction achieves a stable processing condition. The advantage of the combination of horizontal feeding and vertical powder compression is the reduction of uncompacted material compared to the vertical feeding. However, compaction with rolls in vertical position results in asymmetrical densification of powder across the ribbon thickness, since the powder transport takes place by a feeding screw and the transport of the powder is influenced by gravity. The inclined design of feeding possesses the advantages of the aforementioned feeding constructions. It uses

feeding and tamping screws and also the gravity to convey the powder. The inclined position rolls assure less powder leakage [16].

Also the mounting of the rolls can be different. If both rolls are installed in fix positions, the gap width is fixed, so the densification of the powder is defined by the feed screw and the compaction pressure is not adjustable. In terms of process control it is more advantageous, when one of the rolls is movable. This allows to keep the compaction pressure or SCF constant by adapting the GW or the screw speed [19]. The rolls can differ not only in their positions and mountings but also in their width, surface and diameter. A wider roll width results in a higher throughput, which is important, when the roll compactor is used in the commercial production [20]. Various roll surfaces are available; smooth (sm), knurled (kn), serrate, grooved surfaces are some examples. An overview about the ranges of process parameters, providing the characteristic units, types of sealing system (seal) and rolls, roll surface (surf), roll diameter (D), roll width (RW) and applied control system is given in Table 1 considering several roll compactor suppliers.

Table 1. Summary and description of different types of laboratory scale roll compactors.

Roll compactor supplier	Roll compactor	SCF [kN/cm] CF [kN] or HP [bar] roll force [ton]	GW [mm]	RS [rpm]	D [mm]	RW [mm]	Mobility of rolls	Roll surface	Sealing system	Control mechanism
K.R. Komarek Inc. [21]	Komarek B050H	0-13.2 kN/cm	1.5-6.0	0-7.5	100	38	no	smooth, knurled	side-sealing	-
FitzPatrick [22-24]	Chilsonator IR 220	6-90 MPa	-*	4.0-12	200	20	yes	smooth	side-sealing	-
Sahut Conreur [25]	Micro-Compactor MP1	0-25 kN/cm	-*	0-25	150	30	yes	pocketed, knurled, corrugated	side-sealing	-
Freund-Vector Corporation [26, 27]	TF-Mini	1-8 ton	-*	2-10.1	100	35		smooth, axial grooved	side-sealing	-
AlexanderWerk AG [28, 29]	BT120	18-143 bar	1.0 – 5.0	2.8-12.1	120	25	yes	knurled smooth	side-sealing	-
Hosokawa Alpine AG [30]	Pharmapaktor C250	0-100 kN	1.0-3.0	2-5.7	250	30	yes	smooth, knurled	side-sealing	PID, GW and screw speed control
L.B. Bohle Maschienen + Verfahren GmbH [28, 29]	BRC 25	0.5-20.0 kN/cm	0.5-6.0	1-30	250	25	yes	knurled, fine grooved, coarse grooved, smooth	rim-rolls	PID, SCF and GW control
Gerteis Maschinen + Processengineering AG [28, 29]	Mini-Pactor	2.0-20.0 kN/cm	1.0-6.0	1-30	250	25	yes	smooth, knurled, toothed or custom design	side-sealing, rim-rolls	PID, SCF and GW control

*no information has been found in the literature

It was reported, that the rougher the applied roll surface is, the higher is the friction between the powder particles and the roll surface, which can be meaningful, when loose powder has to be compacted. Daugherity et al. evaluated the effect of roll surface on the ribbon thickness and on the manufacturing capability of a Vector Freund roll compactor [31]. In the study of Rambali et al., ribbed roll surface resulted in robust granules for the subsequent tableting step [32].

The bypass of uncompacted powder is one of the difficulties, which has to be overcome during roll compaction. To prevent powder migration outside the compaction area, either a side-sealing (SS) system or rim-roll (RR) sealing system is built in between the feeding and compaction area. The SS system consists of two plates that build a "wall" beside the gap width. The RR sealing system has one roll having edges, while the other roll fits in between these rims creating the RR sealing system [17]. The illustrations of these types of sealing systems and smooth and knurled roll surface are introduced in Figure 3.

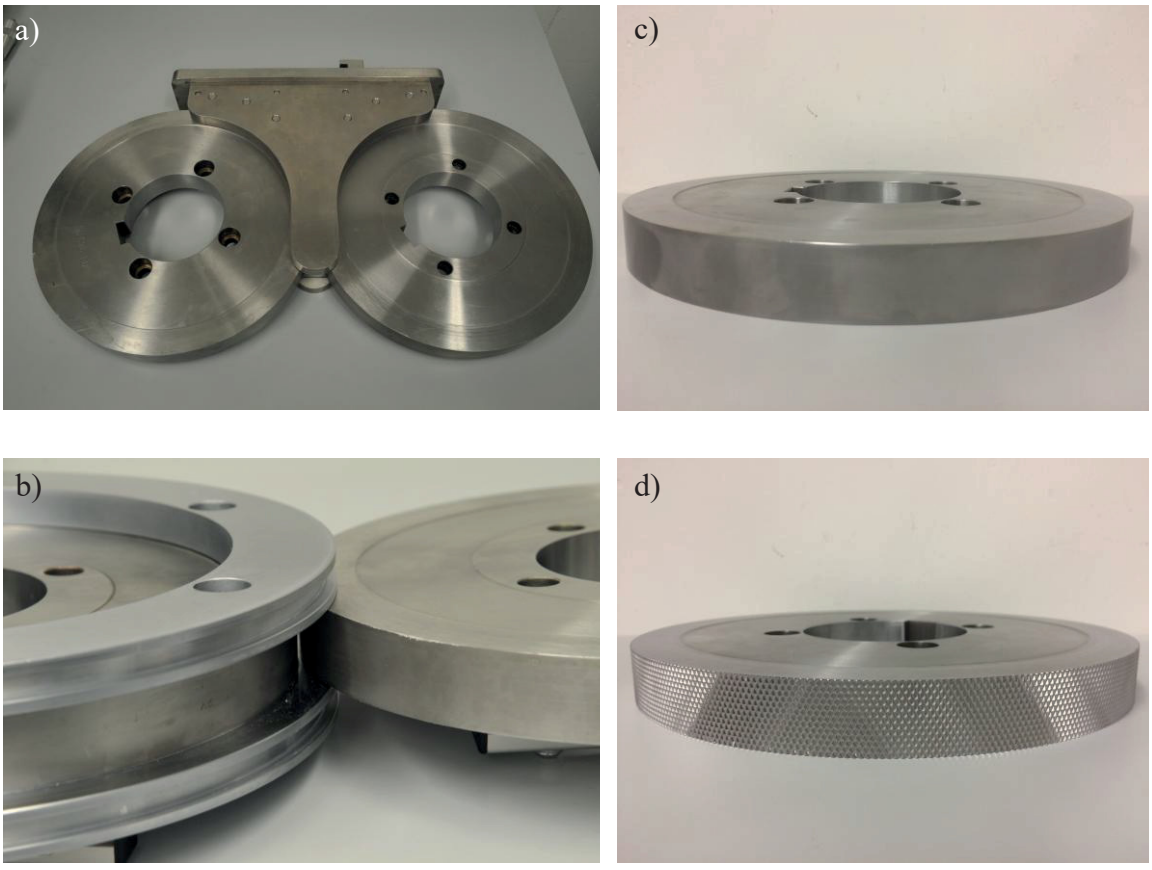

Figure 3. SS sealing system (a) and RR sealing system (b) and smooth (c) and knurled (d) rolls.

The applied sealing system has a major impact on the ribbon quality, and thus also on the granule characteristics. Using RR sealing system leads to a more homogeneous density

distribution in ribbons compared to SS system [33-35]. It is reported in the study of Perez-Gandarillas et al. that comparable overall ribbon density is obtained regardless of the utilized sealing system, while the granule size distribution (GSD) is affected by the type of sealing [36]. Milling of ribbons can take place subsequently after compacting the powders into ribbons, when the milling unit is integrated in the roll compactor or the ribbons are collected first and granulated in a separate milling device [17]. Oscillating mill is a commonly used method in dry granulation, in which the rotor speed, angle of oscillation, rotor type and mesh size are the most significant parameters affecting the granulation performance [37].

Beside the advantages of roll compaction mentioned in the previous section, also several drawbacks have to be overcome. One of the main disadvantages is the production of high amount of uncompacted material, which is termed as "fines" in the literature [38]. The produced fines can be re-compacted in order to improve the yield, nevertheless, the recycling of fines can lead to inappropriate drug uniformity, therefore the re-compaction if fines is not an advisable manner to increase the throughput [9]. The amount of fines can be reduced, when high compaction pressure, RR sealing system and vacuum de-aeration are applied, albeit too high compaction pressure can lead to reduced compactibility of granules [39]. Experiments to densify by compaction only to the degree necessary for non-friable and strength enough granules have been described before. This enhances the flowability without the reduction of the compactibility [40]. Ribbons are often described by heterogeneity in strength and in relative density (RD) across the roll width and along the roll length. The density heterogeneity of ribbons across the width can be improved with RR, while the non-uniform density in the length of the ribbon can be enhanced by the improvement of the powder feeding appeasing the fluctuation of screw feeding [18]. A further disadvantage of roll compaction is the material sticking on the roll surface, which can be decreased by the application of lubricants on the roll surface or in the powder blend [41].

1.2.2 Theory of powder densification

The interparticulate bond formation during dry granulation is described by the following stages: particle rearrangement, particle deformation, particle fragmentation and particle bonding. The particles are rearranged and pre-densified while the powder is conveyed to the compaction zone. The nip or compaction area, where the powder is exerted to

increased compression forces and the brittle particles break and plastic particles deform resulting more contact points between the particles. Particle fragmentation takes place as the compression force increases further. The fractured particles offer new surfaces establishing more contact points between the particles. This progress leads to bonding of particles at molecular level due to the effect of van der Waals forces [2, 16]. The powder densification takes place in the compaction unit. In order to describe the powder densification in detail, further regions shall be defined. A distinction is made between the slipping region, compaction region and the release region [18]. The different regions are introduced in Figure 4, in which *DW* is the drawn-in width, *GW* is gap width, *D* is roll diameter, α is the nip angle and φ is the entry angle.

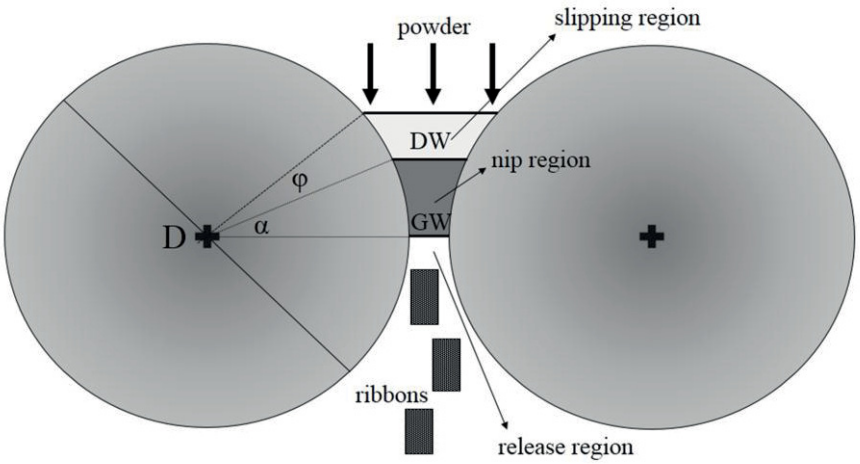

Figure 4. The slipping region, nip region and release region in the compaction unit.

In the slipping region the powder particles move slower than the roll surface. This region begins at the entry angle, where a finite roll pressure is exerted. Once, the powder velocity achieves the roll speed, the nip area is reached, corresponding to the nip angle and the densification of the powder starts [42, 43]. The powder densification takes place in the compaction/nip region, whereby the pressure goes up and achieves its maximum. The powder densification can be described by the densification factor, *DF*, which can be calculated by dividing the DW by the GW. According to this, rolls with smaller diameter have smaller DF compared to a roll pair with bigger diameter at the same GW [9]. A higher pre-densification of the powder and the application of rolls with large diameter

result in a wider DW, which is in linear correlation with the set GW. The schematic presentation of the correlation between the roll diameter and the ratio between the DW and GW is presented in Figure 5.

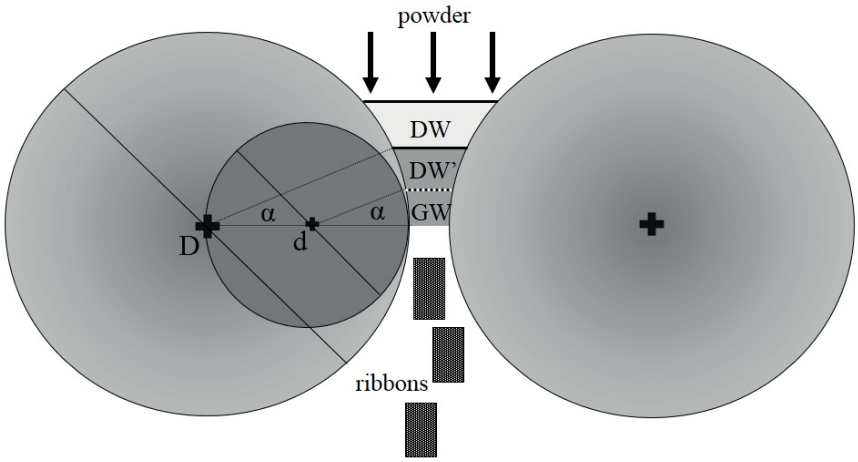

Figure 5. Densification factor dependency on the roll diameter.

Changing the GW leads to the alteration of the powder densification. Larger GW results in a decreased densification. Therefore, if the same degree of densification shall be achieved while using roll compactors with different roll diameter, the GW has to be adapted according to the following Equation 1, Equation 2 and Equation 3 [44].

$$DF_D > DF_d \qquad \text{Equation 1}$$

because,

$$\frac{DW}{GW} > \frac{DW'}{GW} \qquad \text{Equation 2}$$

therefore,

$$\frac{DW}{GW} = \frac{DW'}{GW'} \rightarrow DF_D = DF_d \qquad \text{Equation 3}$$

It is reported from the literature, that the nip angle is independent from the roll diameter [45]. Nevertheless, the nip angle is influenced by the compacted material characteristics, applied roll surface and formulation. Using smooth rolls and or including lubricant in the raw materials, the nip angle is decreased, as the interparticle frictional forces and also the friction between the powder particles and the surface of the equipment are decreased. In contrast, larger nip angle is achieved, when the frictional forces are enlarged utilizing knurled rolls and enhancing the pre-densification of the powder, while the material is conveyed to the compaction zone. The powder densification becomes higher when the nip angle is increased. In the release region the compacted ribbon leaves the compaction unit and enters the milling zone. The thickness of the ribbon can exceed the GW as the compacted material reveals elastic recovery after ejection [46].

The powder densification is influenced by the ratio between the roll diameter and the GW and on the other hand by the RS as well. The RS defines the linear speed, thus also the dwell time of the densification. The selection of the RS depends on the material properties, e.g. flowability and deformation behavior [16]. Materials showing plastic-elastic deformation behaviour are sensitive to dwell time. Setting low RS results in granules with improved flowability and lower friability of granules [22, 47], while shorter dwell time (faster RS) can cause loss of compactibility, therefore increased friability and decreased hardness. In general, in case of plastic-elastic and partly plastic deforming materials, the setting of higher RS is beneficial [48]. The densification of materials with significant elastic recovery requires a certain maximum RS, as the fast release of the ribbon and the short execution under the compaction pressure can cause cracking and weakening of the ribbons. In case of too short dwell time, the ribbon can fall apart [3]. In contrast, for brittle materials, the non-significant effect of the RS on the powder densification has been described in the literature. An extended exposure under the compaction force (CF) has a negligible effect on the ribbon properties, as the fragmentation of brittle particles takes place rapidly [49-51].

1.3 Ribbon density/porosity: the key intermediate product attribute

Some studies revealed ribbon properties, e.g.: ribbon density/porosity and strength governs the GSD, strength and porosity [45, 52-55], which has an effect on tableting/capsule filling

processes [56-58]. Thus, the most important feature in roll compaction is the ribbon density/porosity. In order to obtain granules, possessing the desired quality attributes i.e. granule size and strength, the non-uniform ribbon density distribution is required to be improved. Based on Zinchuk's investigation, granules milled from ribbons with 60-80% relative density possessed appropriate characteristics to obtain tablets with desired quality [59]. Because of this, many research studies focused on the effect of roll compaction process parameters on ribbon density/ribbon porosity and on the analyses of the non-uniform density distribution in ribbons.

A part of these research studies have been published about the understanding of the roll compaction and the improvement of roll pressure distribution on the roll surface, which can be distinguished from each other in their method in terms of investigating the roll compaction process. The first article has been issued by Johanson that introduced a powder mechanics model to predict the separation force and torque and the roll surface pressure based on the physical characteristics of the powder and the roll dimensions [43]. Various mathematical models for roll compaction modeling have been established and the application of roll compaction simulators has been already presented in order to gain a better understanding of the roll compaction process [30, 35, 42, 59-67]. The aim of modeling and prediction of ribbon RD by mathematical models is saving of material and time. However, it is described in the literature, that the models need to be validated by experimental data set, which often leads to an extensive laboratory work [68]. Several investigations have been reported about the agreement between the measured and predicted densities of ribbon strips [35, 69, 70]. Reimer et al. [71] introduced a hybrid modeling using the Styl'One Evolution, which has been established based on the mimicking of ribbons through production of the so called ribblets by the Styl'One Evolution and on the application of an integration model modified after Peter et al. [72].

Most investigations on ribbon density have been conducted experimentally and in-line and off-line methods have been utilized for the ribbon density determination. Since ribbon density data predicted by the mathematical models need to be validated, the improvement of experimental work on the measurement of ribbon RD is essential [73]. The irregular shape of ribbon pieces is one of the difficulties that makes the determination of the apparent volume of ribbons, thus also the off-line determination RD, a demanding task. Wöll et al. described the suitability of a punch method and the usage of NIR (near infra-red) method for porosity determination of ribbons. The porosity measurements by the punch method were used for the calibration of the NIR method. Both measurement

techniques have been found to be appropriate methods for ribbon porosity evaluation [74]. A similar approach for ribbon density measurement, called sectioning method has been introduced by Miguelez-Moran et al. [41], which was compared to micro-indentation and X-ray micro-computed tomography (μCT) in terms of the determination of density distribution in ribbons [52]. They found, that micro-indentation and X-ray μCT result in a finer resolution of the local density variation, while the sectioning method is faster and simple. The suitability of in-gap porosity measurement has been published by Herting et al. in 2007. Using this method, the volume of the ribbon is calculated multiplying the GW, diameter of the rolls, RW, RS and the production time. Then the weight of granules resulted from the milled ribbons was divided by the calculated volume, which led to the determination of the envelope density of ribbons [75]. Later, also other authors reported about the usefulness of in-gap porosity measurement in terms of controlling the downstream granule and tablet properties [76]. Volume displacement methods have frequently been utilized to define the apparent volume of ribbons. Michrafy et al. [69] analyzed the ribbon porosity/ribbon density by mercury porosimetry and light transmission. The density across the ribbon width was measured by mercury porosimetry. The obtained periodic heterogeneity in ribbons as dark and light zones was found to be in correlation with the geometry of the feeding screw, but not with the obtained density data from the mercury porosimetry measurements corresponding to the lighter and darker zones. The authors related the light transmission results to the anisotropy of the microstructure in the ribbon, which influences the light diffusion through the ribbon piece. As the usage of mercury is neither environment nor operator friendly, intrusion with low viscosity oil and powder pycnometry using free-flowing medium such as DryFlow® used for the GeoPyc method has become a more and more commonly used method [20]. Khorasani et al. [77] compared the oil absorption method with the mercury intrusion method, in that the oil absorption method was obtained as a comparative approach for ribbon porosity determination. Considerable amount of work have been published about the application of powder pycnometry, since it is a fast and cost-effective method for envelope density determination [30, 36, 53, 59, 68, 71, 78-85]. Souihi et al. [30] introduced how a roll compaction process transfer between a Hosokawa and an AlexanderWerk roll compactor can be considered correlating the normal stress and the ribbon RD, measured by GeoPyc powder pycnometer. Three different measurement techniques, such as laser-based direct measurement as novel method, volume displacement measurement using

GeoPyc, and manual measurement considering the dimensions of the ribbon samples have been compared in the work of Iyer et al. [86]. In this study, the laser-based technique was obtained to be comparable with the volume displacement technique and to be suitable method to test the RD of ribbons and tablets. Alesso et al. [20] conducted a ribbon porosity evaluation using laser-based direct measurement with the oil intrusion technique. The laser based method was found to be an appropriate approach to acquire ribbon porosity rapidly. Also terahertz imaging system has been reported to be a suitable approach to evaluate the density distribution in ribbons, as the terahertz radiation is able to penetrate the ribbon and the refractive index indicates the variations in density [87]. In the studies of Khorasani et al. [58, 77], NIR chemometric method employing principal component analysis was proved to be a useful online approach to map the ribbon density distribution and the GSD. Also the effect of the roll pressure and RS were investigated. They found that higher roll pressure and slower RS results in lower ribbon porosity, larger granules and less amount of fines. Nevertheless, the NIR radiation showed a marginal penetration depth in the ribbon surface, therefore the density of ribbons cannot be detected considering the whole ribbons, the density resolution only at the surface of the ribbons is possible. Several studies reported about the NIR spectroscopy and NIR chemical imaging to be feasible tools for real-time monitoring of RD [24, 70, 73, 88].

In order to investigate the density in the whole ribbon piece, also tomographic methods are promising tools according to Hancock et al. Zeitler et al. [89] summarized in-vitro tomographic tools, X-ray μCT, magnetic resonance imaging and optical coherence tomography, respectively, as possible methods for structure determination of solid dosage forms. Several studies reported about the expediency of X-ray μCT during investigation of particle packing and particle movement [90, 91], porosity and morphology of granules [92], density distribution in tablets [93, 94] in the last 10 years. Akseli et al. investigated the variation in local ribbon density and its effect on the produced tablets using nondestructive ultrasonic. The findings have been confirmed by X-ray μCT [95]. Wiedey et al. [34] presented the density distribution in all three spatial directions in higher resolution than before. In their further study [96], the applicability of thermographic camera for in-line density distribution determination has been demonstrated. It was shown that the temperature distribution in the thermographic images matched the density distribution measured by X-ray μCT.

2 Aims of this study

Numerous types of roll compactors are on the market, which differ in their configuration, design of roll compaction, performance and the extents to set the process parameters. Because of these discrepancies and the lack of knowledge in this field, the systematical investigation of different types or roll compactors is the main goal of the present thesis. For that purpose, spray-dried mannitol and microcrystalline cellulose and the 50-50 % (w/w) mixture thereof should be used as model materials showing different deformation behaviour. Ribbons should be prepared using inclined, horizontal and vertical roll compaction designs, respectively. The impact of the process parameters, roll compaction design and the type of material on the ribbon and granule characteristics should be systematically investigated within the scope of design of experiments.

Recording the roll compaction process parameters, the control performance should be assessed with highest attention on the control technique of the roll compactor, the precision and the deviations from the set value of the hydraulic pressure (HP)/SCF and GW. Additionally, the settling time of new parameter settings was considered as a critical value of the process control. Beside the obtained dataset, the quality of the produced ribbons and granules should be analyzed in terms of ribbon RD and GSD. The ribbon RD should be measured by two different techniques, using GeoPyc powder pycnometer and X-ray μCT. Both measurement methods should be compared to each other in terms of their benefits and drawbacks. Based on the obtained ribbon RD results, conversion factors might be established introducing a principle method for the roll compaction process transfer.

A further objective of this study was to examine the granule quality by analyzing correlations between the ribbon RD and GSD, as all ribbon batches were milled by the star granulator of the Mini-Pactor using constant granulation settings.

3 Results and discussion

3.1 Control performance of the different types of roll compactors

3.1.1 Introduction and objectives

Roll compaction is a continuous dry granulation method and it is in the very nature of roll compaction as being continuous process, the process has to be robust over a longer period of time in order to maintain the critical process parameters as requested. As roll compaction is a long manufacturing process, the critical process parameters need to be controlled ensuring the process setting is stable, thus robust products being conform to the defined specifications can be produced. The control performance of roll compaction has already been examined in the frame of some previous investigations [97-100]. Singh et al. [99] published a detailed concept to design appropriate control system including cascade and single open loop control configurations/proportional integral derivative (PID) controllers, in order to keep the process parameters within the specifications for a continuous pharmaceutical tablet manufacturing process including a roll compaction step. Different operation modes were examined by Shlieout et al. [97, 98] considering the process parameter consistency and the effect of changing the SCF, GW and RS using a Gerteis Mini-Pactor. Since the control concepts of different roll compactors were simulated [53, 99, 101] and in only some cases experimentally investigated, further analyses of the control of roll compaction process is fundamental.

Less work has been published on the analysis of control strategies for the individual unit operation, roll compaction. In order to control the roll compaction process, the maintenance of the most important process parameters - the SCF, GW and RS – is essential. Most commonly the control is realized by using PID controllers. P stands for the proportional term, which produces an output that is proportional to the current error. Increasing the proportional gain will increase the speed of the control system response. If the proportional gain is too high, the system can become unstable and if the proportional gain is too low, the control action may be too small when responding to disturbances. I stands for the integral term, which is proportional to both the magnitude and duration of the error. If the I-term is too high the present value can overshoot the set value. D stands

for the derivative term, and is based on the rate of change of the process variable. It causes the output to decrease, if the process variable is increasing rapidly. Often, the D-term is set to zero resulting in a PI controller. While commonly the control parameters of the HP or CF are not accessible for the end user, but only for the supplier, the parameters for the gap control can be set by the end user.

In this part of the thesis, the aim was to evaluate the performance of different types of roll compactors regarding the settling time, the deviation of the actual values from the set values and the precision of the SCF/HP and GW in steady-state. The settling time is defined to be the time needed to achieve the new parameter settings according to the set value. Steady-state process condition is described as a constant process, while all actual values of the process parameters achieved the specification of the set value. The roll compaction environment and data recording frequency of the examined roll compactors were different as described in sections 5.2.4.2 and in 5.2.2.

3.1.2 Control performance of AlexanderWerk BT120 roll compactor

The roll compactor of AlexanderWerk used in this work does not possess a gap control system. High deviations are observed between the set process parameters and the actual values. Typical process data of the roll compaction runs regarding mannitol, mixture and MCC 101 are presented in Table 2 using smooth rolls and in Table 3 using knurled rolls. The starting process parameters of the HP and GW are also included in the aforementioned tables: 24 → 18 means that the HP was decreased from 24 bar to 18 bar and 3 → 1.5 means that the GW was decreased from 3 mm to 1.5 mm. The settling time, which was necessary to track the setpoint respecting the HP and GW, is presented in Table 2 and in Table 3. These tables also include the coefficient of variation (CV) of the recorded HP and GW values during the production of the different batches. The CV is the ratio of the standard deviation (σ) and the mean (μ), presented in Equation 4, which represents the robustness of the process. A lower CV indicates less fluctuations during processing.

$$\mathrm{CV} = \frac{\sigma}{\mu} * 100$$ Equation 4

Results in regard to the other roll compactors shown in the next sections are represented following the above described narration.

Table 2. Settling time and steady-state values of process parameters compacting with AlexanderWerk with smooth roll surface.

	Parameter setting			HP [bar]			GW [mm]		
	HP [bar]	GW [mm]	RS [rpm]	time [s]	mean ± s	CV [%]	time [s]	mean ± s	CV [%]
mannitol	30 → 18	0 → 1.5	3	20	15.98 ± 0.15	0.95	50	1.52 ± 0.05	3.04
	24 → 18	2.3 → 2.3	3	0	20.38 ± 0.49	1.33	2	2.29 ± 0.03	2.56
	0 → 60	1.9 → 1.5	3	10	59.26 ± 0.65	1.10	30	1.48 ± 0.02	1.67
	0 → 60	0 → 2.3	3	10	58.25 ± 0.48	0.82	60	2.22 ± 0.08	2.13
mixture	0 → 18	1.5 → 1.5	3	2	17.06 ± 0.24	1.39	6	1.48 ± 0.08	5.29
	36 → 18	1.9 → 2.3	3	0	17.12 ± 0.12	4.22	118	2.29 ± 0.04	1.81
	36 → 60	1.5 → 1.5	3	4	58.27 ± 1.37	2.35	16	1.49 ± 0.11	7.15
	0 → 24	2.2 → 2.3	3	2	22.03 ± 0.38	1.72	47	2.24 ± 0.10	4.37
MCC 101	36 → 18	0.8 → 1.5	3	0	17.18 ± 1.57	9.11	98	1.48 ± 0.11	7.20
	0 → 18	0.7 → 2.3	3	0	18.15 ± 0.56	3.10	90	2.29 ±0.10	4.30
	36 → 48	1.5 → 1.5	3	2	46.74 ± 0.45	0.96	14	1.46 ± 0.06	4.36
	36 → 46	0.8 → 2.3	3	3	43.98 ± 0.14	0.32	74	2.22 ± 0.15	6.77

Table 3. Settling time and steady-state values of the process parameters compacting with AlexanderWerk roll compactor using knurled roll surface.

	Parameter setting			HP [bar]			GW [mm]		
	HP [bar]	GW [mm]	RS [rpm]	time [s]	mean ± s	CV [%]	time [s]	mean ± s	CV [%]
mannitol	24 → 18	3 → 1.5	3	0	18.37 ± 0.61	3.31	40	1.55 ± 0.29	18.67
	18 → 18	1.5 → 3.0	3	0	20.43 ± 0.50	2.45	50	3.01 ± 0.02	0.75
	36 → 60	2.2 → 1.5	3	10	59.02 ± 0.22	0.37	70	1.47 ± 0.03	2.48
	36 → 60	2.2 → 3.0	3	10	58.07 ± 0.33	0.57	30	2.99 ± 0.03	0.96
mixture	0 → 18	3.0 → 1.5	3	50	16.09 ± 0.28	1.74	70	1.47 ± 0.10	7.07
	60 → 18	1.5 → 3.0	3	10	20.12 ± 0.49	2.45	20	3.00 ± 0.06	2.06
	0 → 60	0 → 1.5	3	20	58.61 ± 1.48	2.53	60	1.48 ± 0.03	1.89
	0 → 60	0 → 3.0	3	20	60.03 ± 0.58	0.96	30	2.89 ± 0.15	5.07
MCC 101	24 → 18	3.0 → 1.5	3	0	15.82 ± 2.81	17.79	36	1.52 ± 0.14	9.28
	0 → 18	0 → 3.0	3	40	17.31 ± 0.46	2.68	60	2.93 ± 0.06	2.15
	0 → 60	0 → 1.5	3	121	59.54 ± 0.50	0.84	181	1.47 ± 0.07	4.77
	18 → 60	3.0 → 3.0	3	10	56.16 ± 0.78	1.33	120	2.95 ± 0.13	4.30

The specification of the HP is set at the setpoint HP ± 2 bar and for GW the set value ± 0.1 mm. According to these terms, the deviation from the set value and precision of the HP and GW adjustment were inappropriate to produce ribbons with proper quality compacting with both types of roll surfaces. In general, except some certain batches, the achieved HP was lower than the set parameter. Due to the high standard deviation (SD), the actual HP values were below the lower limit. For instance, in case of setting 18 bar HP at 1.5 mm GW, 15.82 ± 2.81 bar HP and 1.52 ± 0.14 mm GW are achieved, when MCC is roll compacted using knurled rolls, thus the steady-state process conditions are not achieved.

Roll compaction was more difficult when smooth rolls were used. The highest set HP and GW had to be reduced, when MCC was processed and also in case of mixture compacting with 2.3 mm RW. Due to the low friction between the processed powder and the smooth roll surface, higher screw speeds were required to let the material grabbed in between the rolls. Conveying the powder setting the maximum screw speed was not efficient to achieve 3.0 mm GW. Thus, the set value of the gap size was changed to 2.3 mm regarding roll compaction with smooth rolls. In case of MCC 101 the highest set HP was 48 bar, when 1.5 mm GW was set, while adjusting 2.3 mm GW only 46 bar HP was realized as set value. In case of the mixture, 24 bar was the highest feasible HP at 2.3 mm gap size. In addition, in case of MCC and the mixture, the increase of the RS from 3 rpm to 8 rpm was needed to grab the powder into the compaction area at the beginning of the roll compaction process. Thus, 8 rpm RS and 25 - 40 rpm screw speed were set to transport the powder into the gap. After reaching a certain GW, the RS was reduced to 5 rpm and afterwards to 3 rpm to develop the desired gap size presented in Figure 6.

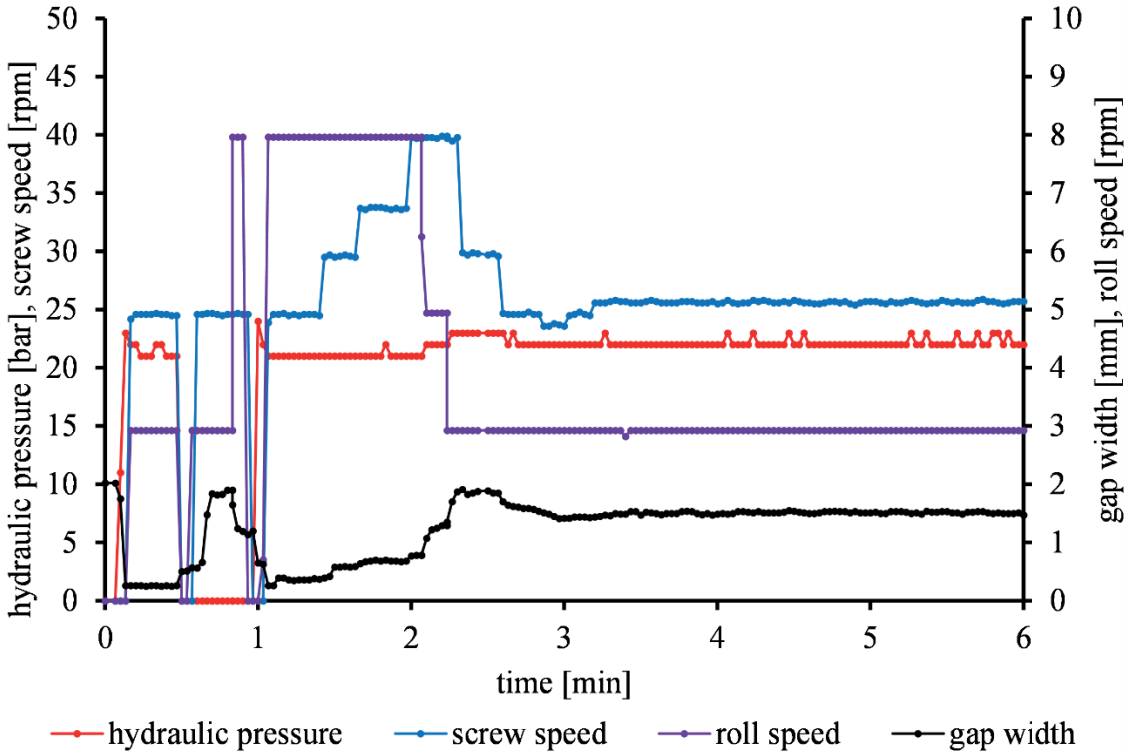

Figure 6. Roll compaction parameters for the mixture using AlexanderWerk BT120 with smooth rolls.

Based on these results, a wider processing space was detected, when knurled roll surface was used. The effect of the material properties was reflected in the progress of the individual roll compaction runs of each material. Due to the proper flowability and non-hygroscopic property of mannitol, the roll compaction with knurled rolls setting the planned process parameter combinations was successfully performed in randomized order, shown in Figure 7.

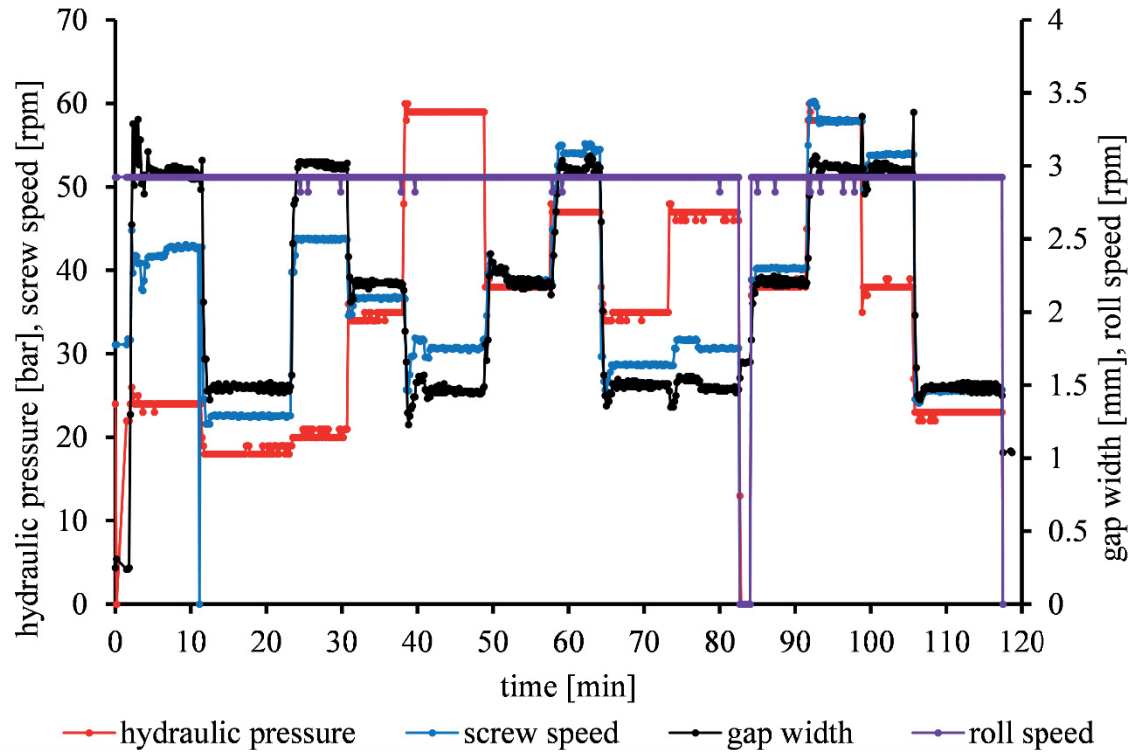

Figure 7. Process parameters of roll compaction of mannitol using AlexanderWerk BT120 with knurled rolls.

However, roll compaction interruptions were needed during the operation using smooth rolls in case of all materials due to the warming up of the machine, while material sticking caused roll compaction breaks using knurled rolls in case of MCC 101 and the mixture. Table 2 and Table 3 provide results for the settling time, which was needed to reach the steady-state process conditions. A longer period of time (3 - 121 s) was necessary to set the HP to the following value, when the previous HP was 0 bar. In the other cases, the set HP was reached in maximum of 10 s in case of knurled rolls and less than 30 s in case of smooth rolls. The speed of the GW adaptation to the following GW value took longer time (30 - 181 s), when 0 mm GW was the previous actual value, or when the amount of conveyed material was not enough to open the gap. This was observed due to insufficient powder flow from the hopper to the screw.

Without a gap control it was difficult to obtain a desired GW. The process showed higher deviations from the set values and low precision. It was not always possible to obtain the desired HP. The use of the smooth rolls made the process more complicated and the factor space for process variables was narrower.

3.1.3 Control performance of L.B. Bohle BRC 25 roll compactor

Roll compaction using the BRC 25 roll compactor was examined using MCC, mannitol and the mixture. The recorded process parameters regarding all materials and used roll surface patterns are presented in Table 4, Table 5, Table 6 and Table 7. The adjustment of the SCF had priority to the GW control compacting with BRC 25. Thus, the obtained periods of time needed to change the GW were longer compared to the time required to set the SCF. No correlation between the length of the adaptation time and the used materials, roll surface or the extent of the process parameter modifications was found in case of the SCF. Even though, the speed of the GW adjustment was depending on the one hand on the PI parameter settings of the GW control loop, on the other hand on the material sticking to the roll surface. The PI parameter setting was kept constant during all roll compaction runs. As presented in Table 4, Table 6 and Table 7, longer adaptation time in case of smooth (0-130), coarse (15-75 s) and fine grooved roll surface (11-72 s) was obtained due to the material sticking on the roll surface. 0 s settling time was obtained, when the GW was kept constant at 3.0 mm gap size, while the SCF was increased from 7 kN/cm to 10 kN/cm compacting MCC 101 using coarse grooved rolls. The deviations of the set value of the actual SCF values were found to be appropriate, when 2 kN/cm was set. However, in case of 10 kN/cm SCF, slightly higher deviations from the set value were observed. The SCF was reached with proper precision, while higher standard deviations of the GW were observed.

Table 4. Settling time and steady-state values of the process parameters compacting with BRC 25 roll compactor using smooth rolls.

		Parameter setting			SCF [kN/cm]			GW [mm]		
		SCF [kN/cm]	GW [mm]	RS [rpm]	time [s]	SCF [kN/cm]	CV [%]	time [s]	GW [mm]	CV [%]
smooth	mannitol	6 → 2	2.3 → 1.5	3 → 2	61	2.02 ± 0.03	1.36	46	1.48 ± 0.07	4.51
		6 → 2	2.3 → 3.0	3 → 2	20	2.00 ± 0.02	1.09	48	2.97 ± 0.08	2.62
		6 → 2	2.3 → 1.5	0 → 4	40	2.01 ± 0.03	1.30	60	1.50 ± 0.03	2.15
		10 → (7) → 2	1.5 → 3.0	0 → 4	20	2.01 ± 0.01	0.74	20	2.98 ± 0.07	2.39
		8 → 10	1.5 → 1.5	2 → 2	38	10.07 ± 0.05	0.66	42	1.48 ± 0.04	2.12
		8 → 10	3.0 → 3.0	2 → 2	15	10.07 ± 0.07	0.41	24	3.05 ± 0.11	1.08
		6 → 10	3.0 → 1.5	4 → 4	40	10.04 ± 0.06	0.57	20	1.48 ± 0.04	3.04
		8 → 10	3.0 → 3.0	4 → 4	0	10.02 ± 0.05	0.52	0	2.98 ± 0.04	1.45
	mixture	0 → 2	0 → 1.5	0 → 2	41	2.01 ± 0.05	2.29	70	1.51 ± 0.12	7.88
		6 → 2	2.3 → 3.0	3 → 2	20	2.01 ± 0.02	0.97	53	3.01 ± 0.07	2.36
		6 → 2	2.3 → 1.5	3 → 4	21	2.01 ± 0.04	2.07	21	1.49 ± 0.08	5.23
		6 → 2	2.3 → 3.0	3 → 4	20	2.00 ± 0.02	1.00	60	3.00 ± 0.06	1.86
		8 → 10	1.5 → 1.5	2 → 2	11	10.04 ± 0.06	0.56	0	1.50 ± 0.04	2.44
		8 → 10	3.0 → 3.0	2 → 2	20	10.03 ± 0.04	0.41	0	2.99 ± 0.05	1.65
		8 → 10	1.5 → 1.5	4 → 4	9	10.04 ± 0.05	0.53	0	1.49 ± 0.04	2.86
		8 → 10	3.0 → 3.0	4 → 4	20	10.05 ± 0.04	0.37	20	2.97 ± 0.04	1.46

	MCC 101	0 →2	0 → 1.5	0 → 2	*					
		10 → 2	1.5 → 3.0	2 → 2	21	2.00 ± 0.02	1.10	40	2.97 ± 0.10	3.37
		6 → 2	2.3 → 1.5	3 → 4	81	1.92 ± 0.19	9.72	120	1.52 ± 0.12	8.02
		6 → 2	2.3 → 3.0	3 → 4	31	1.97 ± 0.11	5.64	41	1.57 ± 0.12	7.81
		0 → 10	1.5 → 1.5	0 → 2	51	10.05 ± 0.09	0.91	130	1.53 ± 0.13	8.73
		8 → 10	3.0 → 3.0	2 → 2	10	10.05 ± 0.05	0.49	20	3.01 ± 0.06	2.03
		5 → 10	2.3 → 1.5	0 → 4	40	10.56 ± 0.08	0.77	20	1.53 ± 0.02	1.39
		2 → 10	1.5 → 3.0	2 → 4	*					

*due to system error, data was not recorded.

Table 5. Settling time and steady-state values of the process parameters compacting with BRC 25 roll compactor using knurled rolls.

		Parameter setting			SCF [kN/cm]			GW [mm]		
		SCF [kN/cm]	GW [mm]	RS [rpm]	time [s]	SCF [kN/cm]	CV [%]	time [s]	GW [mm]	CV [%]
knurled	mannitol	8 → 2	3.0 → 1.5	2	31	2.09 ± 0.05	2.38	46	1.49 ± 0.04	2.38
		10 → 2	1.5 → 3.0	2	28	2.00 ± 0.02	1.07	48	2.98 ± 0.06	1.86
		6 → 10	3.0 → 1.5	2	38	10.07 ± 0.05	0.47	42	1.48 ± 0.04	2.67
		6 → 10	2.3 → 3.0	2	15	10.07 ± 0.07	0.65	24	3.05 ± 0.11	3.63
	mixture	2 → 2	3.0 → 1.5	2	14	2.01 ± 0.04	2.07	9	1.49 ± 0.04	2.80
		4 → 2	1.5 → 3.0	2	18	2.01 ± 0.02	1.11	30	3.00 ± 0.04	1.17
		2 → 10	2.0 → 1.5	2	25	10.06 ± 0.04	0.43	3	1.49 ± 0.02	1.61
		2 → 10	1.5 → 3.0	2	6	10.07 ± 0.02	0.22	19	3.05 ± 0.10	3.30
	MCC 101	8 → 2	3.0 → 1.5	2	40	2.01 ± 0.03	1.25	58	1.48 ± 0.05	3.69
		10 → 2	3.0 → 3.0	2	25	2.01 ± 0.03	1.51	31	3.00 ± 0.09	2.88
		4 → 10	3.0 → 1.5	2	25	10.05 ± 0.04	0.44	56	1.48 ± 0.05	3.66
		6 → 10	2.3 → 3.0	2	15	10.07 ± 0.04	0.37	24	3.04 ± 0.06	2.08

Table 6. Settling time and steady-state values of the process parameters compacting with BRC 25 roll compactor using coarse grooved roll surface.

		Parameter setting			SCF [kN/cm]			GW [mm]		
		SCF [kN/cm]	GW [mm]	RS [rpm]	time [s]	SCF [kN/cm]	CV [%]	time [s]	GW [mm]	CV [%]
coarse grooved	mannitol	8 → 2	3.0 → 1.5	2	50	2.01 ± 0.03	1.28	68	1.50 ± 0.03	2.02
		6 → 2	3.0 → 3.0	2	15	2.00 ± 0.02	0.76	75	3.00 ± 0.05	1.76
		6 → 10	3.0 → 1.5	2	23	10.05 ± 0.06	0.62	17	1.47 ± 0.08	5.38
		8 → 10	1.5 → 3.0	2	11	10.07 ± 0.04	0.44	15	3.01 ± 0.03	0.98
	mixture	0 → 2	3.0 → 1.5	2	11	2.04 ± 0.04	1.81	44	1.48 ± 0.06	3.79
		10 → 2	3.0 → 3.0	2	25	2.00 ± 0.03	1.49	58	3.00 ± 0.04	1.38
		2 → 10	3.0 → 1.5	2	21	10.06 ± 0.03	0.33	24	1.50 ± 0.03	2.17
		8 → 10	1.5 → 3.0	2	33	10.08 ± 0.08	0.77	58	3.01 ± 0.04	1.23
	MCC 101	8 → 2	3.0 → 1.5	2	46	2.00 ± 0.03	1.39	57	1.48 ± 0.03	1.86
		8 → 2	1.5 → 3.0	2	24	2.01 ± 0.02	1.02	36	2.99 ± 0.05	1.70
		2 → (7) → 10	3.0 → 1.5	2	46	10.06 ± 0.05	0.51	46	1.49 ± 0.03	3.17
		7 → 10	3.0 → 3.0	2	48	10.07 ± 0.04	0.38	0	3.01 ± 0.04	1.22

Table 7. Settling time and steady-state values of the process parameters compacting with BRC 25 roll compactor using fine grooved rolls.

		Parameter setting			SCF [kN/cm]			GW [mm]		
		SCF [kN/cm]	GW [mm]	RS [rpm]	time [s]	SCF [kN/cm]	CV [%]	time [s]	GW [mm]	CV [%]
fine grooved	mannitol	6 → 2	1.5 → 1.5	2	28	2.12 ± 0.02	0.92	11	1.50 ± 0.03	1.69
		8 → 2	1.5 → 3.0	2	28	2.03 ± 0.02	1.09	63	2.99 ± 0.06	1.93
		2 → 10	3.0 → 1.5	2	26	10.07 ± 0.03	0.34	37	1.50 ± 0.03	2.17
		6 → 10	2.3 → 3.0	2	30	10.06 ± 0.03	0.30	52	3.01 ± 0.03	1.07
	mixture	10 → 2	3.0 → 1.5	2	43	2.00 ± 0.03	1.31	64	1.48 ± 0.04	2.72
		6 → 2	1.5 → 3.0	2	24	2.02 ± 0.02	1.10	14	3.02 ± 0.08	2.65
		8 → 10	3.0 → 1.5	2	18	10.03 ± 0.06	0.61	68	1.49 ± 0.03	1.99
		0 → 10	0 → 3.0	2	64	10.06 ± 0.03	0.30	67	3.04 ± 0.10	3.26
	MCC 101	8 → 2	3.0 → 1.5	2	45	2.00 ± 0.02	1.05	72	1.49 ± 0.05	3.12
		6 → 2	1.5 → 3.0	2	23	2.01 ± 0.02	1.1	29	2.99 ± 0.04	1.33
		6 → 10	2.3 → 1.5	2	20	10.05 ± 0.04	0.42	17	1.47 ± 0.06	4.01
		4 → 10	3.0 → 3.0	2	19	10.07 ± 0.04	0.35	29	3.01 ± 0.04	1.45

A typical curve of the screw speed is presented in Figure 8 changing the SCF from 8 kN/cm to 6 kN/cm and from 6 kN/cm to 10 kN/cm and the GW from 1.5 mm to 3.0 mm then from 3.0 mm to 1.5 mm. The decrease of the SCF followed a continuous progress, while its increase showed an irregular evolution. Figure 8 shows also how the screw speed was changed with the altered GW. After changing the GW, an overreaction of the screw speed was observed. Then the proper screw speed was set, which led to a constant gap size.

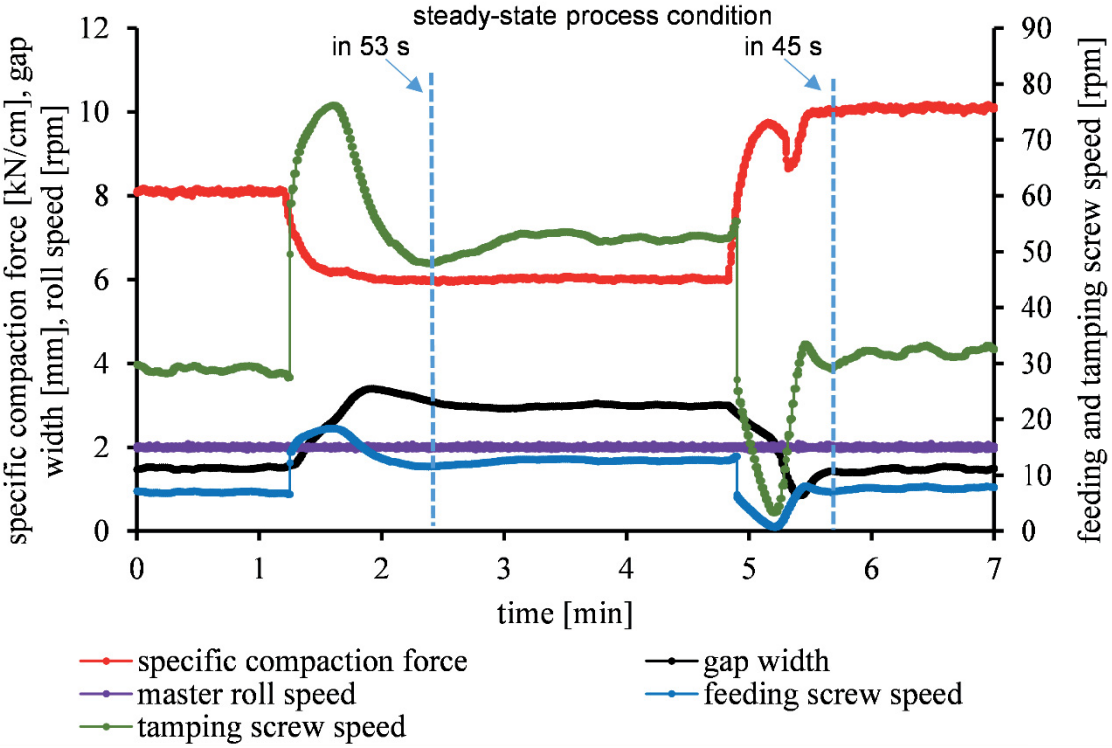

Figure 8. Adjustment of the SCF and GW to the new parameter settings compacting mannitol with BRC 25 using knurled roll surface.

Keeping the SCF at 6 kN/cm, while altering the GW from 3.0 mm to 2.2 mm, similar but moderated overreaction of the screw speed was observed, presented in Figure 9.

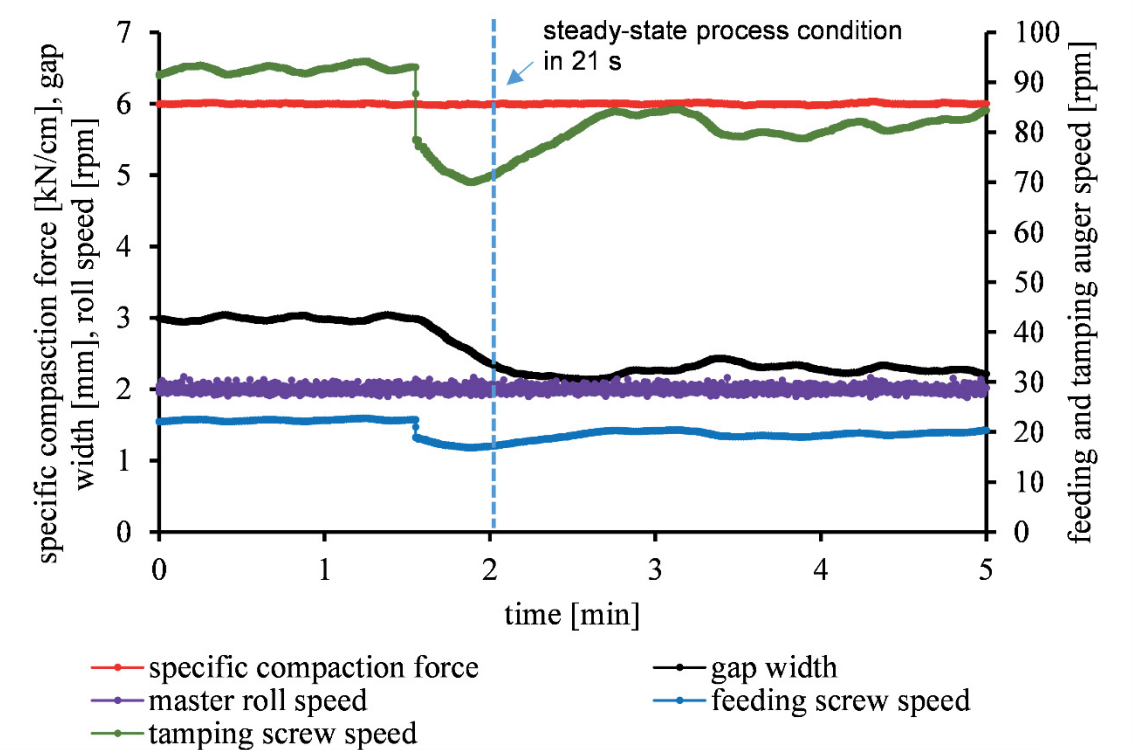

Figure 9. GW adjustment keeping the SCF constant for processing of MCC 101 with BRC 25 using coarse grooved rolls.

In contrast to the previous two examples, the speed of the feeding and tamping screws followed a damped increase and decrease trend until the proper speed was reached, shown in Figure 10. The observed increase of GW is explained by effect of the decrease of the SCF. Compacting the same or slightly less amount of powder setting a decreased SCF opened the gap until the forward value of the SCF was reached.

The gap control of the BRC 25 worked properly. Changes in the process parameters were in most cases compensated within 30 seconds for SCF and within 60 seconds for GW. SCF and GW were controlled with satisfactory deviations from the set values and high precision in steady state for all tested materials and roll surfaces.

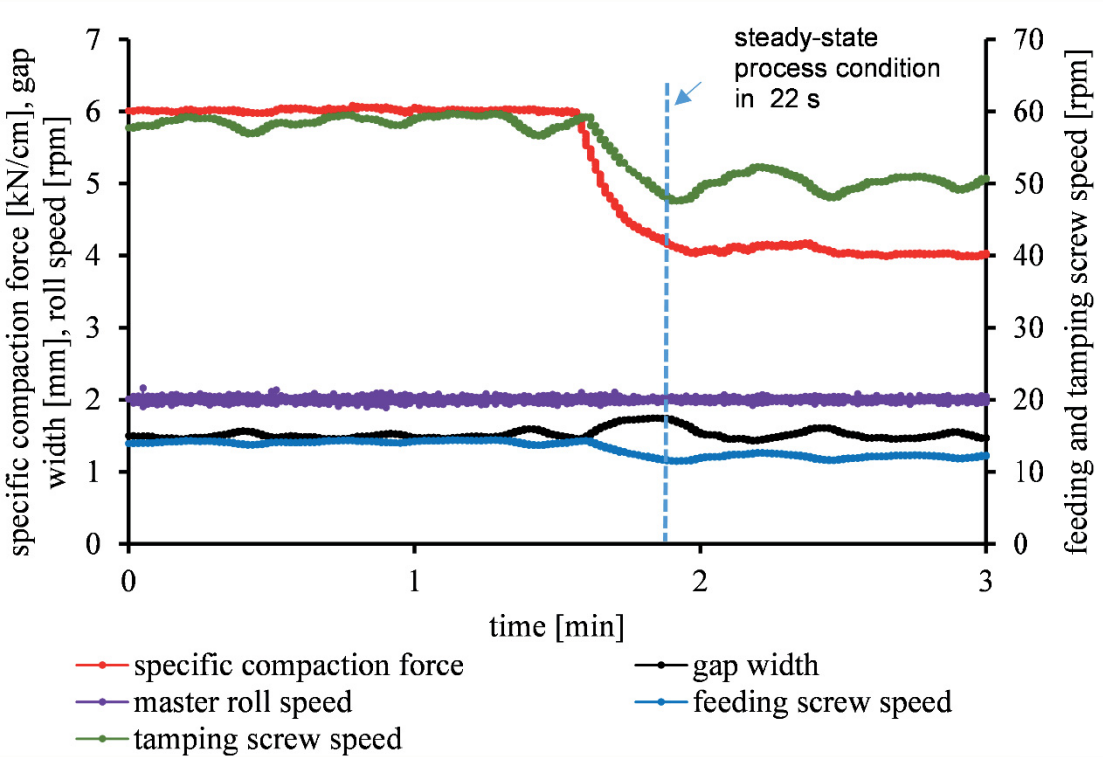

Figure 10. SCF adjustment keeping the GW constant processing MCC 101 with BRC 25 using coarse grooved rolls.

3.1.4 Control performance of Gerteis Mini-Pactor roll compactor

Roll compaction of mannitol using the automatic mode resulted in desired values of the GW with high precision as soon as the steady-state process condition was reached, exhibited in Figure 11.

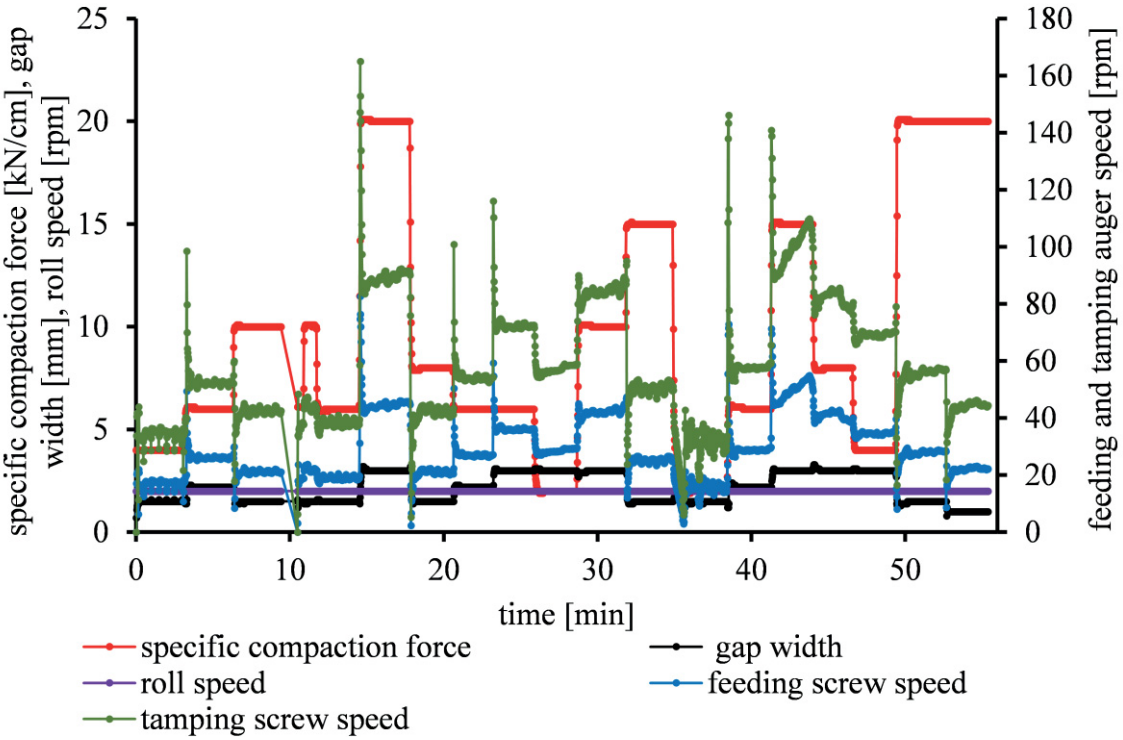

Figure 11. Process parameters of Gerteis Mini-Pactor compacting mannitol using gap control.

Beside the fast adaptation of the GW and SCF, also only small deviations from the set value and high precision of the SCF was observed. The PI control loop was responsible for the realization of a constant GW. The speed of the feeding and tamping augers was adjusted to control the GW, as presented in Figure 12. Increasing the SCF from 4 kN/cm to 6 kN/cm and the GW from 1.5 mm to 2.2 mm, the feeding and tamping screw speed were increased with a great step to convey more amount of powder to open the gap between the rolls. After 10 s, the speed of the feeding and tamping augers were decreased to a constant speed to develop a constant 2.2 mm gap size. Before decreasing the gap size from 2.2 mm again to 1.5 mm the SCF was increased to 10 kN/cm. After the increase of the SCF, the screw speeds jumped to a slightly higher value. This progress of the feeding and tamping auger speeds showed a decrease as soon as the new value of the GW was adjusted. The decrease of the GW was kept until a certain value, while the amount of

transported material was reduced. In order to realize 1.5 mm gap size, the speed of the feeding and tamping screws was adjusted to a higher value.

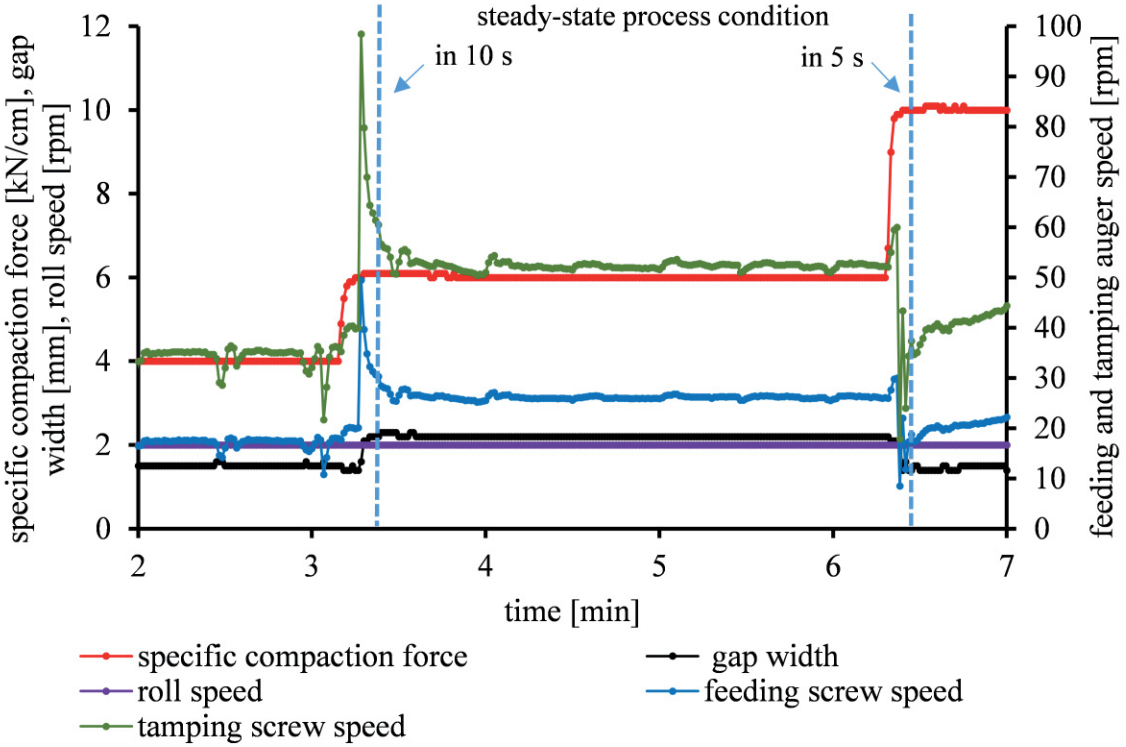

Figure 12. GW control of Gerteis Mini-Pactor operating in automatic mode.

The obtained mean and standard deviations of the SCF and GW and also the period of time needed for the adjustment of the constant parameters are shown in Table 8.

Table 8. Settling time and steady-state values of the SCF and GW compacting mannitol.

Parameter setting			SCF [kN/cm]			GW [mm]		
SCF [kN/cm]	GW [mm]	RS [rpm]	time [s]	SCF [kN/cm]	CV [%]	time [s]	GW [mm]	CV [%]
15 → 2	1.5 → 1.5	2	16	1.98 ± 0.04	4.61	0	1.51 ± 0.07	2.26
6 → 2	3.0 → 3.0	2	9	1.99 ± 0.03	1.48	0	3.01 ± 0.03	0.89
6 → 10	2.3 → 1.5	2	3	10.00 ± 0.02	0.23	8	1.49 ± 0.03	1.91
2 → 10	3.0 → 3.0	2	7	10.02 ± 0.04	0.44	7	2.99 ± 0.04	1.20
4 → 20	3.0 → 1.5	2	9	20.02 ± 0.04	0.19	20	1.49 ± 0.03	2.32
6 → 20	1.5 → 3.0	2	4	20.02 ± 0.04	0.20	6	3.01 ± 0.04	1.41

The time of the process adaptation to new parameter setting of the SCF was observed less than 20 s. The increase of the SCF from 6 kN/cm to 20 kN/cm took place in 4 s, while the decrease from 15 kN/cm to 2 kN/cm was achieved in 16 s. The periods of time to set the GW to the forward value was detected under 20 s. Changing the SCF from 6 kN/cm to 2 kN/cm and keeping the GW constant caused a settling time of the GW of 0 s, because of the small decrease step of the SCF. In contrast, in case of the decrease of the GW from 3.0 mm to 1.5 mm increasing the SCF from 4 kN/cm to 20 kN/cm, 9 s were needed. This longer period of time was necessary, because the speed of the feeding and tamping screws were decreased under the sufficient speed to generate 1.5 mm GW. The PI control loop overreacted slightly by re-setting the speed of the feeding and tamping screws.

3.1.5 Summary

The roll compactors, which were available for the comparison, were of different age. Newer machines from the same suppliers may have different process control capabilities and other implemented innovations in hard- and software for allowing more robust processes. It is easy and valuable to check the settling time and steady state conditions for a given set-up of a roll compactor.

The recorded process data set of the AlexanderWerk BT120 was described by insufficient deviations from the set values and precision compared to the BRC 25 and Mini-Pactor roll compactors. Because of the limitation in the parameter settings in case of MCC and the mixture using smooth rolls and the inacceptable deviations from the set values of the process parameters, a proper control of the HP and the GW are required. To implement a certain control of the GW, an improvement of the feeding unit is needed including the powder transport from the hopper to the feeding screw. Homogenous powder flow from the hopper to the horizontal screw and the adequate powder pre-densification were found to be essential to reach uniform ribbon properties.

The process data set delivered by the BRC 25 roll compactor was found to be more in accordance with the set values and precise compared to the AlexanderWerk BT120 roll compactor regarding all types of materials and roll surfaces. No relationship was found between the deviations of the set values of the BRC 25 roll compactor and the used material or roll surface. Even though, faster GW adaptation was observed, when knurled rolls were used.

The most precise and close to set values data of SCF and GW data were recorded in case of Gerteis Mini-Pactor respecting the process. Also faster process adaptation was observed compared to the BRC 25 after changing the roll compaction parameters.

These facts can be explained by the difference in the control method of the SCF and in the PI parameter setting of the GW control loop. Since the P-portion of the PI control loop was set to 10 in case of BRC 25 and to 12 in case of the Mini-Pactor, the control system of the Mini-Pactor reacted to the GW changes with a stronger response. The I-portion defines the time intervals, in which an error value is calculated as a difference between the actual values and the desired set value. The I-part of the PI control loop was set to 20 s in case of the BRC 25 roll compactor, while this was set to 15 s in the GW control loop of the Mini-Pactor. Because of the more frequent control steps and distinctive response of the control loop operating with the Mini-Pactor, a more consistent roll compaction was observed compared to the BRC 25 roll compactor. In order to achieve a more precise roll compaction process keeping tightly the set values using the BRC 25 roll compactor, the readjustment of the PI-control loop parameter setting is required regarding each type of roll surface.

Other differences between the two roll compactors include the way to control the SCF. While the BRC 25 was using a spindle motor, the Mini-Pactor controlled the SCF by a hydraulic system. The feeding systems and the sealing systems are also of importance for the performance of roll compactors.

3.2 Ribbon relative density

3.2.1 Introduction and objectives

The quality of granules, as being the end product of roll compaction/dry granulation and the starting material of tableting, is highly depending on the quality of ribbons. The ribbon quality is mainly influenced by the choice of excipients, set process parameters, roll compaction design regarding the roll surface and sealing system. Therefore, the effect of HP, SCF, GW, RS, type of sealing system, applied roll surface and the type of compacted material was evaluated on the ribbon RD. The experimental setup was built up based on the full factorial experimental plan, described in sections 5.2.1 and 5.2.2. In order to investigate the effect of different roll compaction designs, the implementation of different types of roll compactors was needed. The RD of ribbons produced by the different roll compactors was measured by GeoPyc powder pycnometry in order to analyze the differences and similarities between the effect of process parameters on the RD depending on the utilized roll compactor. For this purpose, GeoPyc pycnometry was selected as analytical tool, as it is a fast, user- and environmental-friendly method [78].

The further goal of this part of the thesis was to investigate the ribbon RD in high spatial resolution. It was already described in the literature that more detailed information about the RD of ribbons can be obtained, when X-ray µCT is used for the analysis of the ribbon structure [52]. Wiedey et al. [34] described the ribbon RD across the width, along the length and over the thickness of MCC ribbons at spatial resolution using X-ray µCT. Nevertheless, the aforementioned study did not address the RD considering the whole ribbon piece. Therefore, the RD of mannitol ribbons was analyzed across the width and considering the whole volume of the ribbon sample by X-ray µCT. Based on the obtained results, the GeoPyc powder pycnometry and the X-ray µCT were compared with each other.

3.2.2 Investigation of ribbon relative density by powder pycnometry

3.2.2.1 Relative density of ribbons produced by AlexanderWerk BT120

While it was possible to perform the whole experimental plan for all materials using knurled rolls, working with smooth rolls resulted in several difficulties. As the application

of smooth rolls led to diminished internal wall friction, higher screw speeds were required in order to grab the powder between the rolls and to achieve a comparable GW as was used when knurled rolls were implemented. Due to the screw speed limitation of the roll compactor, the maximum achievable GW was 2.3 mm for smooth rolls. At 60 bar HP in case of MCC and 36 bar, 48 bar and 60 bar HP using 2.3 mm gap size in case of the mixture a critical value of the roll compactor was exceeded, thus the process was stopped. The limitation of the screw speed resulted in a reduced processability regarding the GW, when smooth rolls were used. The processability using smooth rolls was also limited considering the maximum achievable HP in case of MCC and mixture. As MCC and the mixture were processed at high relative humidity [28], the moisture content of the aforementioned powders increased. Amidon et al. showed that the flowability of MCC decreases with increased relative humidity. Thus the cohesion was increased and the frictional forces and electrostatic charges may have been reduced [102]. In contrast, this reduction of processability was not observed for the roll compaction of mannitol, which is explained by its non-hygroscopic property and spherical shape [103], hence by its better flowability compared to MCC and mixture. Lower screw speed resulted in a more efficient powder feeding, thus an easier and less problematic powder transport was obtained from the hopper into the compaction zone and also the warming up of the machine was found to be less extensive. Therefore, the range of processability using smooth rolls was influenced by the behaviour of the manufactured material.

The RD of ribbons produced with smooth rolls is plotted against the set HP in Figure 13 a), while the RD of the knurled ribbons is introduced in Figure 13 b). In both cases, the ribbon RD raised with increasing HP. For the design using smooth rolls, denser ribbons were obtained, when 1.5 mm GW was adjusted at high HP setting. This observation aligned only in some cases, when knurled rolls were implemented, e.g.: mixture ribbons manufactured with 24 bar, 48 bar and 60 bar HP were slightly denser, when 1.5 mm GW was adjusted compared to ribbons produced with identical HP but at 3.0 mm GW. The difference between the RD of mannitol ribbons and the other both investigated materials was conspicuous; roll compaction of mannitol resulted in a significantly higher ribbon RD, than the processing of MCC and mixture. Nevertheless, it can be seen, that the mixture ribbons show comparable RD results to the mannitol ribbons, when it was compacted using high HP. Comparing the RD results, higher ribbon RD was obtained for all investigated materials, when roll compaction was accomplished using a pair of smooth rolls. Due to the low friction between the powder particles and the smooth roll surface, the

grabbing of the powder particles was not sufficient, thus the pre-densification of the material was higher compared to knurled rolls. Furthermore, the inhomogeneous surface of the knurled rolls provided a greater roll surface area to get in contact with the powder particles during grabbing and densification [104]. Since the roll surface area was greater, while the set HP was the same, the achieved compaction pressure was lower than the one exerted in case of smooth rolls.

Based on the obtained RD results, an acceptable model (R^2= 0.787, Q^2= 0.682) was achieved for roll compaction using smooth rolls. The quality of the model can be explained by the absent responses in case of mixture and MCC. An excellent model (R^2= 0.953, Q^2= 0.935) was obtained, when the roll compaction was investigated using knurled rolls. In both models, the most significant term was the HP. The quadratic term of HP was found to be significant in case of smooth rolls shown in Figure 14 a), while the term of fraction of MCC (Mater) follows the HP in the significance in the model of knurled rolls presented in Figure 14 b). Increasing the fraction of MCC had a negative effect on the RD; setting the same parameters, more porous ribbons were produced when MCC was compacted, while the compaction of mannitol led to denser ribbons. The GW had a minor, negative influence on the ribbon RD only in case of smooth rolls. Lower GW resulted in higher ribbon RD. The GW did not have a significant effect on the RD in case of knurled rolls, due to sticking of the material to the roll surface. Consequently, the production of ribbons led to thinner ribbons as the set GW. The two-fold interaction between the HP and type of material (HP*Mater) was observed as a significant term, shown in Figure 14 b) meaning that increasing the HP by one level resulted in a higher increase in RD when MCC was used than was the case for mannitol.

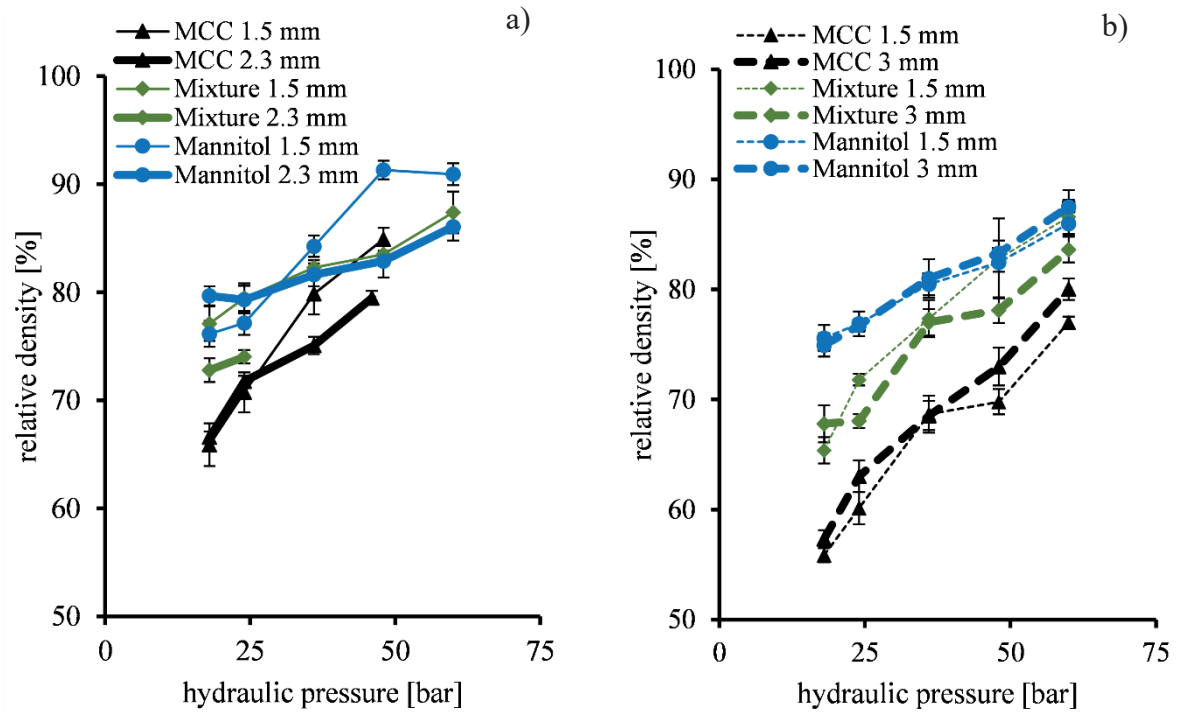

Figure 13 a), b). RD of MCC, mannitol and mixture ribbons produced by AlexanderWerk BT120 roll compactor using smooth (a) and knurled (b) roll surface (mean±s, at least n=3).

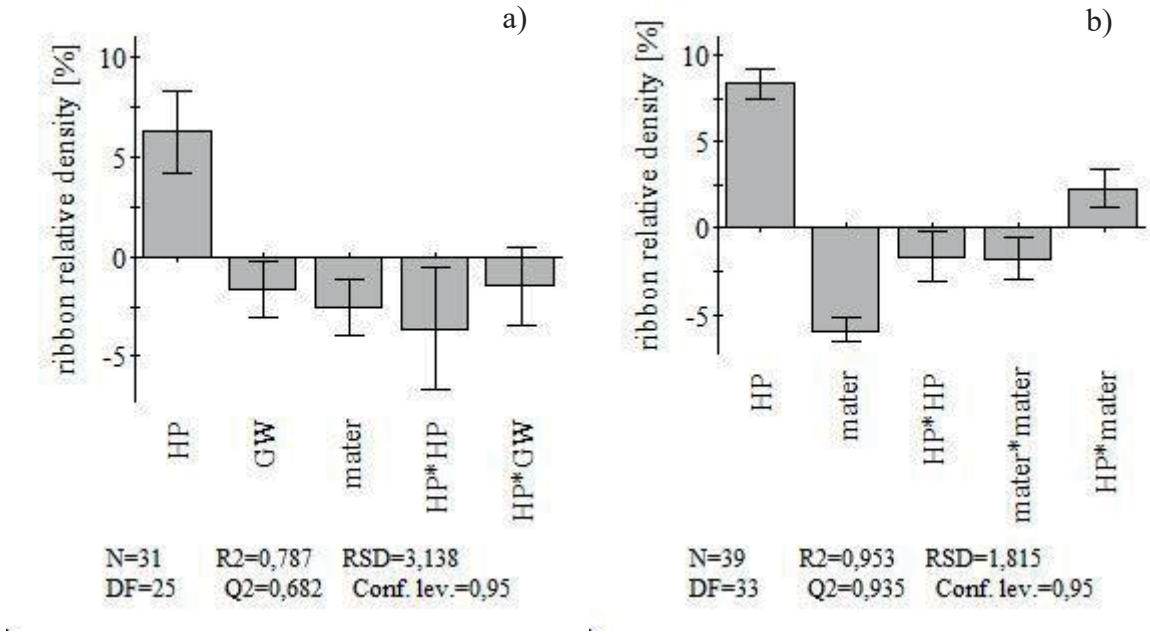

Figure 14 a), b). Coefficient plots of the model terms analyzing the ribbon RD obtained by AlexanderWerk BT120 roll compactor using smooth (a) and knurled (b) rolls.

3.2.2.2 Relative density of ribbons produced by Hosokawa Alpine Pharmapaktor C 250

The RD of MCC, mixture and mannitol ribbons is presented in Figure 15 a). The increase of the SCF led to denser ribbons independent of material type. As in case of the AlexanderWerk BT120, the mannitol ribbons were denser compared to MCC and mixture ribbons. The effect of the process parameters is presented in the coefficient plot, in Figure 15 b). The SCF was found to be the most significant term in the model (R^2= 0.972, Q^2= 0.962). An inverse effect of the GW was obtained; the lower the set GW, the higher was the RD. As the results indicate, the fraction of MCC had a significant effect on the ribbon RD, which is also proven by the statistical analysis. The two-fold interaction between the SCF and type of material (SCF*Mater) had a significant effect on the RD, which is shown in detail in the interaction plot, exhibited in Figure 16. Equivalent to the results for the AlexanderWerk BT120, the effect of the SCF was higher when the fraction of MCC was high, and lower when mannitol was processed.

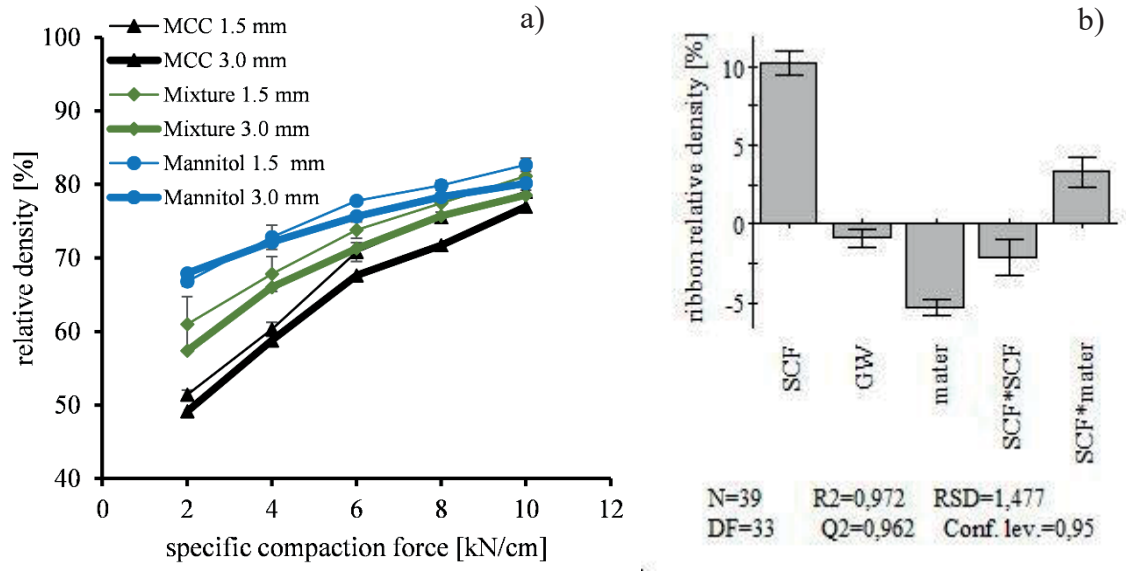

Figure 15 a), b). RD of MCC, mannitol and mixture ribbons (a) produced by Hosokawa Alpine Pharmapaktor C250 roll compactor setting 1.5 and 3.0 mm gap width (mean±s, at least n=3) and coefficient plot (b) of the model terms.

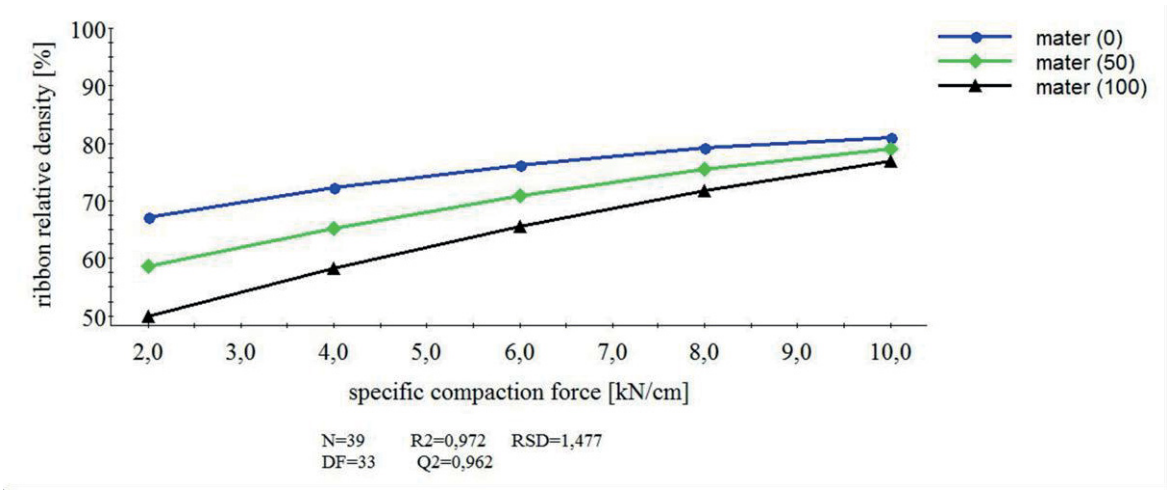

Figure 16. Interaction plot of the SCF and type of material respecting the ribbon RD obtained by Hosokawa Alpine Pharmapaktor C250.

3.2.2.3 Relative density of ribbons produced by L.B. Bohle BRC 25 roll compactor

An increasing trend of the ribbon RD was observed, when the SCF was incremented, as presented in Figure 17 a) and b). As it is described in case of the previous roll compactors, also the compaction using BRC 25 roll compactor resulted in more porous ribbons, when MCC and mixture were processed compared to mannitol. However, the effect of the increase of the SCF by one level on the ribbon RD was more conspicuous in case of MCC and the mixture compared to mannitol. As expected, ribbons that were manufactured setting 1.5 mm GW in most cases showed higher RD compared to ribbons produced by adjusting 3.0 mm GW, except mannitol ribbons when setting 1.5 mm GW and 4 rpm RS. The direct effect of the SCF and the inverse effect of the fraction of MCC were obtained as most significant terms in the model (R^2= 0.964, Q^2= 0.946). The set RS and GW were found to be significant terms; the smaller the GW and the lower the RS were, the denser were the compacted ribbons. The RS was obtained on the one hand as significant main factor, on the other hand two-fold interactions with the GW and the fraction of MCC were determined. The two-fold interactions between the RS and GW and RS and fraction of MCC are introduced in Figure 18. The slight significance of the RS in the model is comprehensible, as MCC shows plastic deformation behaviour, which is described to be time dependent [70, 105]. The effect of the RS on the ribbon RD is propagated in Figure 19.

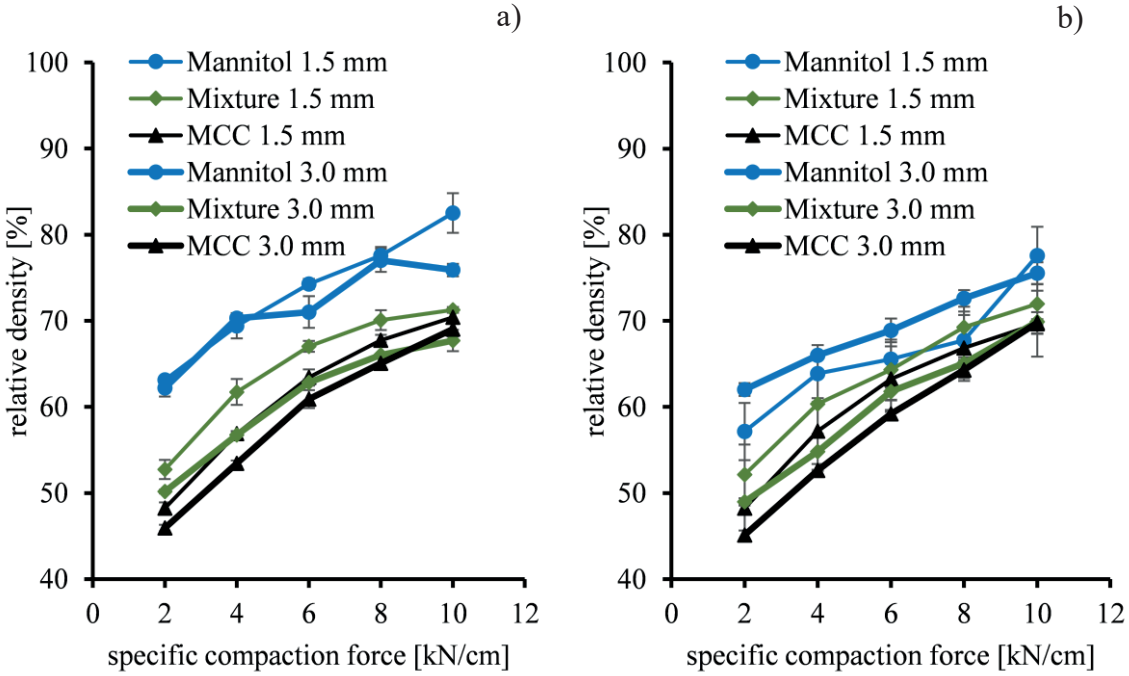

Figure 17 a), b). MCC, mixture and mannitol ribbon RD manufactured by BRC 25 roll compactor using 2 rpm RS(a) and 4 rpm RS (b) (mean±s, at least n=3).

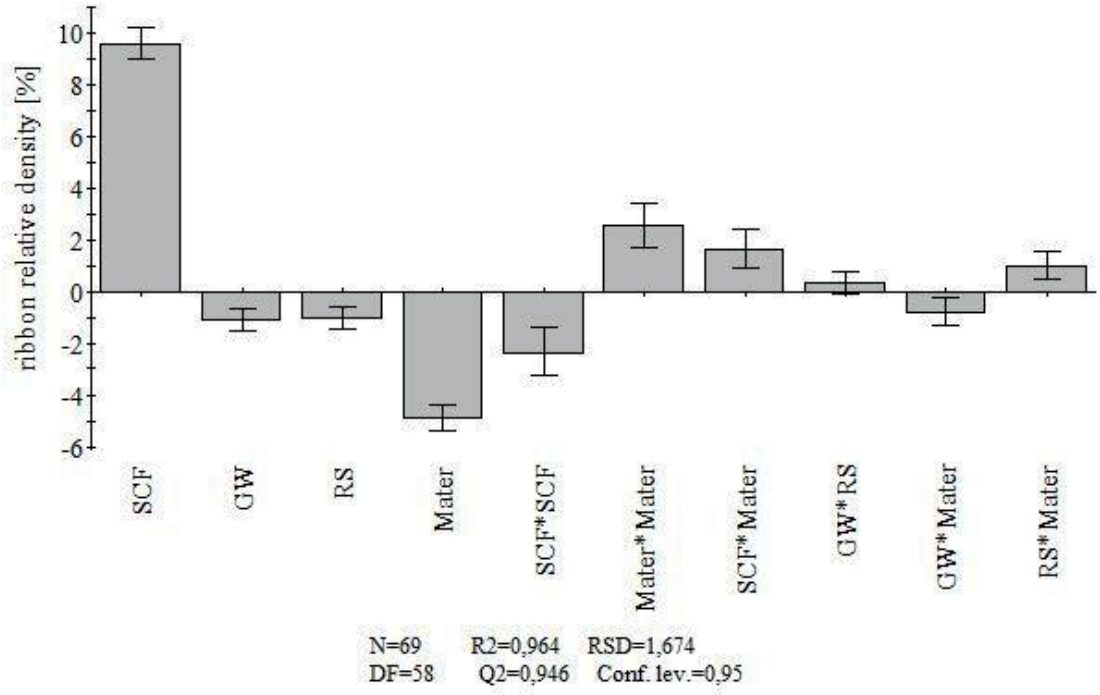

Figure 18. Coefficient plot of the model terms analyzing the ribbon RD obtained by L.B. Bohle BRC 25 roll compactor.

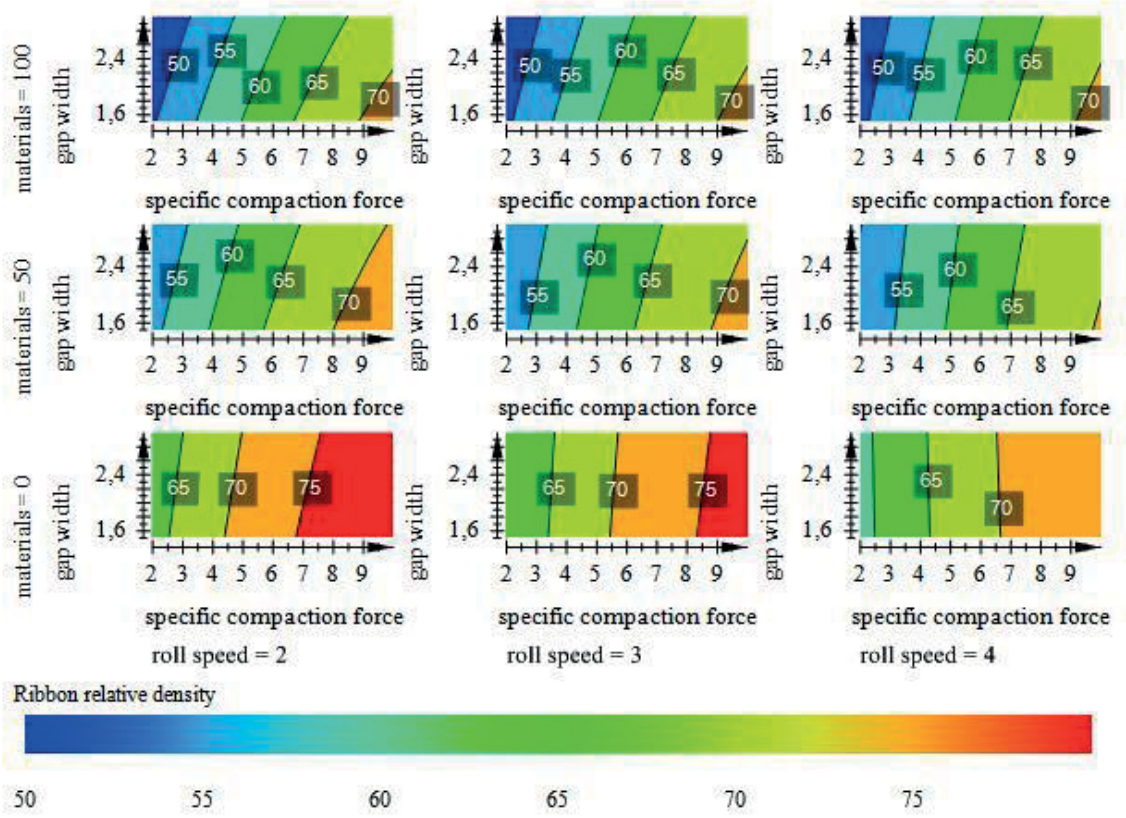

Figure 19. 4 D contour plot of the correlation between ribbon RD, SCF, GW, RS and fraction of MCC using BRC 25 roll compactor.

3.2.2.4 Relative density of ribbons produced by Gerteis Mini-Pactor

Mannitol ribbons were produced to investigate the impact of the process parameters on the ribbon RD. The effect of different sealing systems, RR and SS assembly and the effect of different types of roll surfaces, smooth and knurled rolls, also were examined during the work with this roll compactor. In Figure 20 a), b) and Figure 21 a), b) the RD of mannitol ribbons produced is depicted. The highest RD results were observed, when SS assembly and a pair of smooth rolls were used for roll compaction. In contrast, the lowest ribbon RD were obtained, when smooth rolls and RR were utilized. No clear statement can be made about the effect of the knurled roll surface in correlation with the used sealing system, as setting 4 kN/cm and 10 kN/cm SCF resulted in identical RD values, however obvious interaction between the sealing system and knurled roll surface was not found considering the remaining RD. A good model (R^2= 0.899, Q^2= 0.875) of the examined factors was established, which showed that the SCF and its quadratic effect were found to be the most significant factors followed by the type of sealing system. SS system resulted in higher RD compared to rim-rolls. The results plotted in Figure 20 a), b) and Figure 21 a), b) embrace the influence of the sealing system and the roll surface on the ribbon RD.

The coefficient plot, shown in Figure 22, exhibits the slightly significant effect of the roll surface on the ribbon density. The implementation of a pair of smooth rolls allowed the compaction of denser ribbons compared to a pair of knurled rolls. The effect of the two-fold interaction between the type of sealing system and roll surface shows that a comparable densification of mannitol can be achieved when RR were used with knurled surface as it was observed in case of SS system using smooth rolls. High SCF, the usage of SS assembly and smooth rolls resulted in the densest ribbons. The GW was not found to be a significant parameter, as the sticking of mannitol on the roll surface was discernible during the whole roll compaction process. The adhesion of the material on the roll surface prevented to compact ribbons having thickness equal to the adjusted GW. 2 rpm and 4 rpm RS-s were investigated in the design of experiment (DoE) of the Gerteis Mini-Pactor. Based on the ribbon RD results, the RS was obtained to be an insignificant process parameter, as presented in Figure 22.

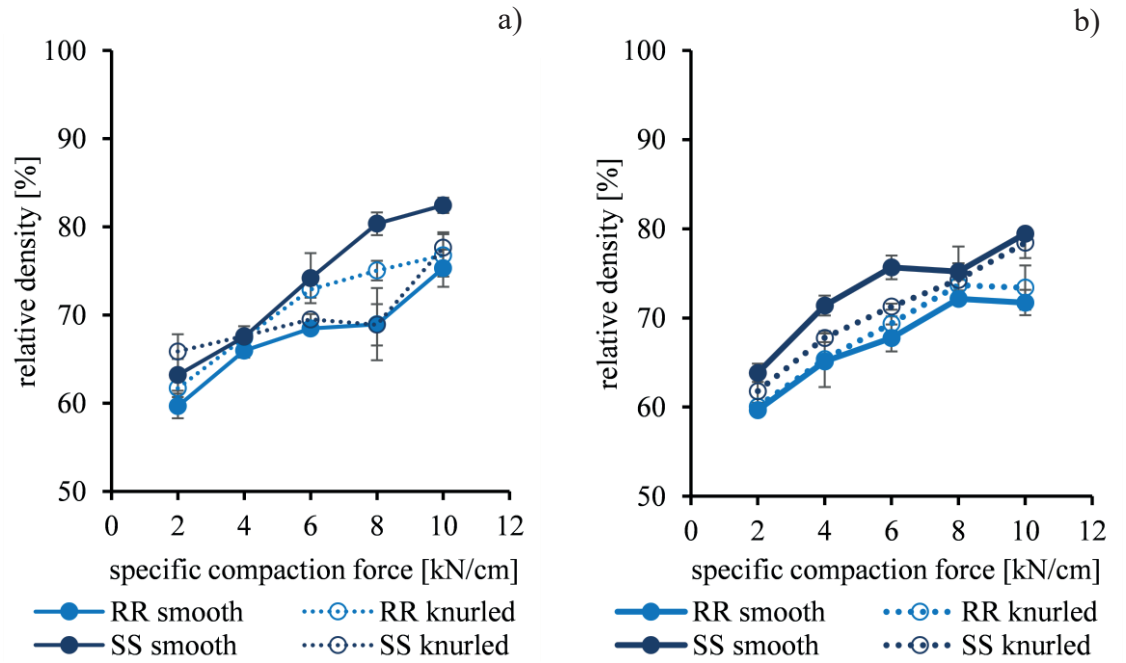

Figure 20. a), b). Correlation between ribbon RS, SCF and roll compaction design setting 1.5 mm GW and 2 rpm RS (a) and setting 3.0 mm GW and 2 rpm RS (b) obtained by Gerteis Mini-Pactor compacting mannitol using smooth and knurled rolls and RR and SS assemblies (mean±s, at least n=3).

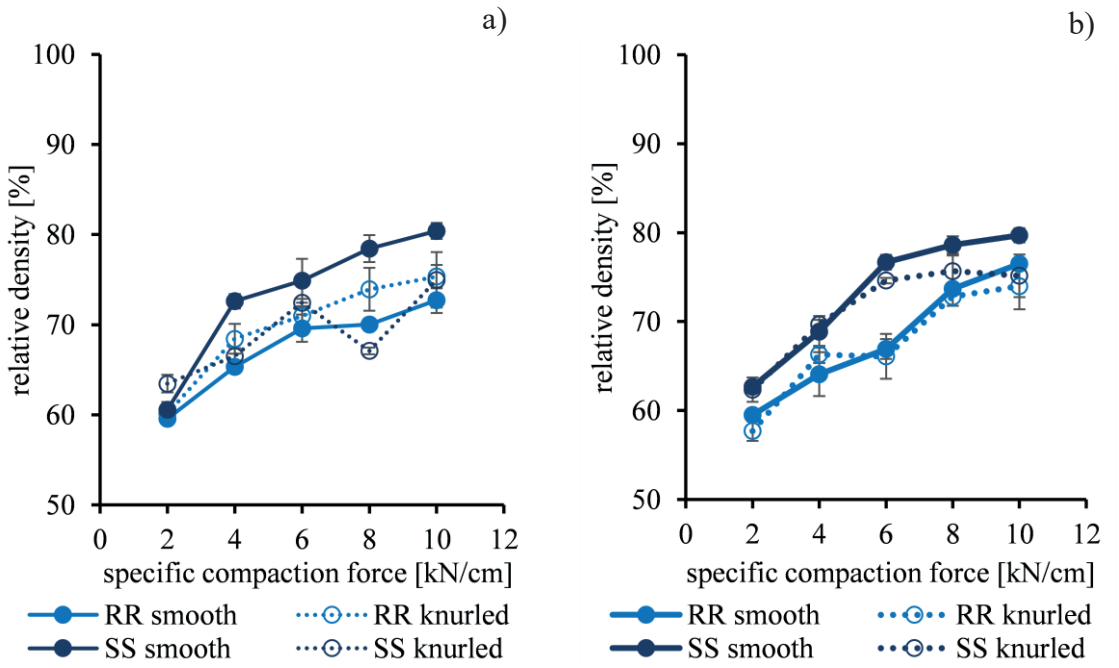

Figure 21. a), b). Correlation between the ribbon RD, SCF and roll compaction design setting 1.5 mm GW and 4 rpm RS (a) and setting 3.0 mm GW and 4 rpm RS (b) obtained by Gerteis Mini-Pactor compacting mannitol using smooth and knurled rolls and RR and SS assemblies (mean±s, at least n=3).

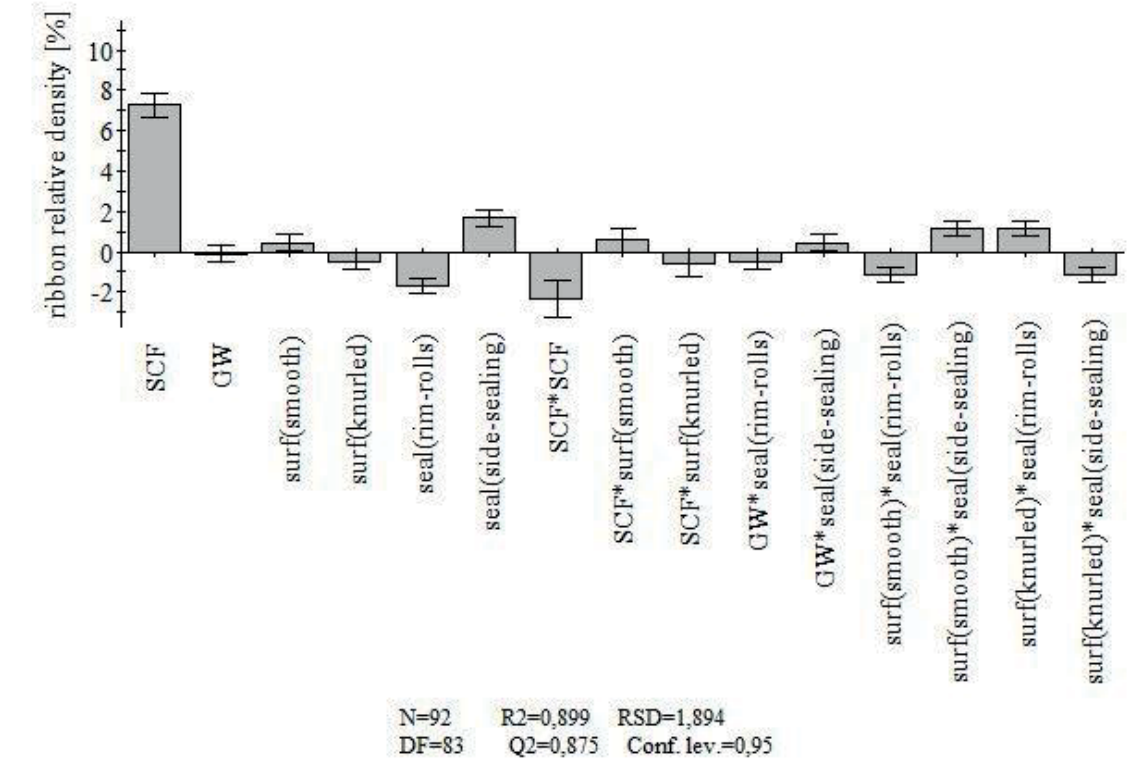

Figure 22. Coefficient plot of the model terms evaluating the ribbon RD obtained by Gerteis Mini-Pactor.

3.2.2.5 Compression behaviour of MCC 101 and mannitol during roll compaction and die compaction

As presented in the previous sections, the mannitol ribbons were always denser than the corresponding MCC ribbons. The observed differences in RD between mannitol and MCC ribbons can be explained by the structure of the raw material and the different deformation behaviour. Heckel analysis revealed yield pressures of 63.7±0.9 MPa for MCC and 135.7 ±0.3 MPa for mannitol, indicating that MCC shows a rather plastic deformation behaviour and mannitol is predominantly brittle. The higher yield pressure of mannitol represents a higher resistance to deformation compared to MCC. This is not in line with the results shown above, where mannitol ribbons were denser for all roll compactors and at all levels.

To explain this fact, the particle morphology has to be taken into account. As is displayed in the scanning electron microscope (SEM) pictures in Figure 23, the mannitol particles were porous spheres, while MCC particles were irregular shaped and more fibrous. It can be assumed that during compaction the spray-dried mannitol particles can easily break even at low pressures. Only after the initial collapse of the sphere the higher resistance to deformation would set in. For MCC however, no sudden collapse at low pressures would be expected.

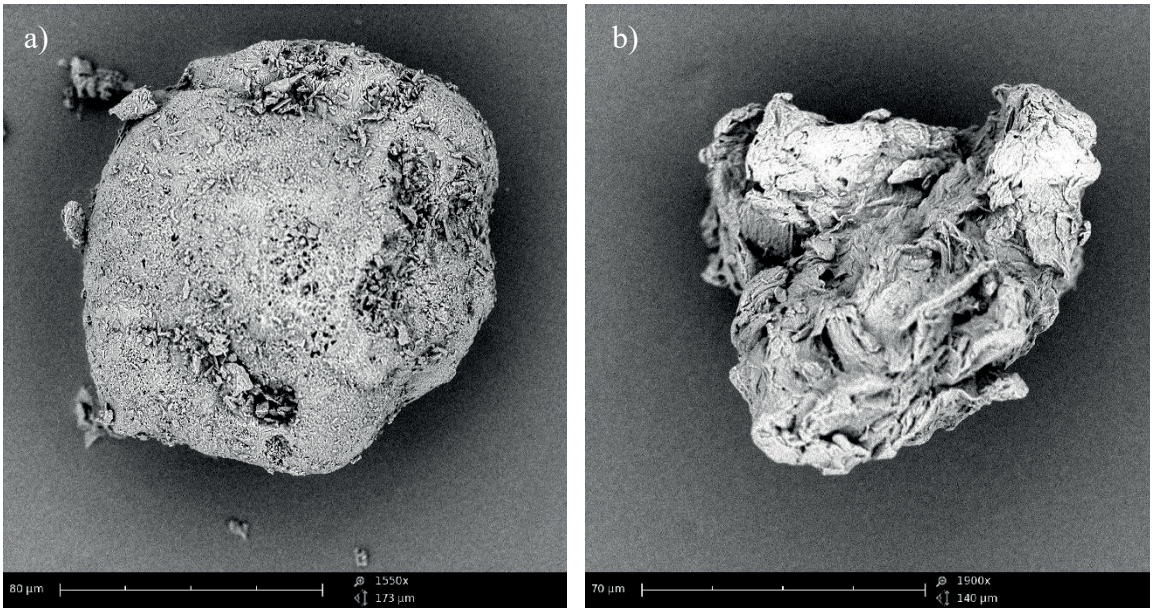

Figure 23. a), b). SEM pictures of a mannitol particle (a) and of a MCC particle (b).

Figure 24 a) shows the in-die determined RD of tablets during compression at the corresponding compression pressure. At very low pressures the RD of mannitol increased

rapidly and showed higher values than MCC, supporting the hypothesis stated above. At higher pressures however, the RD of mannitol increased at a lower rate, so that the profiles cross at about 53 MPa and in the following MCC tablets showed a higher RD. This behavior at higher pressures is still not explanatory for the observations during roll compaction, in which the RD profiles of MCC and mannitol converge at higher forces/pressures, but never cross. A full explanation of this behaviour can be derived from the data shown in Figure 24 b). Here the RD - determined out-of-die - of tablets compressed at 5 different compression pressures is plotted against the maximum pressure during compression. This way the elastic recovery, which takes place between roll compaction and the determination of ribbon density, is also taken into account.

The mannitol tablets showed a higher RD at all levels. The difference is the largest at 50 MPa, at 100 MPa and at 150 MPa the profiles converge without crossing. This behaviour matched the observations during roll compaction and supports the hypothesis that due to the morphology the mannitol particles are compressed to high RD at low pressures, even though the yield pressure is higher than for MCC.

At higher pressure the profiles in Figure 24 b) diverge again, but these high pressures seem not to be realized during roll compaction.

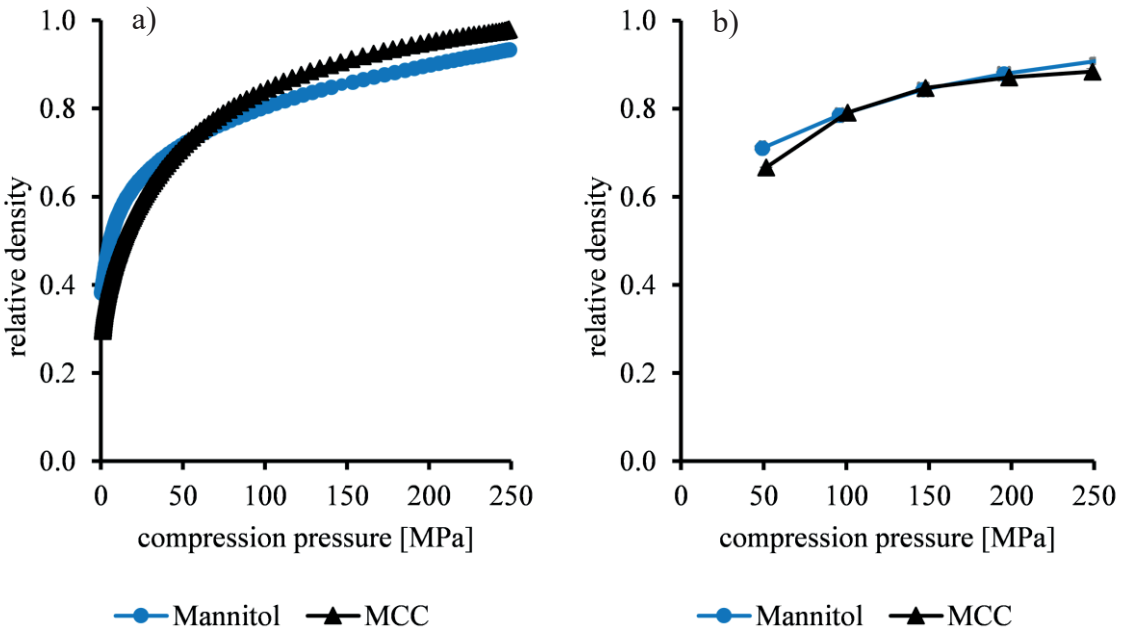

Figure 24. a), b). Deformation of MCC and mannitol (n=10; mean±CI): "in-die" (a) and "out of die" (b) RD of tablets over compression pressure.

3.2.3 Ribbon density characterization by X-ray µCT

3.2.3.1 Relative density characterization using ROTHIST

One of the three cross sections and the corresponding trend of density distribution across the ribbon width are exemplary presented in Figure 25 for ribbons produced by AlexanderWerk BT120 using smooth rolls and in Figure 26 for ribbons manufactured by Mini-Pactor using smooth rolls. The AlexanderWerk ribbons were produced setting 18 bar HP, 2.3 mm GW and 3 rpm RS, while the Mini-Pactor ribbons were manufactured setting 2 kN/cm SCF, 1.5 mm GW and 2 rpm RS. The trend of the ribbon RD across the ribbon width in both aforementioned graphs aligned with the data reported in the literature [33, 34, 52, 106]; the ribbon edges were found to be less dense compared to the middle part of the ribbon. A slightly different trend of RD was observed in case of ribbon 1 in Figure 26 compared to the RD trends of the AlexanderWerk ribbons and Mini-Pactor ribbon 2, as no difference in RD was obtained between the middle part and the edges of the ribbon. The obtained trends of RD were characteristic of the selected position and were not influenced by the applied roll compaction design or parameter setting.

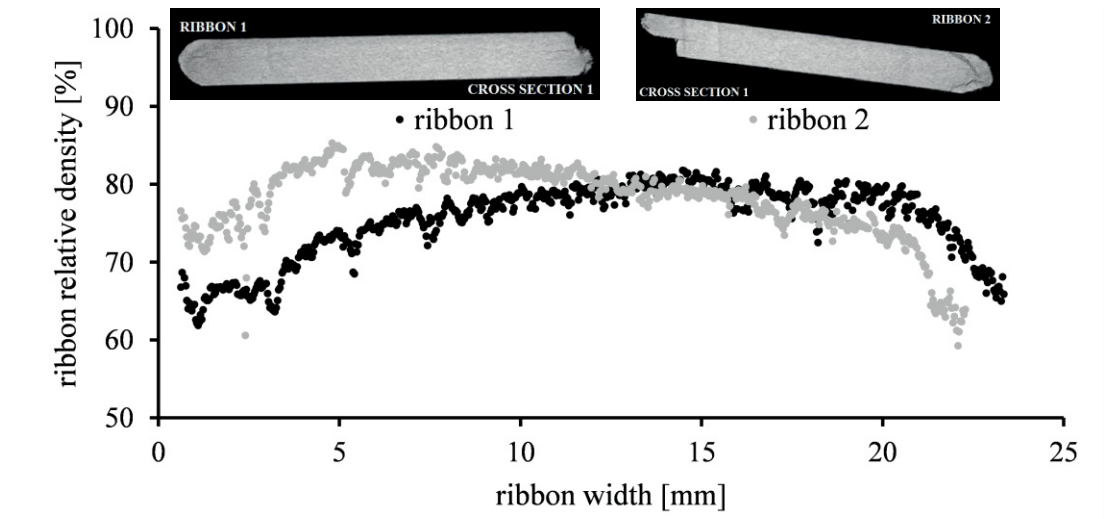

Figure 25. RD evaluated by ROTHIST of two mannitol ribbons produced by AlexanderWerk BT120 setting 18 bar HP, 2.3 mm GW, using smooth rolls and the corresponding cross section images of the ribbons.

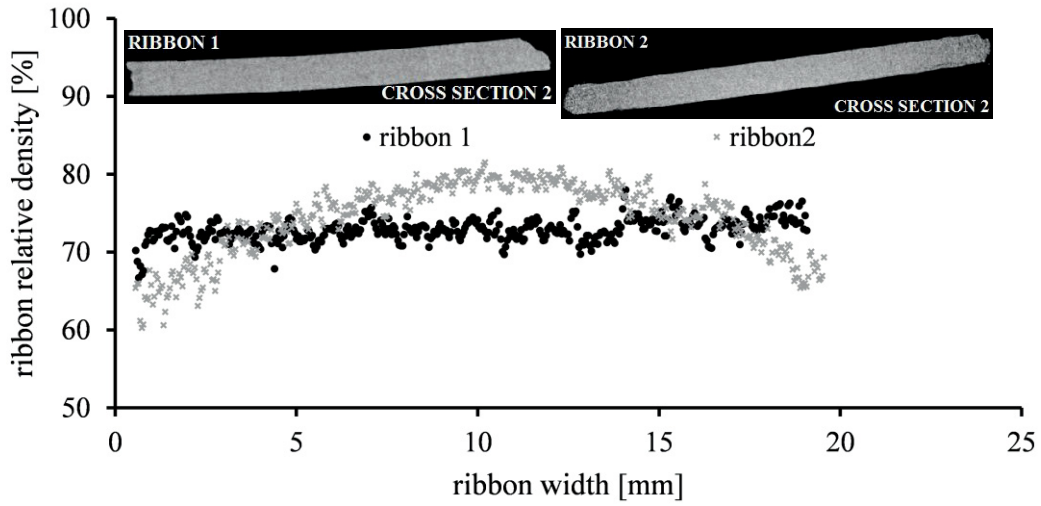

Figure 26. RD evaluated by ROTHIST in two different mannitol ribbons produced by Mini-Pactor setting 2 kN/cm SCF, 1.5 mm GW and 2 rpm RS, using SS system, smooth rolls and the corresponding cross section images of the ribbons.

3.2.3.2 Relative density evaluation using UHIST20 and UHIST50

Investigating the RD by the UHIST20 and UHIST50 evaluation methods, the ribbon RD was calculated from the GVs averaged from the GVs of 20 and 50 layers. This allowed the investigation to calculate the RD across the ribbon width considering the whole ribbon. Thus, the obtained RD values were evaluated depending on their position across the ribbon width. Using this evaluation method, only the Mini-Pactor ribbons were evaluated. Exemplary, the RD values evaluated by UHIST20 are presented in Figure 27 and the RD values obtained by UHIST50 are shown in Figure 28 for the mannitol ribbon 2 from the batch produced by 2 kN/cm SCF, 1.5 mm GW and 2 rpm RS using smooth rolls. The RD trends presented in the aforementioned figures are comparable to each other. It can be also observed that the SD values of RD in the middle of the ribbon are smaller compared to the SD obtained from the edge of the ribbon. Comparable SD values were obtained by evaluating the RD by UHIST20 and UHIST 50, however lower SD was expected in case of the evaluation by UHIST50, as the number of the layers grouped was 2.5 more compared to the evaluation by UHIST20.

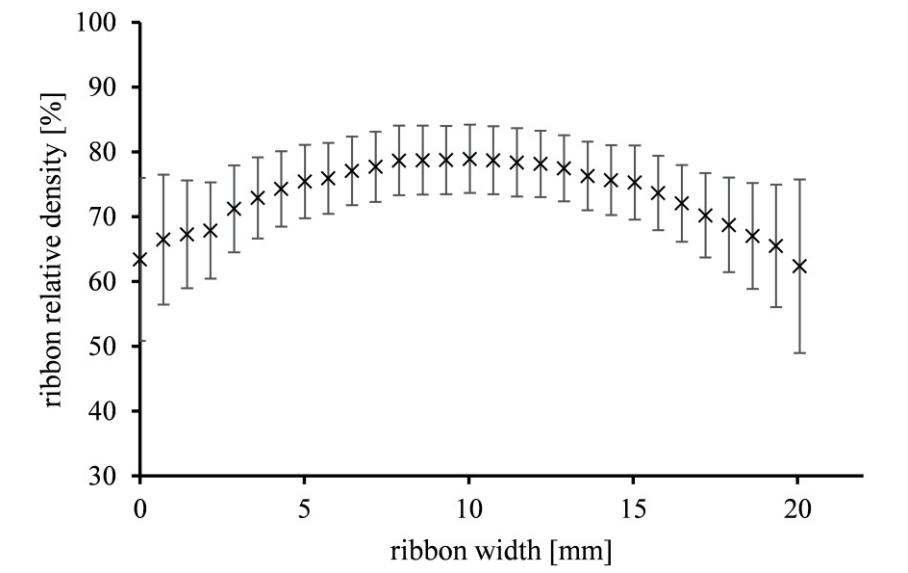

Figure 27. RD evaluated by UHIST20 of Mini-Pactor ribbons produced by 2 kN/cm SCF, 1.5 mm GW and 2 rpm RS using smooth rolls (n=20; mean±s).

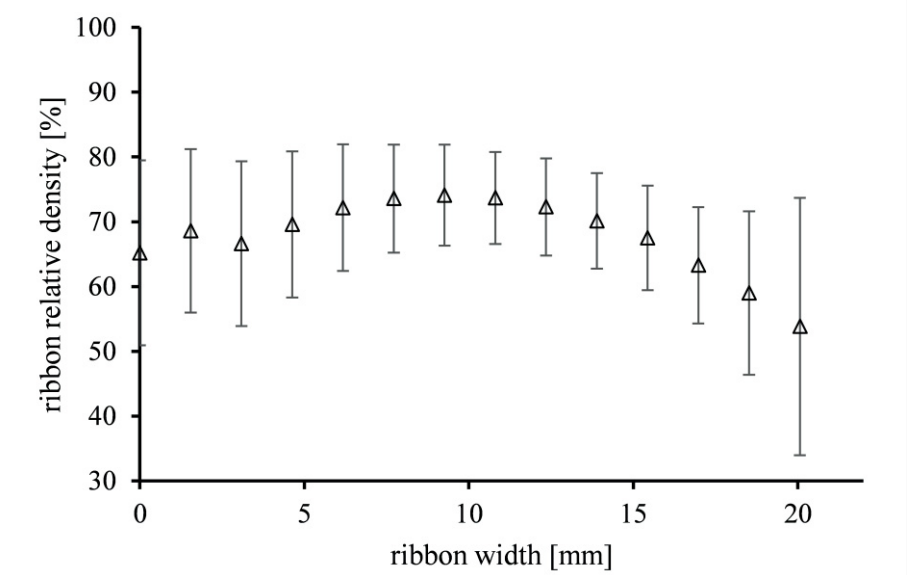

Figure 28. RD evaluated by UHIST50 of Mini-Pactor ribbons produced by 2 kN/cm SCF, 1.5 mm GW and 2 rpm RS using smooth rolls (n=50; mean±s).

3.2.3.3 Relative density results obtained by GeoPyc, ROTHIST, UHIST, UHIST20 and UHIST50

The ribbon pieces being selected for the RD evaluation by X-ray μCT had different length 2.5-4.0 cm. Therefore, the investigation on RD by UHIST examining the whole ribbon sample was based on different amount of data. Using the UHIST software, the average ribbon RD was calculated considering each individual layer in the ribbon. This type of

evaluation was done in case of the mannitol ribbons produced by the AlexanderWerk BT120 roll compactor at 18 bar and 60 bar HP and for the mannitol ribbons produced by the Mini-Pactor at 2 kN/cm and 10 kN/cm SCF and 2 rpm RS. Not only the average RD values were calculated considering the whole ribbon, but also the calibration between GVs and RD of tablets were made considering the whole tablet, which might lead to more accurate determination of density compared to the ROTHIST evaluation, which conducts the calibration between the GVs and the RD of tablets using two cross sections, while for ribbons 3 cross sections were examined as described in 5.4.2.1.

The compared RD data set of the AlexanderWerk BT120 ribbons obtained from the measurements conducted by GeoPyc powder pycnometry and X-ray μCT UHIST are presented in Figure 29 for smooth rolls and in Figure 30 for knurled rolls. The highest RD results were obtained from the evaluation conducted by the X-ray μCT measurements using UHIST software, while the lowest RD values were received by the GeoPyc powder pycnometry, in case of the roll compaction design using smooth rolls. In contrast, the RD values performed by GeoPyc powder pycnometry were found to be the highest, and the lowest RD values were resulted by the X-ray μCT measurements using ROTHIST software. The observation that the RD defined by powder pycnometry is lower, than the RD measured by the X-ray μCT can be explained by the volume determination of ribbons during the measurement using GeoPyc. As explained in Equation 8, the envelope density can be obtained when the weighed mass of ribbon is divided by the obtained volume of ribbon measured by the GeoPyc powder pycnometer. If too large volume is determined by the GeoPyc, the envelope density is obtained to be too low. Finally, this low envelope density is divided by the helium density of the powder, which results in the RD of the ribbon, which is lower than it might be as the ribbon volume was overestimated. The overestimation of the ribbon volume is one of the main disadvantages of the powder pycnometry.

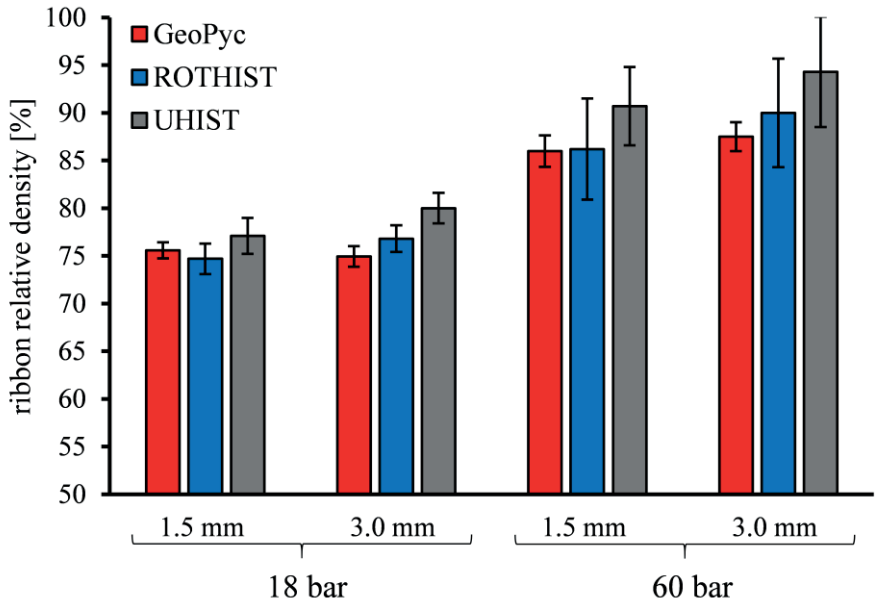

Figure 29. Comparison of RD measured by GeoPyc powder pycnometry and X-ray µCT using ROTHIST and UHIST software of mannitol ribbons produced by AlexanderWerk BT120 roll compactor using smooth rolls (mean±s, n>2).

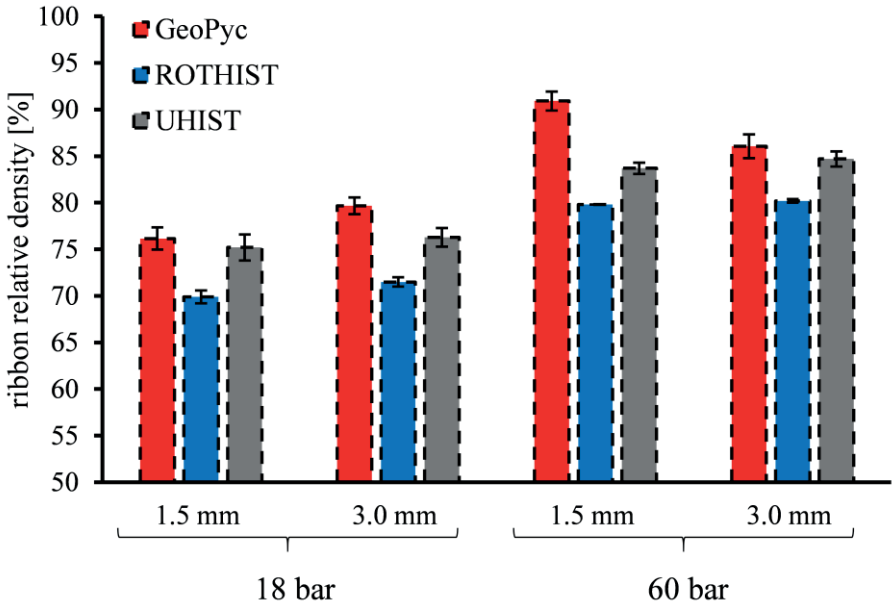

Figure 30. Comparison of RD measured by GeoPyc powder pycnometry and X-ray µCT using ROTHIST and UHIST software of mannitol ribbons produced by AlexanderWerk BT120 roll compactor using knurled rolls (mean±s, n>2).

In case of the Mini-Pactor ribbons, the RD results performed by GeoPyc powder pycnometry, X-ray µCT measurements using the ROTHIST, UHIST, UHIST20 and UHIST50 software were compared for both roll compaction designs; using a pair of

smooth rolls and a pair of knurled rolls. The RD results of ribbons manufactured with smooth rolls are depicted in Figure 31. It can be observed that as in case of the roll compaction design of AlexanderWerk BT120 using smooth rolls, also in case of the Mini-Pactor, the UHIST evaluation method resulted in the highest RD values, and the lowest RD values were obtained by GeoPyc powder pycnometry. This was not observed in case of each investigated batch produced by the Mini-Pactor using knurled rolls. The RD values of the batches manufactured at 10 kN/cm SCF were found to be comparable, when the RD was measured and evaluated by any of the used methods, as presented in Figure 32. The RD of those knurled Mini-Pactor ribbons, which were manufactured at 2 kN/cm SCF, were found to be different depending on the used measurement method as in case of ribbons produced with smooth rolls. All UHIST evaluation methods led to comparable results, however it could be observed that the UHIST evaluation resulted in the highest RD values independently from the set process parameters and applied roll compaction design.

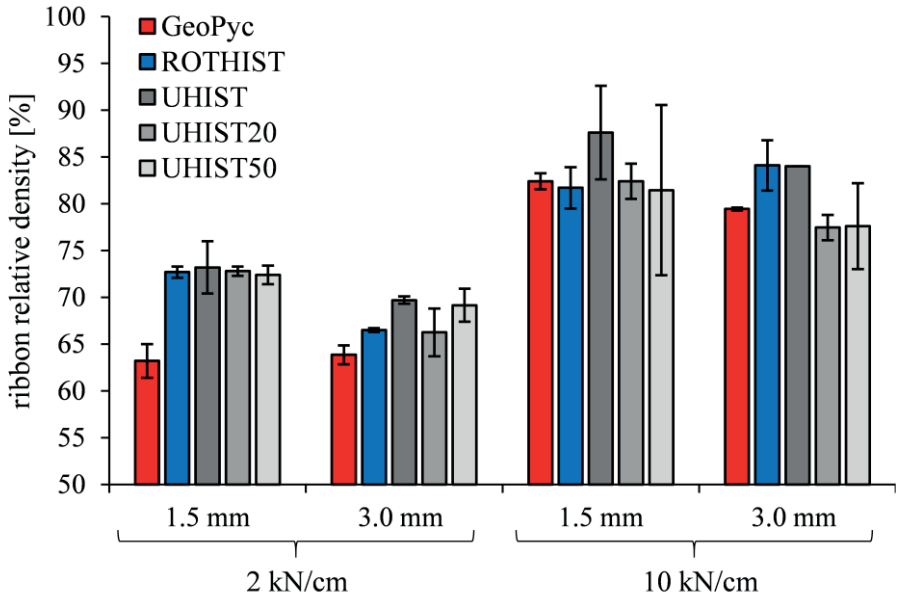

Figure 31. Comparison of RD measured by GeoPyc powder pycnometry and X-ray µCT using ROTHIST, UHIST, UHIST20 and UHIST50 software of mannitol ribbons produced by Mini-Pactor roll compactor using smooth rolls (mean±s, n>2).

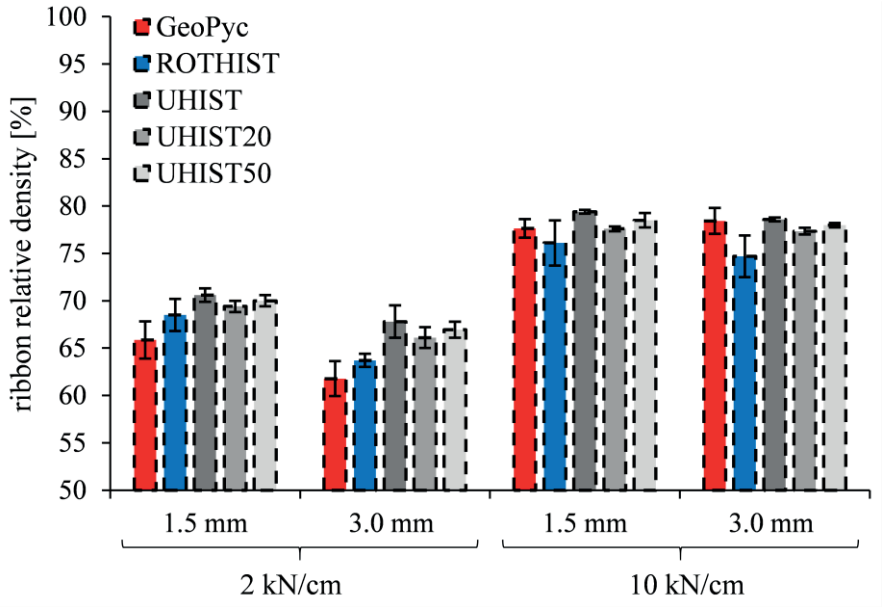

Figure 32. Comparison of RD measured by GeoPyc powder pycnometry and X-ray µCT using ROTHIST, UHIST, UHIST20 and UHIST50 software of mannitol ribbons produced by Mini-Pactor roll compactor using knurled rolls (mean±s, n>2).

In Figure 29 and in Figure 31, high SD of the RD results (4.1-5.8%) obtained by X-ray µCT using ROTHIST and UHIST were observed for ribbons produced at 60 bar HP or at 10 kN/cm SCF. Therefore, the RD values of the investigated samples measured by GeoPyc and X-ray µCT using ROTHIST, UHIST, UHIST20 and UHIST50 software were tabulated in Table 9. The GeoPyc results were comparable to each other, however the RD data showed high variability within the same batch, when it was measured by X-ray µCT. Those RD values can be considered as valid values, which are between 53.9 and 92.9%, as the calibration between the GVs and tablet RD was performed in this range of RD. Therefore, the RD values marked with red in Table 9 are invalid according to the performed calibration (R^2=0.9966). Based on this observation, it can be stated that calibrated range of RD might restrict the application of X-ray µCT, when subjects with high RD are to be measured. Nevertheless, ribbons with RD above 80% are rarely aimed in the pharmaceutical industry, thus this method is suitable for RD measurements, when the RD of subject of interest fits into the calibrated range.

In case of knurled ribbons, presented in Figure 30 and in Figure 32, small SD values of RD (<3.1%) were obtained in case of each evaluation method.

Table 9. Raw data of RD of AlexanderWerk BT120 and Mini-Pactor ribbons produced at 60 bar HP/10 kN/cm SCF and 1.5 mm and 2.3 mm/3.0 mm GW using smooth rolls.

Measurement method and evaluation technique	sample	RD [%] - AlexanderWerk BT120 ribbons		RD [%] – Mini-Pactor ribbons	
		60 bar HP, 1.5 mm GW	batch 60 bar HP, 2.3 mm GW	10 kN/cm SCF, 1.5 mm GW	10 kN/cm SCF, 3.0 mm GW
GeoPyc	1	89.9	85.0	81.4	79.3
	2	90.7	87.3	82.9	79.5
	3	92.3	85.0	82.9	79.6
	4	90.8	87.0		
X-ray µCT - ROTHIST	1	80.9	84.2	83.8	86.9
	2	91.5	95.7	79.5	81.4
X-ray µCT - UHIST	1	87.8	90.2	84.1	84.0
	2	93.5	98.4	91.1	84.0
X-ray µCT –UHIST20	1			80.5	76.1
	2			84.3	78.8
X-ray µCT –UHIST50	1			83.5	75.9
	2			79.4	79.3

The RD determination by X-ray µCT is based on the obtained GV. Thus, it can be concluded that the X-ray µCT might be a more accurate method compared to the GeoPyc powder pycnometry, as it takes into account only the powder particles and so, the included hollows in the ribbons can be excluded from the calculation of the RD. In contrast, the volume determination by powder pycnometry considers the cavities in the ribbons resulting in the overestimation of the ribbon volume and thus, in the underestimation of the ribbon RD.

3.2.4 Discussion and summary

The SCF/HP was found to be the most significant process parameter ($p < 0.001$) in each roll compaction model. This observation aligns with data reported in the literature [9, 53, 73, 84, 105, 107]. For an AlexanderWerk BT120 roll compactor, Khorasani et al. revealed that a higher roll pressure results in denser/less porous MCC 101 ribbons [108]. The

quadratic term of the SCF/HP can be explained by the non-linear increase of the RD, with the linear increase of the SCF/HP.

As it was observed in the current investigation, including an AlexanderWerk BT120 roll compactor, the effect of the GW ($p= 0.033$) was found to be significant only, when smooth rolls were used. For the same roll compactor, the ribbon RD was not affected by the GW when knurled rolls were applied. Different observations can be found in the literature in regard to the influence of GW on the roll compaction process. On the one hand, the significant effect of the GW is described [109], as it was observed in the model ($p< 0.001$) of BRC 25, Pharmapaktor C250 and AlexanderWerk BT120 using smooth rolls in this study. The smaller the GW was set, the denser the ribbons were obtained. It is already published in the literature, that the alteration of the GW has an inverse effect on the RD, independent of the type of processed materials and roll compaction design [68, 72, 110]. Daugherity et al. [31] studied the effect of the serration of the roll surface on the ribbon thickness. It was found, that greater serration results in thicker ribbons compared to roll compaction using identical parameter settings but less serrated rolls. This observation proved indirectly, that the roll surface influences the ribbon quality and the manufacturing capability of the roll compactor. On the other hand, the roll compaction study on the Mini-Pactor and on the AlexanderWerk BT120 using knurled rolls showed contradictive results compared to the previously described ones, as an insignificant effect of GW was obtained. This observation resulted due to the marginal material sticking on the roll surface. The non-significant effect of the GW was also published, when a Hosokawa Bepex Pharmapaktor C250 was investigated [81], however only a narrow range of GW (1-2 mm) was investigated and one knurled and one smooth roll were utilized. The sticking of the compacted material, mainly in case of mannitol, caused difficulties in producing ribbons with similar thickness as the GW was set. The conveyed material was compacted at a smaller gap size than it was set, which led to a higher powder densification. A similar limitation of the roll compaction process was already described earlier [55].

The RS was found to be an insignificant process parameter in the most of the introduced models. One exception was observed, in case of the BRC 25 roll compactor, in which case the effect of RS on the ribbon RD was slightly significant. As it was introduced in the contour plot in Figure 19, the higher the RS, the lower was the density of the ribbons from MCC and mixture. Al-Asady et al. investigated the roll compaction process using an AlexanderWerk WP120 roll compactor. In this study, the GW was kept constant using an

automatic control system by changing the screw speed and hence also the feeding rate of the powder. Higher HP results in more powder consolidation, while lower RS at constant powder feeding rate results in weaker ribbons. The RS had a significant inverse effect on the ribbon density and strength for MCC, as less time was available for the formation of bonding forces between the powder particles [105]. Therefore, it can be concluded, that inverse effect of RS on the ribbon RD is in alignment with the literature for MCC and mixture ribbons. Mannitol particles, as being a brittle material, replies with fragmentation on a certain compaction force, which behaviour was found to be independent from the roll compaction dwell time [111]. Nevertheless, the RS was not included in the model in case of mannitol ribbons produced by the Mini-Pactor, which was also reported in the literature [107].

Beside the SCF and its quadratic term, the fraction of MCC was achieved as a significant factor ($p \leq 0.001$), in case of all roll compactors that processed the different model materials. The higher the fraction of MCC was, the lower the ribbon RD was obtained. The quadratic term of the fraction of MCC was found to be significant in case of AlexanderWerk BT120 using knurled rolls ($p = 0.008$) and for BRC 25 roll compactors ($p < 0.001$) as well. In each investigation, roll compaction of mannitol resulted in the densest ribbons. The difference in the RD between mannitol and MCC ribbons can be explained by the structure of the raw material and through the different deformation behaviour (see section 3.2.2.5).

The investigation of the roll compaction design showed, that both, the type of sealing system and the type of roll surface had a significant effect on the roll compaction process. The impact of the sealing system type was investigated solely in case of Mini-Pactor, as it is the only supplier, which provides both types of sealing assembly. The sealing system was found to be a significant factor ($p < 0.001$) affecting the ribbon RD. SS sealing system resulted in the densest ribbons, when smooth rolls were used. The effect of the roll surface was obtained less significant ($p = 0.022$) compared to the effect of the sealing system. It was also reported, that an irregular roll surface evocate an uneven pressure distribution on the roll surface compared to smooth rolls resulting in a “soft crown area” on the surface of the ribbon [2]. Wiedey et al. reported, that RR sealing assembly results in more homogenous density distribution in ribbons compared to SS [34]. The two-fold interaction of the sealing system and roll surface ($p < 0.001$) described the effect of the roll compaction designs in combination. According to this term, the application of RR using knurled rolls can result in comparable ribbon RD to those ones achieved by manufacturing using SS

smooth rolls. Although, the data set collected shows that the densest ribbons were achieved when SS sealing system was used with smooth roll surface.

Two different measurement techniques for RD determination were compared to each other in order to investigate the advantages of the applied methods. The GeoPyc powder pycnometry is a fast and cost-effective method, which enables to measure the RD of laminated, non-laminated and broken ribbons (e.g. ribbons produced by RR sealing system). Using the X-ray μCT, the RD can be determined in the function of the position in the ribbon considering the individual layers (ROTHIST), grouped layers (UHIST20 and UHIST50) or all the reconstructed layers (UHIST). Thus, not only the local density distribution can be investigated, but also the overall ribbon RD considering the whole volume of ribbon in a higher spatial resolution compared to the data set obtained by powder pycnometry. Since the X-ray μCT is an expensive tool to measure the ribbon RD, the powder pycnometry might be still accurate enough to measure the RD of ribbons, as this parameter is a key quality attribute of roll compaction/dry granulation in order to produce granules or tablets in the required quality. The calibration of the GVs and tablet densities is a demanding task and requires longer preparation time to achieve the reliable calculation of RD from the obtained GVs. In the frame of a development of solid dosage forms, in which ribbons are (one of the) intermediate products, the RD o ribbons might be compared to each other, when the RD values were measured by the same method.

In order to compare the GeoPyc and X-ray μCT ROTHIST, UHIST, UHIST20 and UHIST50 evaluation methods with each other more accurate, the same ribbon piece might be measured first by the X-ray μCT and the obtained data set might be evaluated by the four aforementioned methods. As the X-ray μCT is non-destructive, the same ribbon pieces could be measured by GeoPyc powder pycnometry. This would exclude the variability in RD between the different pieces of ribbons used for the various measurements.

3.3 Establishment of a conversion factor (c_f)

3.3.1 Introduction

A process transfer between roll compactors with different geometries requires the maintenance of the critical quality attributes of ribbons and granules. To accomplish a successful roll compaction process transfer, among others the comparison of the ribbon RD as a critical quality attribute of the roll compaction process is necessary.

Combining the Reynolds approach [53], latent variable models and design of experiment and using experimental data set to establish the OPLS model, Souihi et al. [30] challenged a roll compaction process transfer between a horizontal feeding roll compactor using HP as measure for roll pressure and a vertical feeding roll compactor applying SCF as unit for compaction pressure. The SCF, GW, RS, screw speed, RW, RD and the dimensionless ratios of GW to roll diameter and RS to screw speed were investigated as process variables. Comparable ribbon porosities could be achieved, the measured values were found to be very well estimated by the predicted values, whereas the root mean square error of prediction was 1.0 for comparable batches to the training dataset. However, the established model was appropriate for the used formulation, the model needs to be improved as the root mean square error of prediction increased to 2.7, when the formulation was changed. A further drawback of this method is the need for calibration of the roll pressure of the AlexanderWerk roll compactor, since the extents of both roll compactors are different. The authors applied 0.286 kN/bar calibration coefficient. No explanation was given in the study, how accurate and in which way the establishment of the calibration coefficient was accomplished.

Since the conversion of a certain roll pressure into CF is not given by the roll compactor supplier, the transfer technology may be based on the ribbon RD, since it is easy to measure. To fulfil these requirements, the parameters of the roll compaction process must be adapted. For the most types of roll compactors, the SCF (kN/cm) or CF (kN) is used as a measure to exert a certain CF on the roll surface. The SCF is the CF per 1 cm roll width. Other roll compactors have the attribute to set HP in bar or in MPa. Therefore, a further goal of this part of the thesis is to introduce a theoretical way developing different conversion factors, which enables to convert certain HP/SCF values into new settings in order to obtain ribbons of comparable density. For this purpose, the ribbon RD results

obtained in the experiments using the BRC 25, Mini-Pactor and the AlexanderWerkBT120 roll compactors were used to establish conversion factors.

3.3.2 Conversion factor between the AlexanderWerk BT120 and Mini-Pactor

The ribbon RDs obtained by compacting with the Mini-Pactor were measured to be between 63.2 - 82.4 %. Setting 18 bar, 24 bar, 36 bar, 48 bar and 60 bar HP using the AlexanderWerk BT120 roll compactor resulted in ribbon RD between 76.2 - 90.9 %. These original results are presented with "x" dots in Figure 33, where the c_f is understood as 1 m^2. The trend of the RD values of both roll compactors were similar to each other, however there is a systematic shift in the RD profiles observed. When the set HP values are multiplied by 0.8 m^2 c_f, the trend of the ribbon RDs of both compactors are coinciding, presented in circle shaped dots in Figure 33. The calculated settings of the HP according to Equation 5 are 14.4 bar, 19.2 bar, 28.8 bar, 38.4 bar and 48.0 bar.

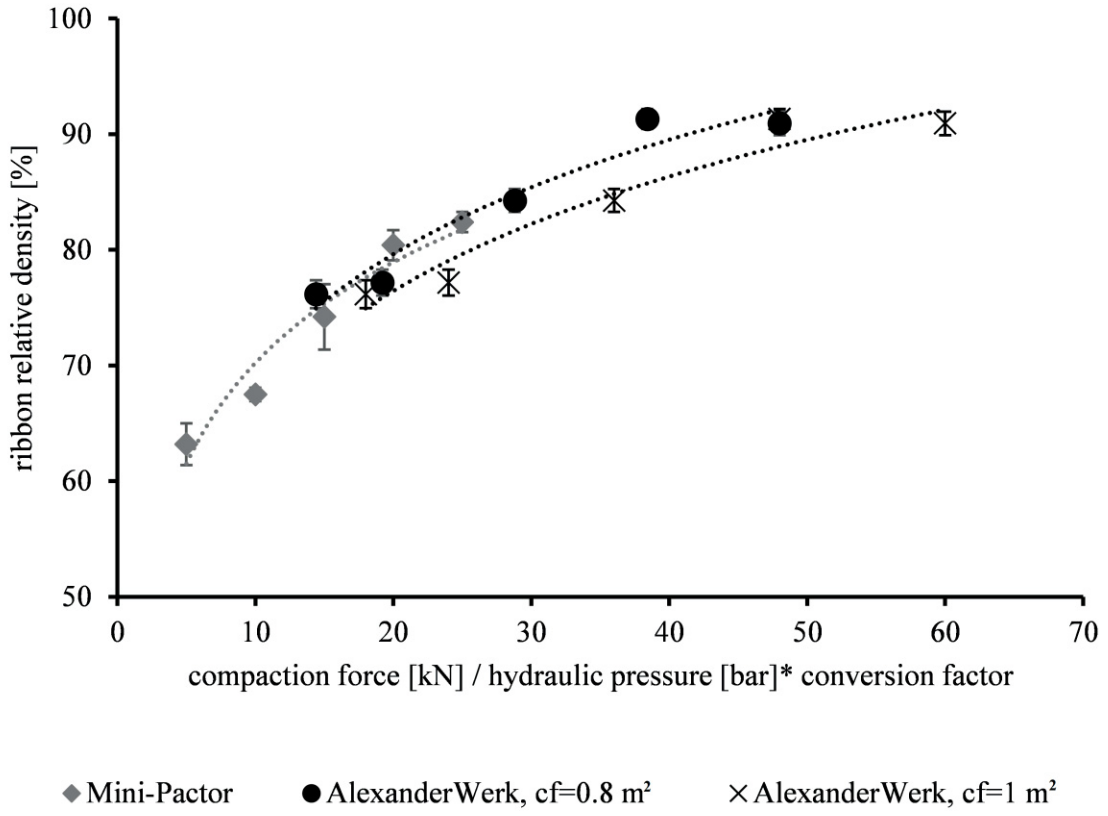

Figure 33. Conversion of the HP into CF using AlexanderWerk BT120 and Mini-Pactor manufacturing with smooth roll surface and SS sealing system setting 1.5 mm GW (mean±s, n=at least 3).

3.3.3 Conversion factor between the Mini-Pactor and BRC 25 roll compactor

Ribbons are produced setting the same SCF, GW and RS compacting with the BRC25 and with the Mini-Pactor roll compactors. The set process parameters are presented in Table 13 and Table 18. The extents of the roll force considering both roll compactors are the same. When those mannitol ribbon RD values are compared that are emanated from the same roll compaction design, smooth roll surface and RR sealing system, a difference between the corresponding relative density values is obtained. Setting the same SCF, GW and RS, the mannitol ribbons produced by the BRC 25 roll compactor are achieved to be denser compared to the mannitol ribbons compacted by Mini-Pactor. The ribbon RD results considering both roll compactors are exhibited in Figure 34 a) and b). As an outcome of the comparison of the mannitol ribbon RD-s obtained by the roll compaction using BRC 25 and Mini-Pactor, the need for the establishment of a c_f is identified, though the adjusted extents, e.g. SCF considering both roll compactors are the same. To set the proper SCF to obtain comparable ribbon RD values, when BRC 25 is used, the originally set SCF values shall be multiplied by 1.6. Plotting the calculated new settings of the SCF, 3.2 kN/cm, 6.4 kN/cm, 9.6 kN/cm, 12.8 kN/cm and 16 kN/cm respectively, the trends of the BRC 25 and Mini-Pactor results show an overlapping above each other, which indicated that sufficient conversion of the SCF setting of the BRC 25 roll compactor is achieved compared to the Mini-Pactor settings. When 4 rpm RS are adjusted using both type of roll compactors, the ribbon RD results are found to be identical, without any conversion of the parameter setting of the BRC 25 roll compactor.

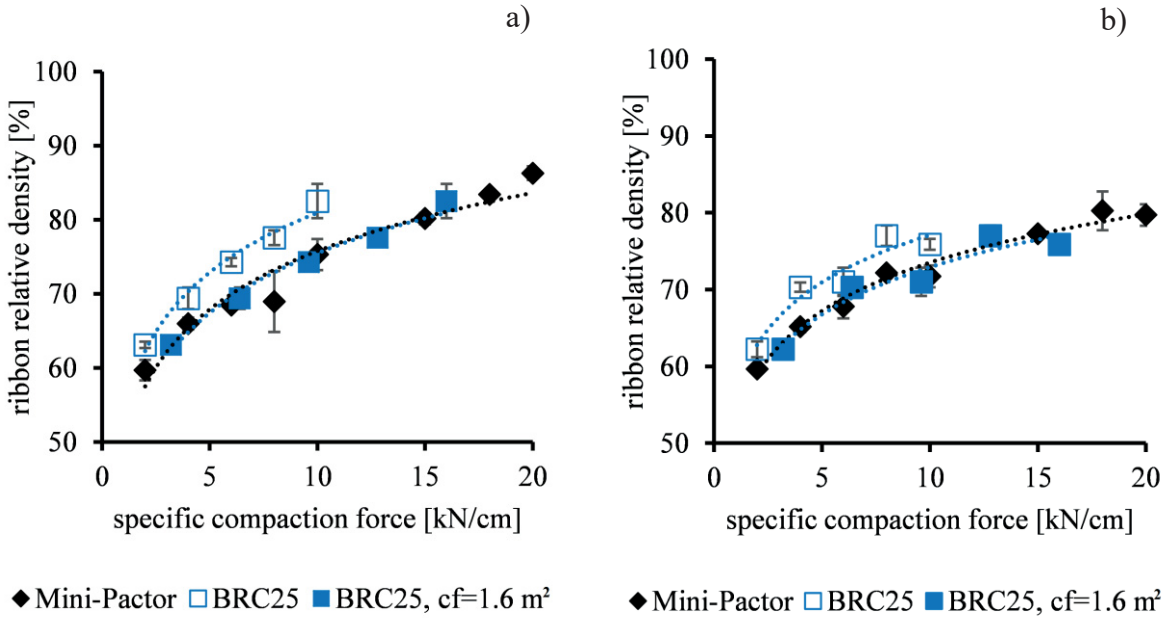

Figure 34. a), b). Conversion of the SCF of the BRC 25 using with the c_f of 1.6 m^2 (mean±s, at least n=3) setting 1.5 mm GW (a) and 3.0 mm GW (b) and 2 rpm RS.

In a recent study [84], contrary results were detected compacting mannitol using both types of roll compactors, although different types of roll compaction designs were used, when ribbons were manufactured using the Mini-Pactor and the BRC 25 roll compactors. The process parameter setting was identical with the one used setting of BRC 25 (RR, smooth rolls), while the roll compaction design of the Mini-Pactor consisted of SS assembly in combination with knurled rolls. As described in section 3.2.2.4, the sealing system and the roll surface affect the ribbon RD. Thus, when the roll compaction process shall be transferred, it is suggested to keep the roll compaction design identical for the establishment of a c_f in order to realize the best performance of the process translation.

3.3.4 Summary

In order to present a principle method, how a roll compaction process can be transferred, when the extents of the roll pressure are different a conversion factor was established between the AlexanderWerk BT120 and Mini-Pactor roll compactors. Multiplying the originally set HP with 0.8 m^2 resulted in the proper settings of the HP to obtain ribbons with comparable RD-s that were achieved by the Mini-Pactor. Furthermore, another example was introduced using the data sets of the Mini-Pactor and BRC 25 roll compactors using smooth RR, as the extents of the CF-s are the same. Using the same

sealing system and setting the same SCF, GW and RS, the ribbons produced by the BRC 25 roll compactor were achieved to be denser compared to the mannitol ribbons compacted by Mini-Pactor. The adapted setting of the SCF regarding the BRC 25 roll compactor was calculated from the original set SCF of the BRC 25 multiplied by 1.6 m^2 c_f.

Since the various roll compactor suppliers do not provide any c_f in order to calculate the CF into roll pressure [39], a principle method was presented, how a roll compaction process can be transferred, when the extents of the roll pressure are different. In order to accomplish a process transfer following the introduced methodology, some limitations need to be considered. The GW, RS, roll compaction design (used sealing system and roll surface), laboratory environment have to be kept identical or at least as similar as possible. In the presented case study, the RS was not kept identical, but this difference was neglected, as the RS does not have a significant effect on the ribbon RD, when brittle material is compacted. The process transfer compacting the plastic material, MCC was not considered so far, as the relative humidity was not kept identical, when the different roll compactors were used. The different relative humidity in the laboratory results in different moisture content of the raw material, which influence the compressibility of MCC. Targeting a certain ribbon RD, the required compaction pressure decreases with increasing moisture content [112]. A c_f was established between the AlexanderWerk BT120 and Mini-Pactor roll compactors. Multiplying the originally set HP with 0.8 m^2 resulted in the proper settings of the HP to obtain ribbons with comparable RDs that were achieved by the Mini-Pactor. Through the presented example, a fast and simple way was introduced to transfer the roll compaction process between different types of roll compactors.

3.4 Characterization of granule size distribution

3.4.1 Introduction

During roll compaction/dry granulation, ribbons possessing certain RD and strength are milled into granules after leaving the compaction zone. The ribbon characteristics are influenced by the process parameters of the feeding and compaction unit, as described in the previous sections. The quality of granules depends on the one hand on the ribbon characteristics, thus indirectly on the set process parameters and used compaction design and on the other hand on the utilized milling method [23]. There are two critical quality attributes of granules, the GSD and the porosity [57]. Due to the nature of roll compaction/dry granulation, no liquid binder is utilized, which is one of the reasons for the high amount fines and hence for the bimodal GSD. Several research studies are published dealing with the different roll compaction/dry granulation process conditions resulting less amount of fines. Herting et al. investigated the roll compaction/dry granulation of MCC-theophylline mixtures having different particle size. It is described that the median granule size was increased with the decrease of the particle size of MCC and theophylline. Further postulation from their study is that granules milled from denser ribbons have higher granule size [75]. In the study of Perez Gago, ribbons compacted from pure materials MCC 101, mannitol and from 6 different mixtures thereof containing 15-85% MCC 101 were milled and the GSD was evaluated [113]. It was shown that the higher the MCC 101 proportion in the mixture, the more amount of fines was produced. The percentiles of the granules were directly influenced by the SCF and its quadratic term, the GW and the type of material. High SCF, low portion of MCC 101 in the mixture and low GW resulted in larger granule size. These results aligned with the results of ribbon RD, since high SCF, high portion of mannitol and low GW led to denser ribbons. The investigation of Mangal et al. [114] focused on the control of GSD by adjusting the impeller speed of the conical rasp sieve, milling ribbons compacted at different SCFs. The results of this study exhibited that increased impeller speed led to higher amount of fines and decreased median particle size, while the increased SCF resulted in robust ribbons and hence in larger granule particles, which aligned with results published in the literature [75]. Furthermore, it was obtained that the RS had a significant effect on the d50 values, when MCC ribbons were milled [114].

Nevertheless, no systematical study has been published in the literature describing the effect of roll compaction design in combination with the process parameters on the GSD. Therefore, in this part of the thesis, it was aimed to investigate the GSD of milled MCC, mixture and mannitol ribbons compacted by the AlexanderWerk BT120, L.B. Bohle BRC25 and the Gerteis Mini-Pactor roll compactors. As the granulation method was kept constant using the oscillating star granulator of the Gerteis Mini-Pactor, the effect of the milling process parameters on the GSD could be excluded. The obtained d50 values, cumulative distribution, density distribution and the amount of fine fraction were evaluated in terms of roll compaction parameters and designs. Fine fraction was defined as particles under 90 µm.

3.4.2 Particle size distribution of the model materials

In order to understand and derive the effect of process parameters and roll compaction designs on the GSD, the particle size properties of the raw materials have been characterized as first. The median particle size of the mannitol, mixture and MCC powders are tabulated in Table 10. The comparison of the cumulative and the monomodal density distribution between mannitol, mixture and MCC powders is depicted in Figure 35 a) and b).

Table 10. Median particle size of mannitol, mixture and MCC powders measured by dynamic image analysis (mean±s, n=3).

Mannitol	Mixture	MCC
164.2±11.9 µm	97.7±12.7 µm	64.8±4.1 µm

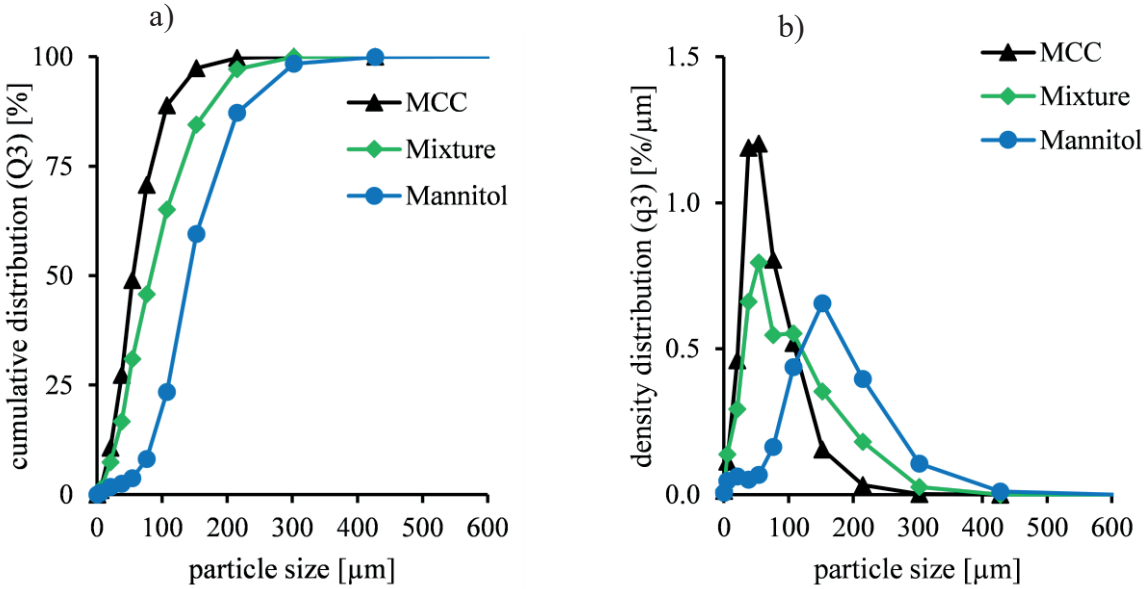

Figure 35. a) and b). Cumulative distribution (a) and density distribution (b) of mannitol, mixture and MCC powders (mean, n=3).

It can be observed that mannitol has a wider particle size distribution compared to MCC, while the trend of the particle size distribution of the mixture particles is between the particle size distribution of MCC and mannitol.

3.4.3 Granule size distribution of granules obtained by AlexanderWerk BT120

3.4.3.1 Mannitol granules

The d50 values of the obtained granules milled from ribbons compacted with smooth and knurled rolls are presented in Figure 36 a) and the corresponding amount of fine fraction is presented in Figure 36 b). An increase in the median particle size of the granules was observed compared to the uncompacted mannitol particles, as expected. The increase of the HP slightly increased the median particle size of granules milled from smooth ribbons. The d50 values of the mannitol granules were found to be between 550 and 700 µm, except two batches of granules. Milling of knurled ribbons compacted with 48 bar and 60 bar HP setting 1.5 mm GW resulted in a decreased d50 value of 360.1 µm and 372.7 µm. Except of these aforementioned batches of granules, granules obtained from knurled ribbons showed higher d50 values compared to granules obtained from the smooth ribbons, although denser ribbons were obtained from the roll compaction design using smooth rolls

than in case of knurled rolls. The highest amount of fines was 7.8% in case of the knurled compaction design setting 48 bar HP and 1.5 mm GW, while compacting with smooth rolls at 48 bar HP and 2.3 mm GW resulted in granules with a maximum fine fraction of 8.9%. These batches with the highest amount of fines had the smallest d50 values. All other granule batches were characterized by a fine fraction ≤ 5.6%.

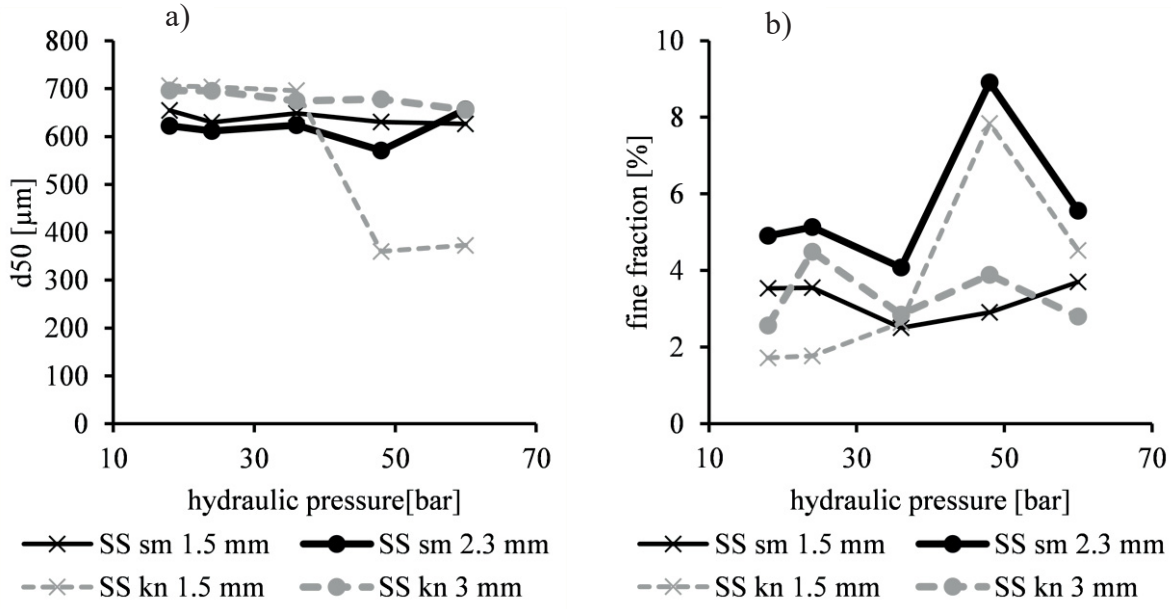

Figure 36. a) and b). Median particle size of mannitol granules (a) and amount of fine fraction (b) obtained milling of ribbons manufactured using smooth and knurled roll surface (mean, at least n=2).

In Figure 37 and Figure 38, the bimodal density distributions of mannitol granules are depicted. The density distribution of the granule batches milled from ribbons compacted with smooth rolls were found to be comparable to each other, as shown in Figure 37. The density distribution of granules milled from knurled rolls and setting 48 and 60 bar HP and 1.5 mm GW, and 18 bar HP and 3.0 mm GW was shifted to the larger granule size, indicating high amount of granules with larger particle size. The maximum values of the density distributions of the aforementioned batches were found to be less than 500 µm.

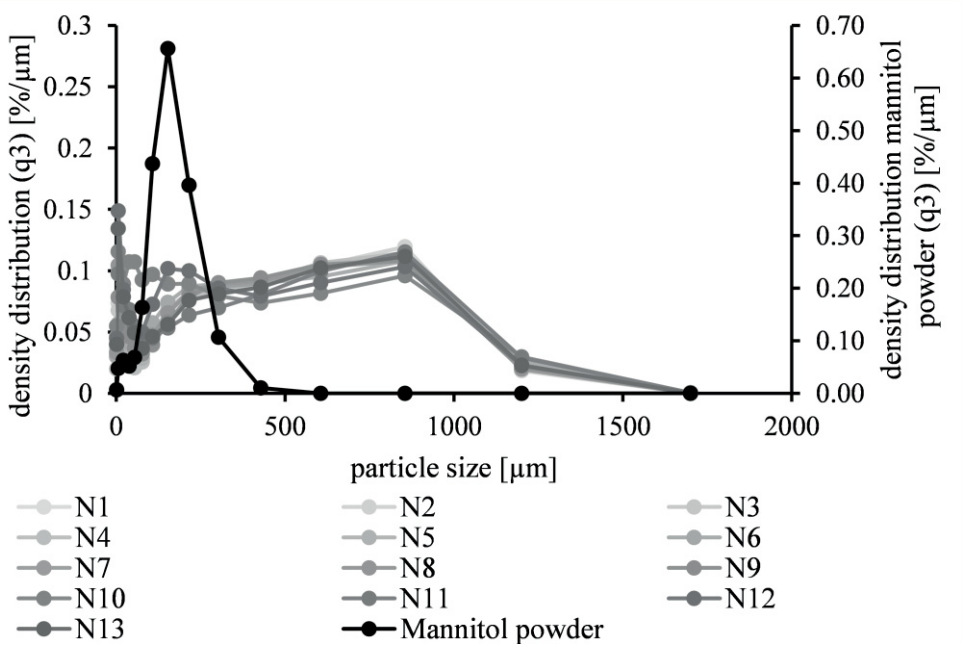

Figure 37. Density distribution of mannitol powder and granules milled from ribbons compacted with smooth rolls and different parameter settings (mean, at least n=2).

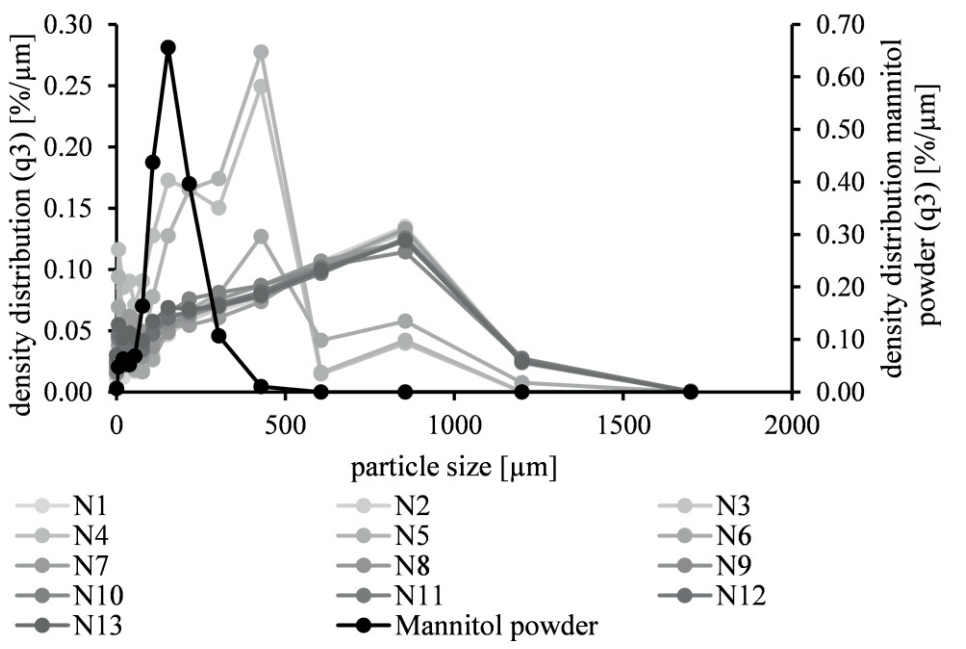

Figure 38. Density distribution of mannitol powder and granules milled from ribbons compacted with knurled rolls and different parameter settings (mean, at least n=2).

3.4.3.2 Mixture granules

The median particle size of the mixture granules are presented in Figure 39 a), which range was found to be between 385.1 and 761.7 µm. Ribbons produced at high HP and low GW resulted in the largest median particle size of the granules for both types of roll surfaces. This observation is alignment with the expectations, as these ribbons showed the highest density. The largest median particle size was generated from knurled ribbons. The amount of fine fraction was found to be between 9.6 and 33.2%, which results are represented in Figure 39 b). The increase of the HP resulted in reduced amount of fines. The usage of smooth rolls led to higher amount of fines compared to the compaction design applying knurled rolls. Comparing the trend of the d50 values with the trend of the amount of fines, it can be concluded that granule batches having larger median particle size include less amount of fines.

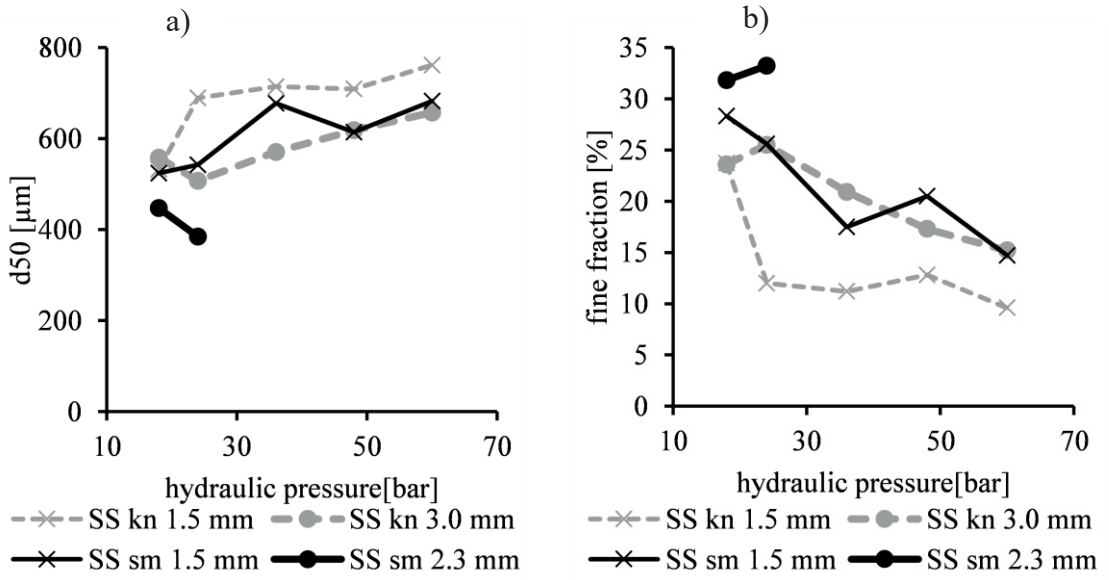

Figure 39. a) and b). Median particle size of mixture granules (a) and amount of fine fraction (b) obtained milling of ribbons manufactured using smooth and knurled roll surface (mean, at least n=2).

The application of different types of roll surfaces led to different density distributions. Application of smooth rolls during roll compaction resulted in higher amount of fines, as depicted in Figure 40 compared to the density distribution of granules derived from the roll compaction using knurled rolls in Figure 41.

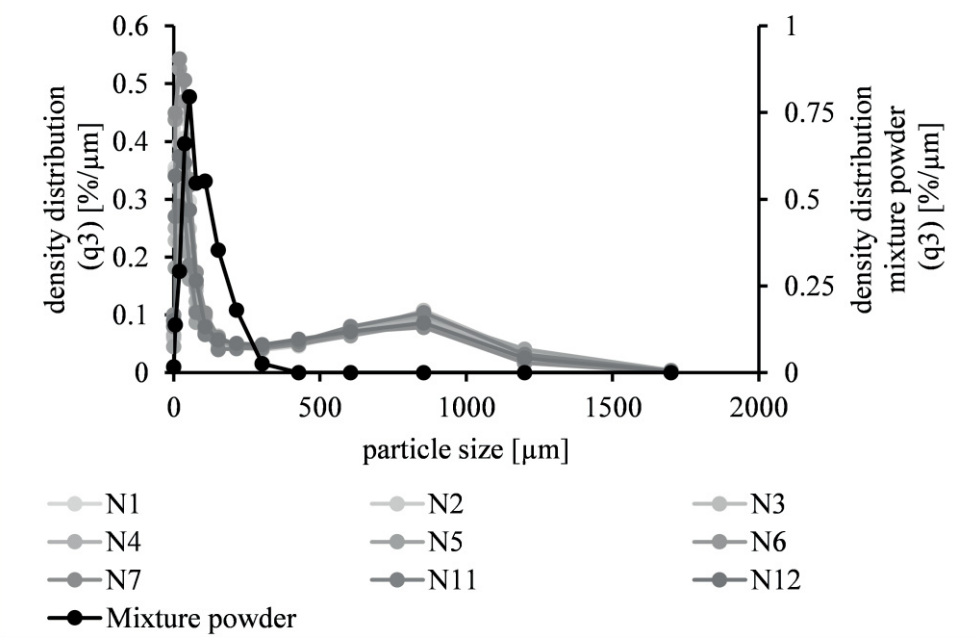

Figure 40. Density distribution of mixture powder and granules milled from ribbons compacted with smooth rolls and different parameter settings (mean, at least n=2).

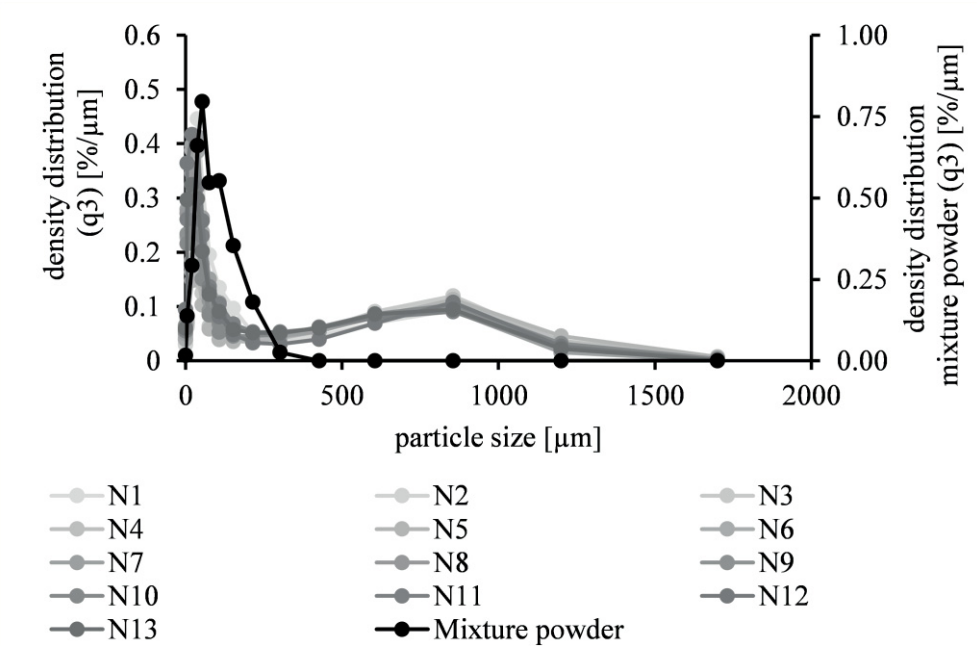

Figure 41. Density distribution of mixture powder and granules milled from ribbons compacted with knurled rolls and different parameter settings (mean, at least n=2).

3.4.3.3 MCC granules

Comparable median particle size of granules were obtained after milling the MCC ribbons, which is exhibited in Figure 42 a). The increase of the HP during roll compaction did not result in larger d50 values of the granules, but a decreasing trend in the amount of fines has been observed, when the HP was increased from 24 bar to 60 bar, as shown in Figure 42 b).

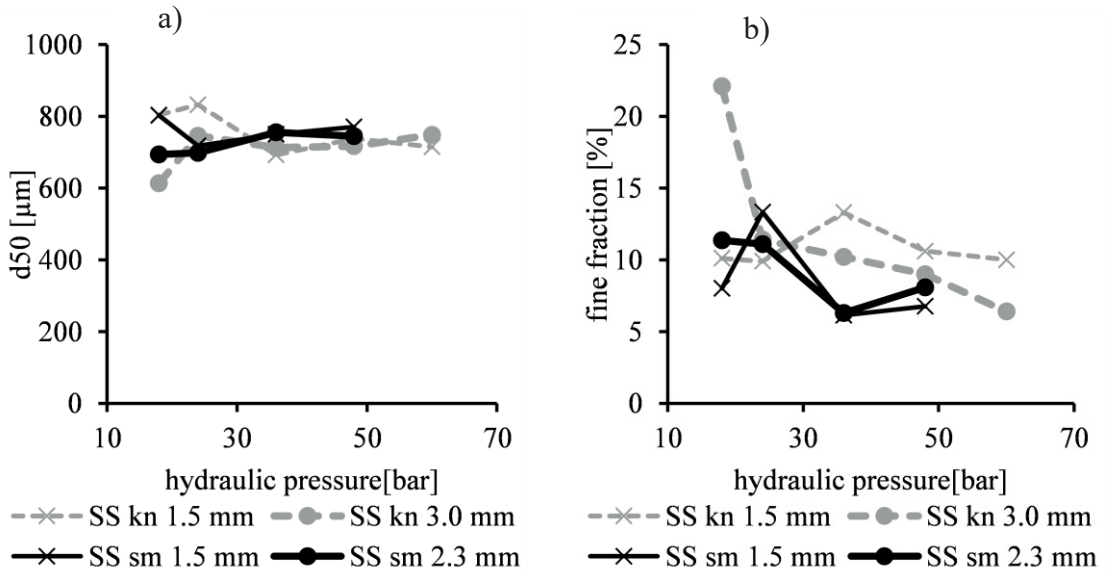

Figure 42. a) and b). Median particle size of MCC granules (a) and amount of fine fraction (b) obtained milling of ribbons manufactured using smooth and knurled roll surface (mean, at least n=2).

The density distribution of the granules milled from ribbons with smooth surface is shown in Figure 43, while the density distribution of granules obtained from ribbons compacted by knurled rolls is depicted in Figure 44. In terms of larger granule sizes, no difference was observed between the aforementioned density distributions, but higher portion of fines was detected, when knurled rolls were used during compaction.

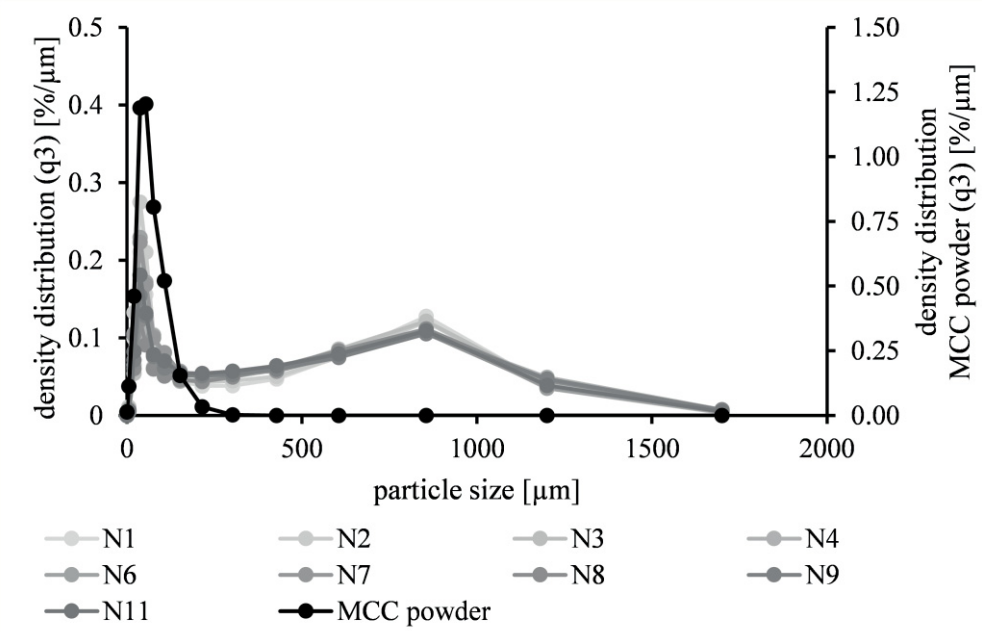

Figure 43. Density distribution of MCC powder and granules milled from ribbons compacted with smooth rolls and different parameter settings (mean, at least n=2).

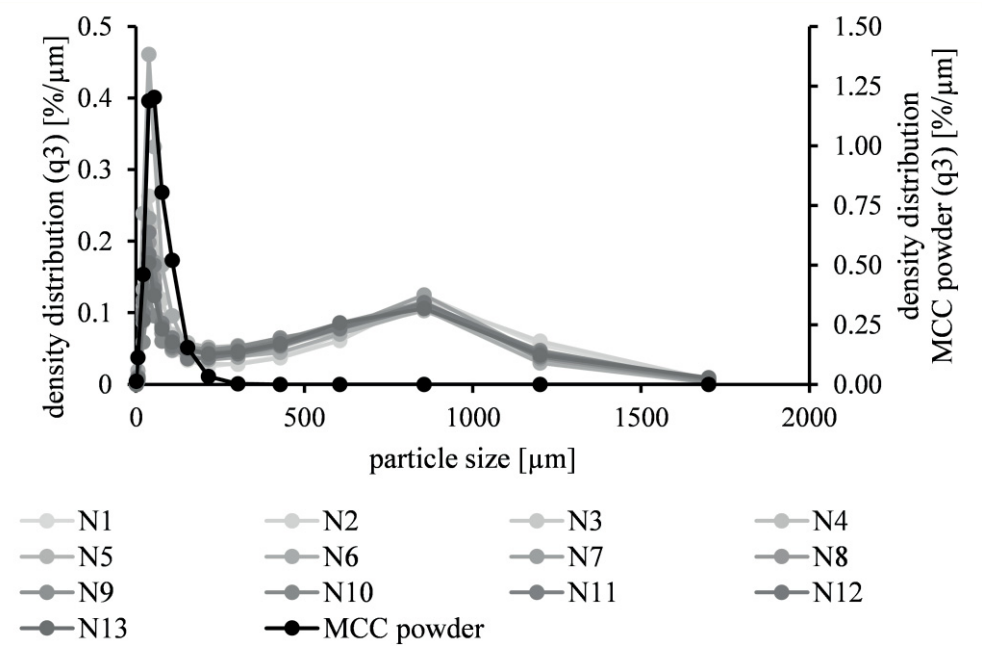

Figure 44. Density distribution of MCC powder and granules milled from ribbons compacted with knurled rolls and different parameter settings (mean, at least n=2).

3.4.3.4 Statistical evaluation of the granule size distribution of mannitol, mixture and MCC

In order to construe the effect of roll compaction process parameters and to understand the influence of the type of material on the median particle size and amount of fines, the results were evaluated using multiple linear regression. Figure 45 a) and b) represent the coefficient plot of those factors, that were found to be significant in terms of the median particle size and fine fraction of granules milled from ribbons compacted with smooth rolls. The coefficient plots of the obtained model for the median particle size and fine fraction of granules resulted from roll compaction applying knurled rolls is shown in Figure 46 a) and b). The R^2=0.735 and the Q^2=0.613 indicates a good model for the d50 values, while the model of the amount of fine fraction was found to be excellent with R^2=0.910 and the Q^2=0.857. In case of each model, the quadratic term of the type of material was obtained to be the most significant factor (p-value<0.001). The largest granules were obtained, when MCC ribbons were milled, followed by the mixture granules. The HP (p-value=0.036) and GW (p-value=0.008) showed a significant influence on the median particle size, when smooth rolls were used during compaction. In Figure 45 b) the significant effect of the quadratic term of the material type (p-value<0.001) is presented, indicating low amount of fine fraction obtained for the mannitol granules. The HP was obtained to be a significant model term (p-value=0.002), while the interaction between the HP and GW was slightly significant (p-value= 0.041).

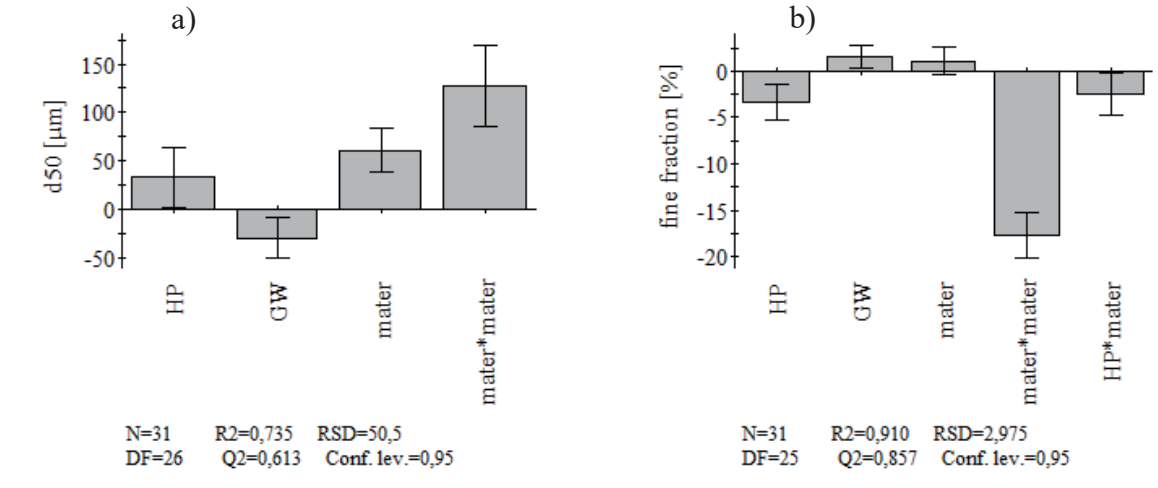

Figure 45. a) and b). Coefficient plots of d50 value (a) and amount of fines (b) obtained from the mannitol, mixture and MCC granules milled from smooth ribbons.

The coefficient plot of median particle size and fine fraction of granules milled from ribbons compacted with knurled rolls are exhibited in Figure 46 a) and b). The R^2=0.503

and the Q^2=0.152 values of the model of the median particle size indicates a poor model, whereas good model was obtained for the amount of fine fraction (R^2=0.813, Q^2=0.716). In contrast to the observations when smooth rolls were used for compaction, the roll compaction design applying knurled rolls was not characterized by the significant effect of the HP and the GW in case of the d50 values. In contrast, similarly as in case of the model with smooth rolls, the type of material (p-value=0.002) and its quadratic term (p-value=0.019) were significant model terms. In addition, the two-fold interaction between the HP and GW (p-value=0.039) and between the HP and type of material (p-value=0.036) were found to be significant factors. The generation of fines was observed to be influenced the most by the type of material (p-value<0.001) and its quadratic term (p-value<0.001) and by the set HP (p-value=0.011). Mannitol granules milled from the densest ribbons showed the lowest fine fraction compared to the mixture and MCC granules.

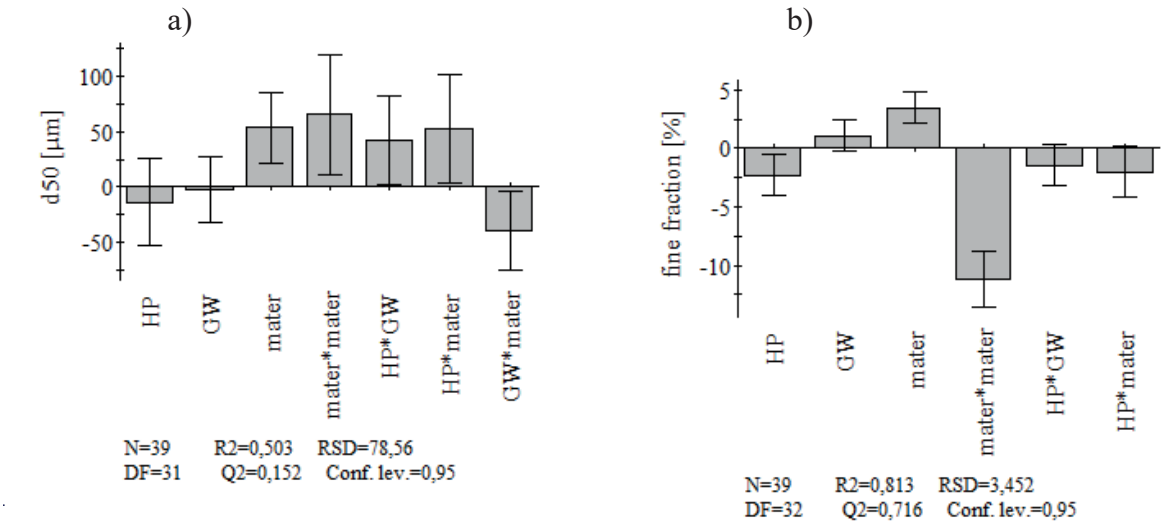

Figure 46. a), b). Coefficient plots of fine fraction of granules obtained from ribbons produced with smooth (a) and knurled (b) rolls.

3.4.4 Granule size distribution of granules obtained by BRC 25

The median particle size of the MCC, mixture and mannitol granules is presented in Figure 47 a), b), c) and d). In case of the most granule batches, the median particle size increased, when high SCF was set. 2 rpm RS resulted into granules having the d50 value between 400-800 µm except the mixture granules produced by setting 2 kN/cm and 4 kN/cm SCF

and 3.0 GW. Setting 4 rpm RS, a wider range of d50 values was obtained between 200 and 800 µm compared to the aforementioned range of particle size. The largest median particle size was obtained in case of the MCC and mannitol granules. Considering the RD values of the corresponding ribbons, the lowest d50 value was expected to be obtained from the MCC and mixture ribbons with lower RD. This expectation was proved in case of the mixture granules at each experimental setting of compaction, but not for MCC. Setting 3 mm GW and the RS at 4 rpm, the median particle size of MCC granules were the largest at each adjusted SCF. In contrast, decreasing the GW from 3.0 mm to 1.5 mm, the largest granule sizes for d50 were obtained in case of mannitol. The densest mannitol ribbons led to the highest median particle size of granules only, if the GW was set at 1.5 mm and the SCF was adjusted to 6 kN/cm or below.

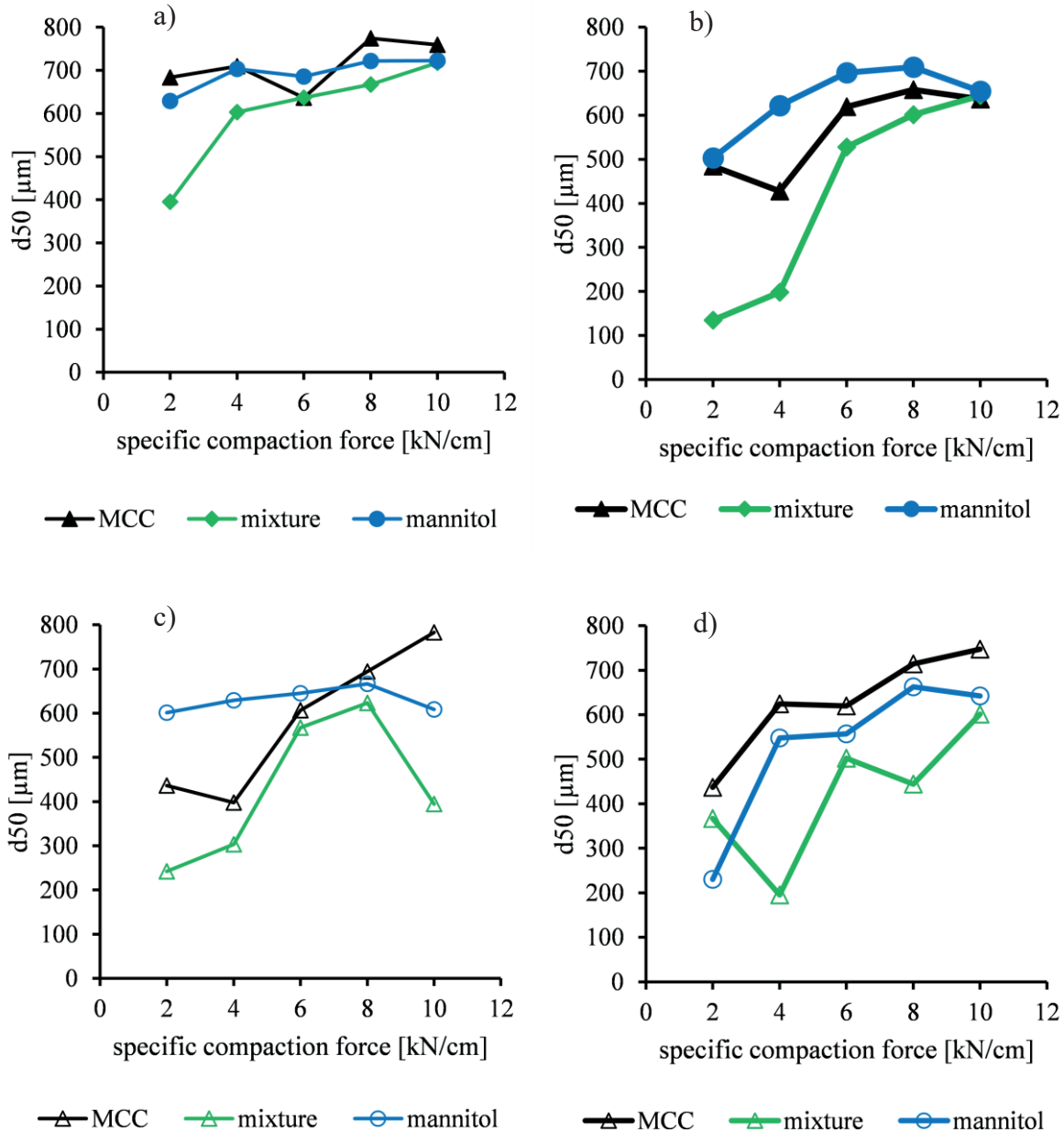

Figure 47. a), b), c) and d). Median particle size of MCC, mixture and mannitol granules obtained after milling of ribbons compacted by the BRC 25 roll compactor setting 1.5 mm GW and 2 rpm RS (a), 3.0 mm GW and 2 rpm RS (b), 1.5 mm GW and 4 rpm RS (c) and 3.0 mm GW and 4 rom RS (d) (mean, at least n=2).

The fine fraction results of the MCC, mixture and mannitol granules are presented in Figure 48 a), b), c) and d). The less amount of fines were observed for the parameter settings of 1.5 mm GW and 2 rpm RS for each type of material, while the highest fine fraction of granules was resulted, when 3.0 mm GW and 2 rpm and 4 rpm RS were adjusted during roll compaction. The highest fine fractions were obtained from the mixture

and MCC granules setting 2 rpm and 4 rpm RS and 3 mm GW and setting 1.5 mm GW and 4 rpm RS. It was also to be expected that the amount of fines decreases with increasing SCF, as more dense ribbons tend to go through abrasion less after breaking into pieces during milling [37]. This decreasing trend of the fine fraction at each parameter setting combination was observed only in case of mannitol granules. In contrast, higher fine fractions were obtained although the SCF was increased for some granule batches of MCC and mixture.

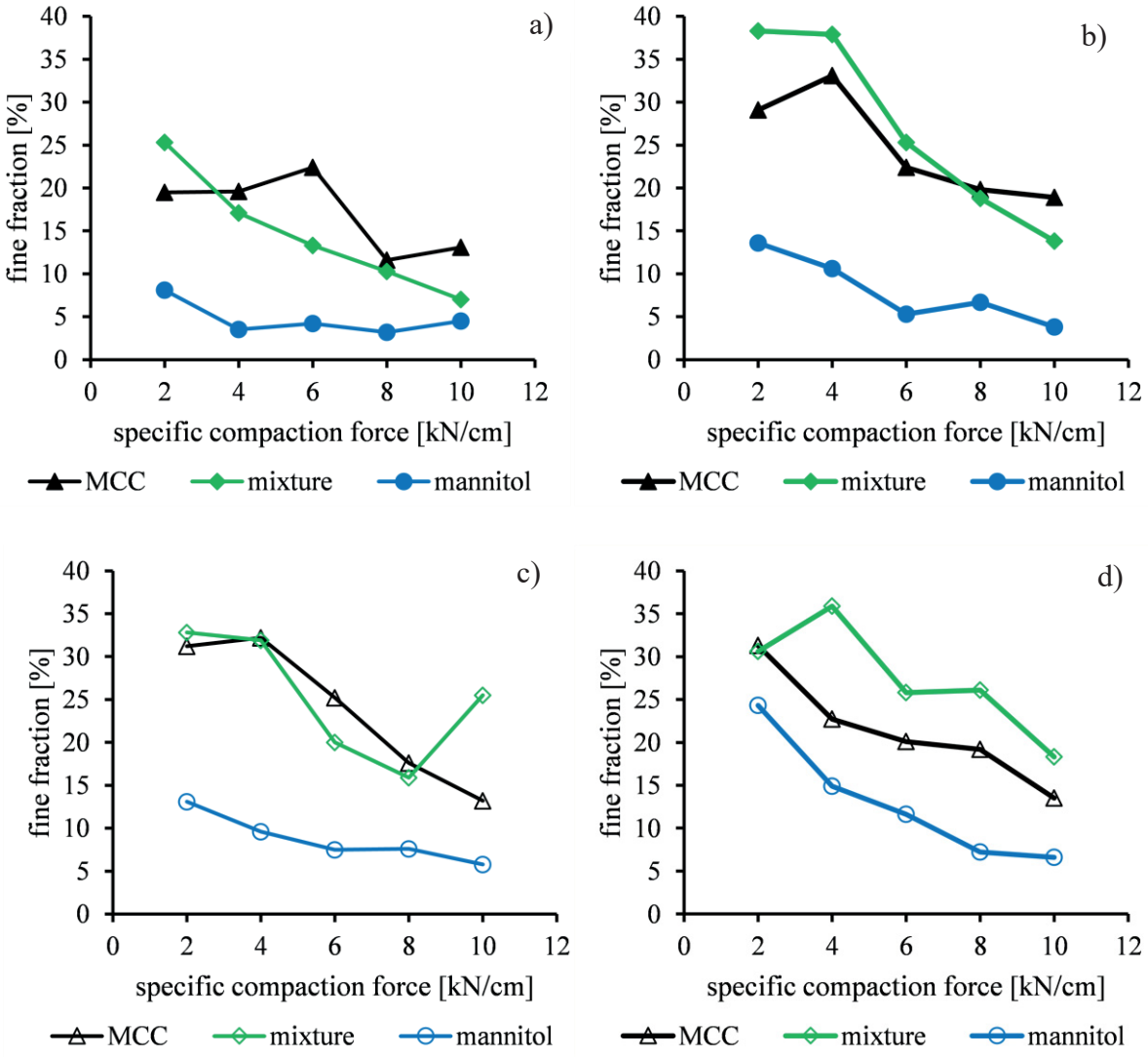

Figure 48. a), b), c) and d). Fine fraction of MCC, mixture and mannitol granules obtained after milling of ribbons compacted by the BRC 25 roll compactor setting 1.5 mm GW and 2 rpm RS (a), 3.0 mm GW and 2 rpm RS (b), 1.5 mm GW and 4 rpm RS (c), 3.0 mm GW and 4 rpm RS (d) (mean, at least n=2).

In Figure 49 a) and b) the coefficient plots of model terms for median particle size and amount of fine fraction are presented. For both responses, good models were established with an R^2=0.715 and Q^2=0.615 for the d50 value and R^2=0.845 and Q^2=0.795 for the

amount of fine fraction. The most significant factor was found to be the quadratic term of type of materials, which means that larger median particle size and lower amount of fines are to be expected when MCC and mannitol ribbons are milled compared to the mixture ribbons using the same milling parameters. The second most significant factor was the SCF in both models. The higher the SCF was set, the larger granules were obtained, while the fine fraction was reduced. The GW and RS also were found to be significant terms in both models. The lower gap and RS were adjusted during roll compaction, the larger median particle size of granules was obtained. Using larger GW and faster RS led to higher amount of fines.

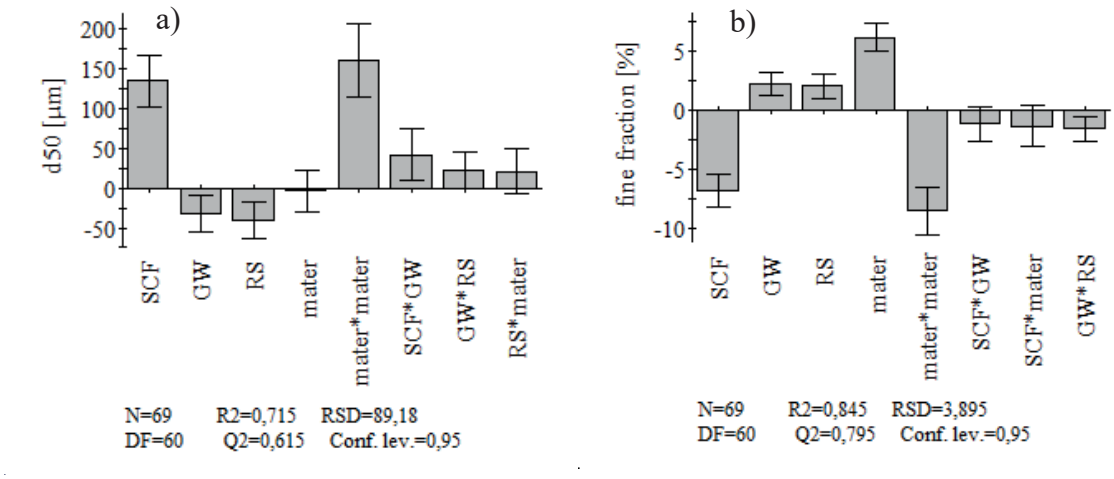

Figure 49. a), b). Coefficient plots of model terms for median particle size (a) and amount of fines (b) of granules obtained from milling ribbons compacted by BRC 25.

The interaction between the SCF and GW was obtained to be significant only for the d50 values. At low SCF, the increase of GW led to larger median particle size, while no particle size enlargement could be observed at higher SCF, when the GW was increased. The aforementioned interaction between the SCF and GW is exhibited in Figure 50.

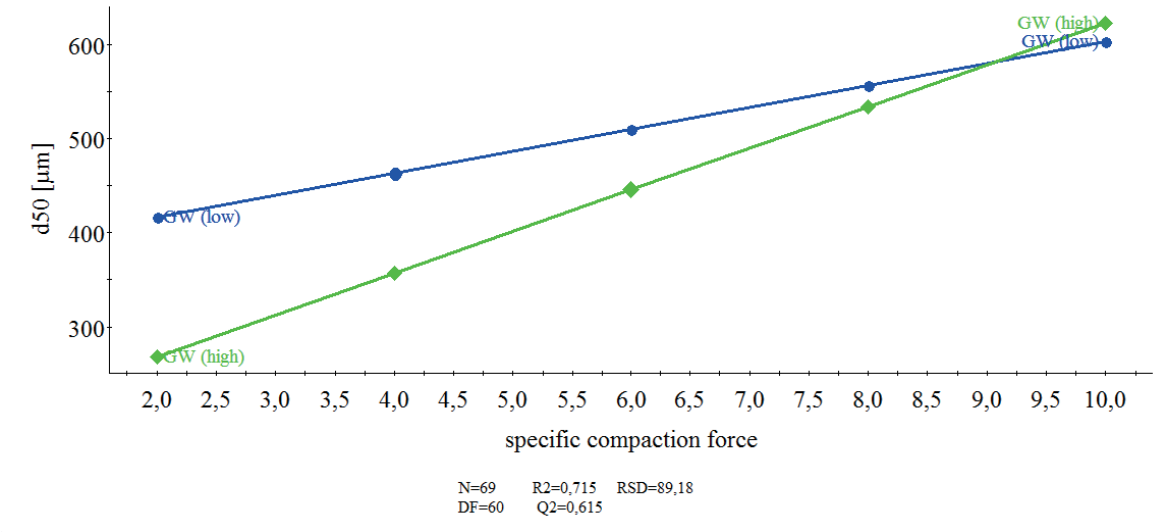

Figure 50. Interaction plot presenting the influence of the set GW depending on the adjusted SCF.

The interaction term of RS and GW had a slightly significant effect on the amount of fines, which is explained in detail by the 4D contour plot in Figure 51.

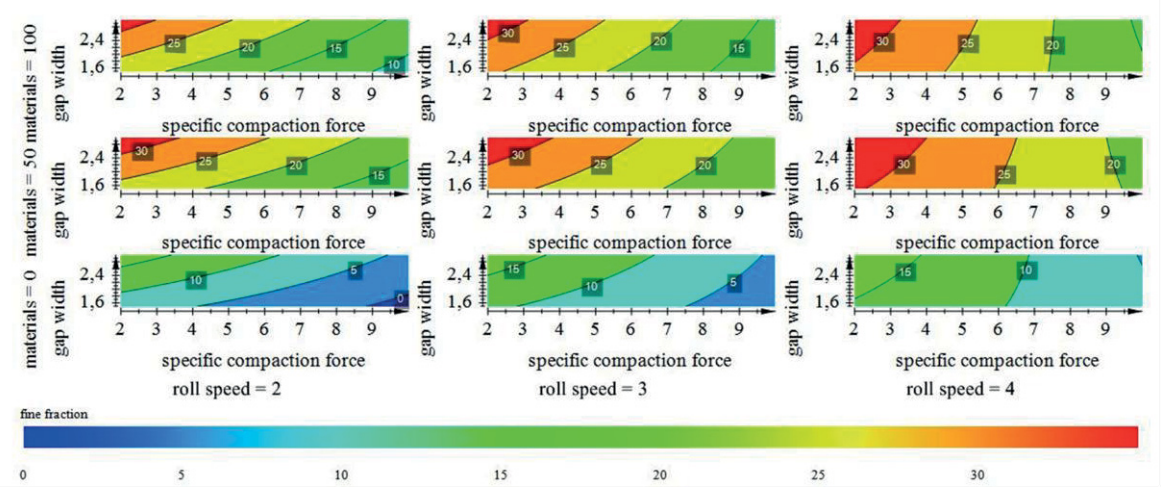

Figure 51. 4D contour plot of fine fraction of granules milled from ribbons compacted by BRC25 roll compactor.

The effect of the GW on the quantity of fines depends on the set RS. The decrease of the amount of fines decreasing the GW from 3.0 mm to 1.5 mm was found to be the most efficient, when 2 rpm RS was set. Less decrease in fine fraction as obtained, when the same change in the GW was taken at 4 rpm RS. The steepest decline of fines was observed for the plastic model material MCC and also for mixture granules containing 50% MCC.

3.4.5 Granule size distribution of granules obtained by Mini- Pactor

The median particle size of the mannitol granules are depicted in Figure 52 a), b), c) and d). The different roll compaction designs are differentiated in the figures. RR sealing system is presented in light blue colour, while the SS in dark blue colour. The continuous line shows results from the smooth rolls, while the dotted lines those ones that are from the knurled rolls. The usage of the SS system led to slightly smaller median particle size compared to the granules obtained from roll compaction designs using RR. The same observations for the d10 values were described by Perez-Gandarillas et al. [36]. In the aforementioned study, the same roll compactor and model material were used. As presented in Figure 52 a) b), c) and d), increasing the SCF, larger granules were obtained. The largest d50 values were obtained between 409.2 and 707.9 µm, when 1.5 mm GW and 2 rpm and 4 rpm RS were set for roll compaction. Setting 3.0 mm GW, the median particle size of granules was obtained between 222.3 and 678.9 µm.

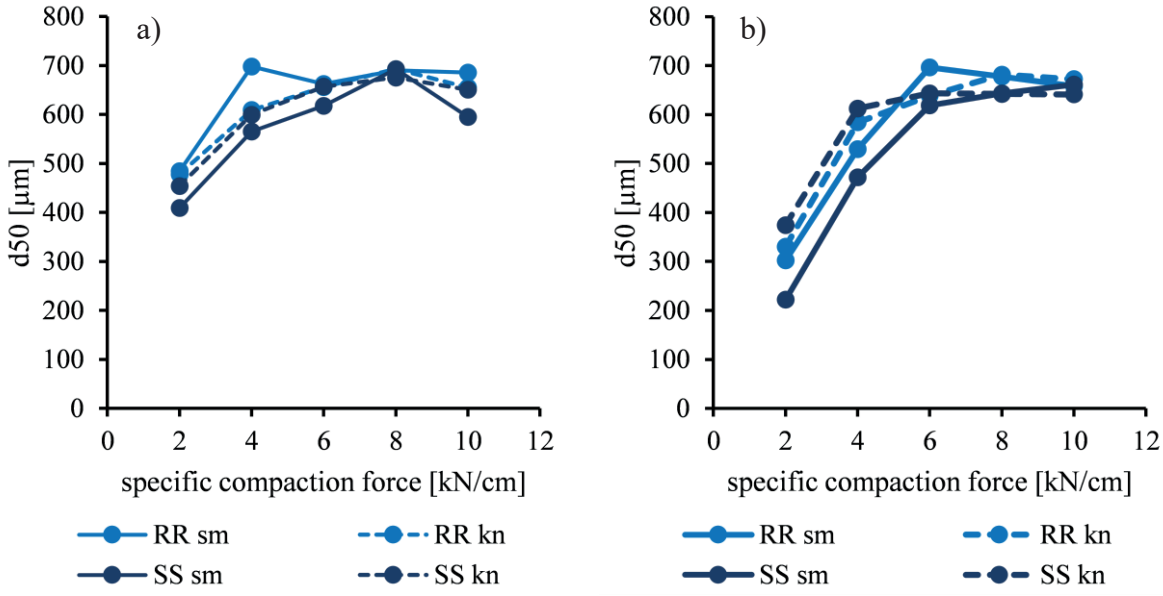

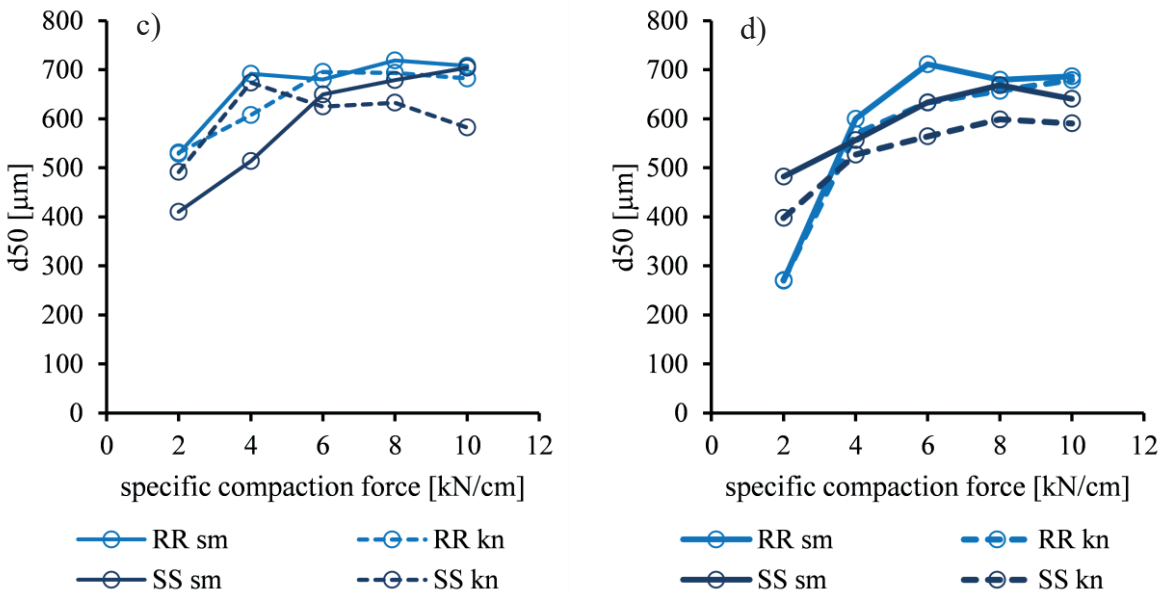

Figure 52. a), b), c), d). Median particle size of mannitol powder and mannitol granules obtained after milling of ribbons compacted by the Mini-Pactor roll compactor setting 1.5 mm GW and 2 rpm RS (a), 3.0 mm GW and 2 rpm RS (b), 1.5 mm GW and 4 rpm RS (c) and 3.0 mm GW and 4 rpm RS (d).

Good model of the examined factors was obtained (R^2=0.845, Q^2=0.803) for the response d50 value. The model terms of the evaluation of the d50 values are presented in Figure 53. The most significant factor are the SCF and its quadratic term (p-value <0.001), followed by the two-fold interaction between GW and SCF (p-value <0.001) and the main component, GW (p-value <0.001). As it was presented in Figure 22, the ribbon RD was not affected by the GW, however the median particle size was influenced by the set GW. The sealing system was found to be a significant model term (p-value<0.001), proving that RR sealing system leads to larger median particle size, while using SS system smaller d50 values are to be expected. In contrast to the type of sealing system, the type of roll surface was not found to be a significant model term.

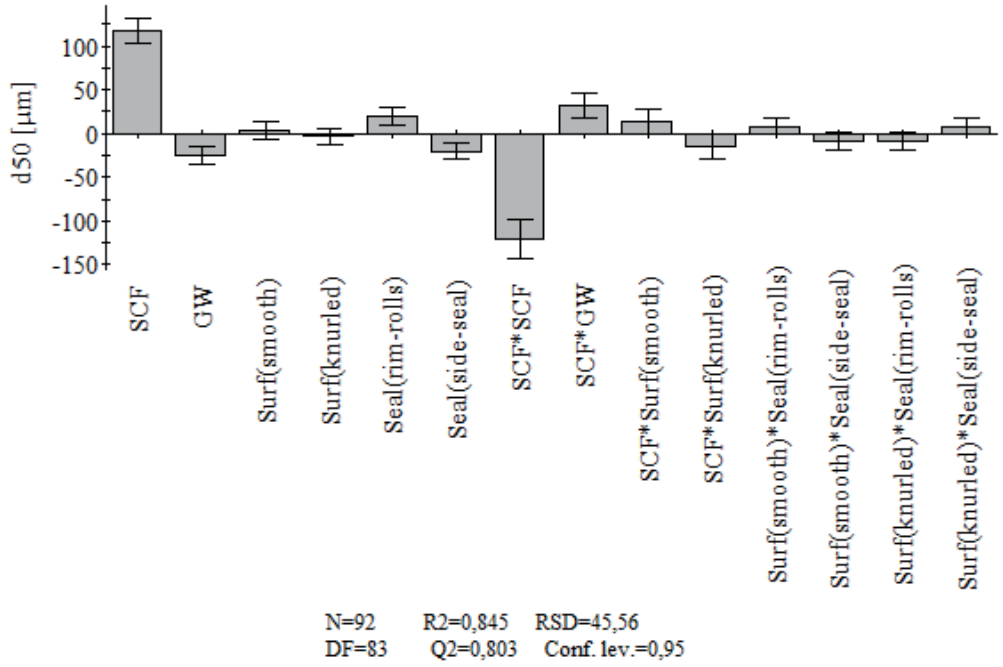

Figure 53. Coefficient plot of the model terms analyzing the median particle size of mannitol granules milled from Mini-Pactor ribbons.

Setting the SCF up to 8 kN/cm, less amount of fines was obtained, while 10 kN/cm SCF resulted higher amount of fines, as presented in Figure 54. This was observed for each batch of granules, which were milled from ribbons that were compacted at 1.5 mm GW and 2 rpm RS. Higher amount of fines were observed at 10 kN/cm SCF, when 3.0 mm GW and 2 rpm and RS were set in case of each roll compaction design except SS using smooth rolls, while setting 1.5 mm GW and 4 rpm RS, the roll compaction designs SS with smooth rolls and knurled rolls led to higher amount of fines, when 10 kN/cm was set, compared to 8 kN/cm SCF. This can be explained by the significance of the quadratic term of the SCF, presented in Figure 55. The model of amount of fine fraction was found to be appropriate, as R^2=0.663 and Q^2=0.568 were obtained. The most significant factor were the SCF (p-value<0.001) and its quadratic term (p-value<0.001). In contrast to the model of the median particle size, the GW was not found to be a significant model term for the quantity of fines. Considering the generation of fines, the roll compaction designs had significant effect compared to their influence on the median particle size, as the two-fold interaction between the type of sealing system and type of roll surface was obtained to be significant (p-value <0.001). The least amount of fines could be achieved, when RR with smooth rolls were used. The application of SS system with knurled rolls also was

advantageous to achieve less fine fraction. The two-fold interaction between the SCF and type of sealing system (p-value <0.017) and between the roll speed and type of roll surface (p-value <0.027) showed significant influence of the amount of fine fraction.

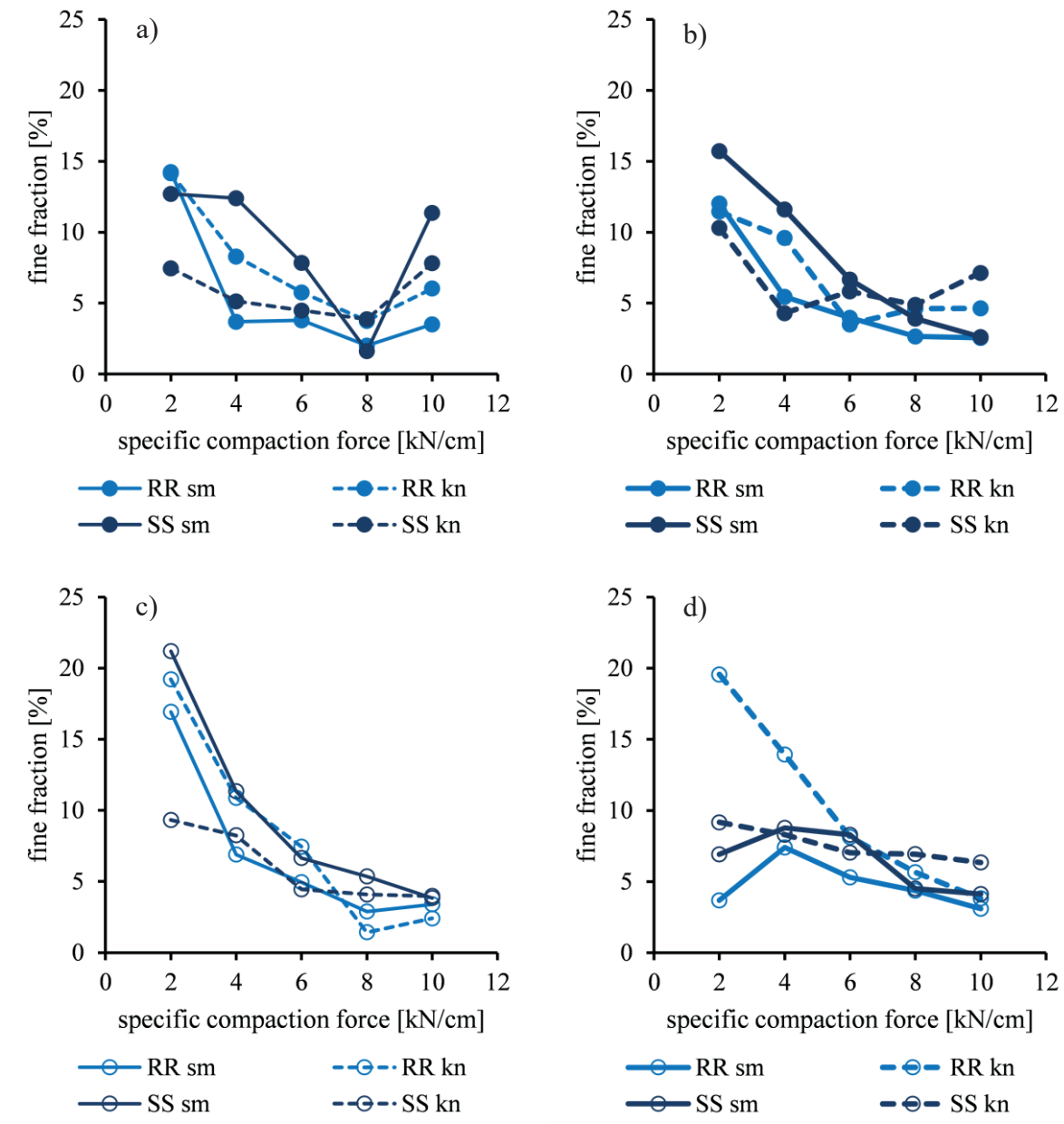

Figure 54. a), b), c), d). Fine fraction of mannitol granules obtained after milling of ribbons compacted by the Mini-Pactor roll compactor setting 1.5 mm GW and 2 rpm RS (a), 3.0 mm GW and 2 rpm RS (b), 1.5 mm GW and 4 rpm RS (c) and 3.0 mm GW and 4 rpm RS (d).

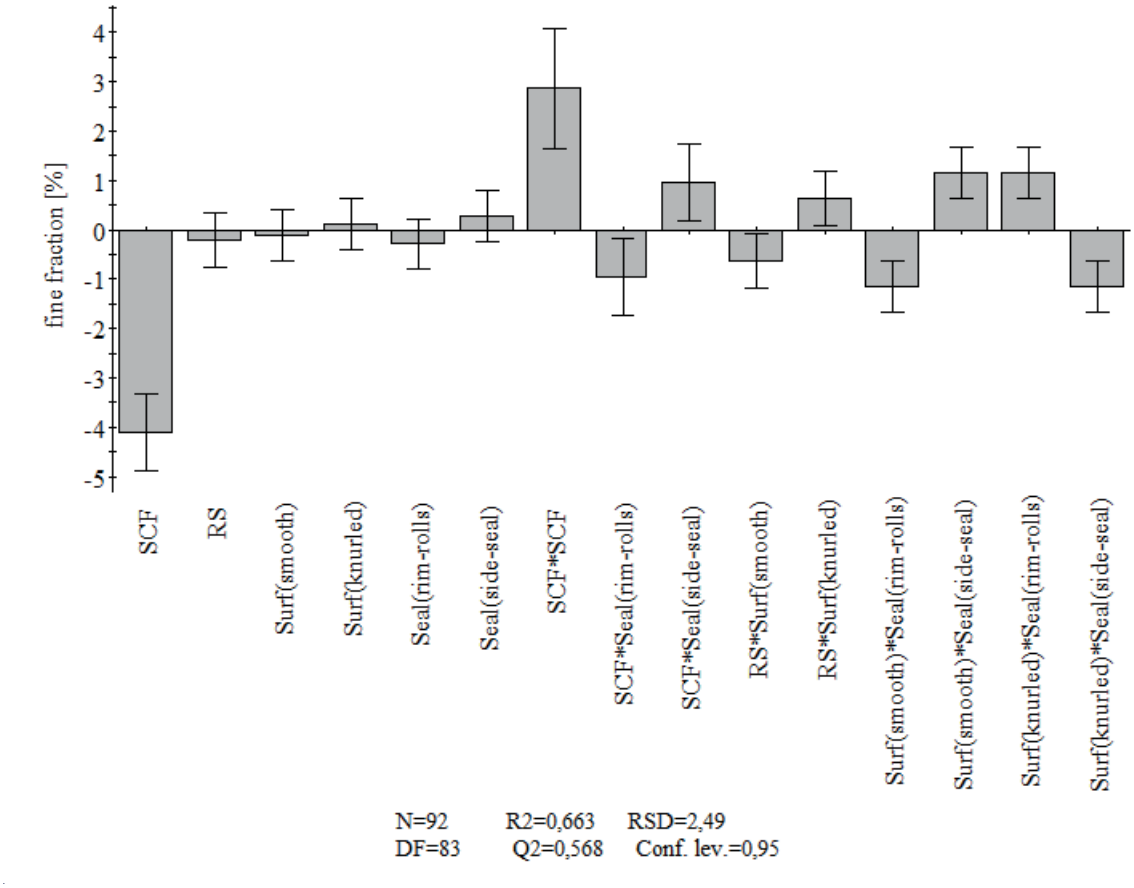

Figure 55. Coefficient plot of model terms analyzing the amount of fines of mannitol granules obtained from Mini-Pactor ribbons.

The aforementioned two-fold interactions are presented in the 4D contour plot in Figure 56. Based on the 4D contour plot, it is obvious, that the increase of the SCF decreased the fine fraction the most, when RR sealing system was used. At the same SCF, the increase of RS from 2 rpm to 4 rpm resulted in the decrease of the amount of fines, when smooth rolls were used, while in case of knurled rolls, the same change of RS increased the quantity of fines.

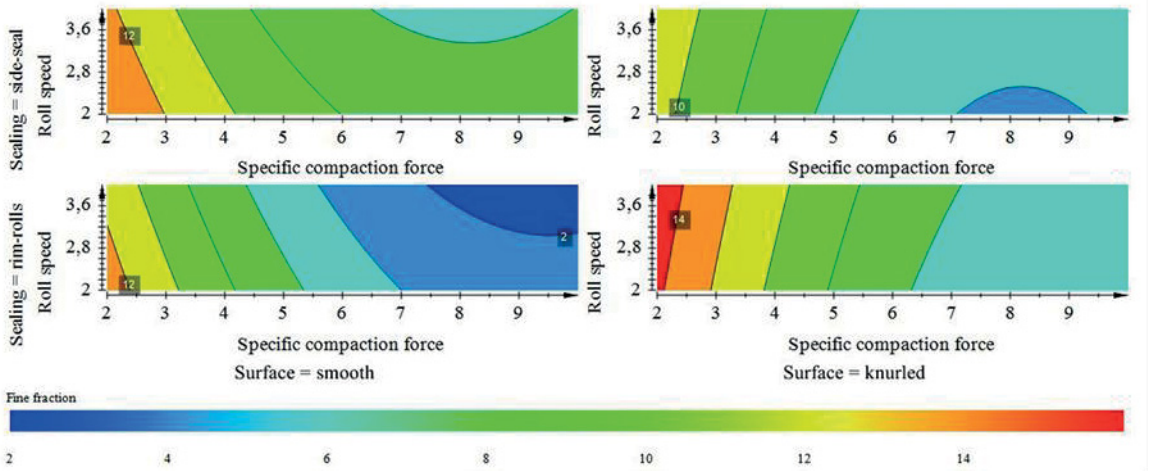

Figure 56. 4D contour plot of fine fraction obtained after milling mannitol ribbons compacted by Mini-Pactor roll compactor.

3.4.6 Summary

In case of each evaluated model, the quadratic term of the type of material was obtained to be the most significant model term. The largest d50 values were obtained for MCC, while the less amount of fines was obtained in case of mannitol showing brittle deformation behavior. In general, it can be concluded that high SCF/HP, low set GW and RS led to the largest d50 values and the less amount of fines for each type of material.

Considering the effect of process parameters and roll compaction designs, some differences were observed between the results of GSD-s using different types of roll compactors. For the granules obtained from ribbons compacted by the AlexanderWerk BT120 roll compactor, the HP and GW were found to be significant factors for both responses, when smooth rolls were used for roll compaction. In contrast, only the HP was found to be significant main factor in the model of fine fraction, when knurled rolls were used for compacting ribbons. Depending on the used type of roll surface, different amount of fines were obtained. When smooth rolls were used, the highest amount of fines was generated from mannitol and mixture ribbons. The milling of MCC ribbons resulted in the highest amount of fines, when knurled rolls were applied for roll compaction. The lowest amount of fines was achieved from mannitol ribbons produced with knurled rolls. Mirtic et al. [37] investigated the correlation between the density (porosity) of the ribbons and the obtained amount of fines. In this study, the same type of materials and roll compactor (AlexanderWerk BT120) were used. MCC and mannitol ribbons with different densities (70-85%) were milled with constant milling parameter settings. The quantity of fines from

MCC ribbons was found to be independent from the MCC ribbon density, while mannitol ribbons with low density resulted in higher amount of fines compared to denser ribbons. In contrast, it was shown in the current study that the quantity of fines depends the most on the type of material and the set hydraulic pressure. As described in section 3.2.2.1, setting different HP-s for roll compaction, MCC and mannitol ribbons with different densities were obtained. These ribbons resulted in certain amount of fines depending on the type of material and set HP applied during roll compaction. Denser ribbons resulted in less fines, which was observed in the study of Khorasani et al. [58]. This alteration between the study of Mirtic et al. and the current study might be explained by the range of ribbon density evaluated. Mirtic et al. evaluated ribbons in the range of density between 70-85%, while the current study investigated ribbons in the density range of 65-90%.

The largest median particle size was obtained for MCC and mannitol granules, when the BRC 25 roll compactor was used for manufacturing of ribbons. The lowest d50 values were obtained in case of the mixture granules, as it was observed for the mixture granules milled from ribbons compacted by the AlexanderWerk BT120 roll compactor. At each set SCF, small amount of fines was obtained, when 1.5 mm and 2 rpm RS were set in case of mannitol granules. These finding is in good agreement with the data described in the study of Ingelbrecht et al. [48], in which lactose, as brittle model material was evaluated. The highest amount of fines were resulted by the milling of mixture ribbons.

As observed for the granules of the BRC25 roll compactor, also in case of the Mini-Pactor granules, the d50 values were the highest, when 1.5 mm GW was adjusted for roll compaction. A clear effect of the roll compaction design could not be derived from the raw data, however the statistical evaluation proved that the application of RR sealing system leads to higher granule size independent of the used roll surface. The fine fraction was influenced the most by the set SCF and its quadratic term followed by the two-fold interaction of the type of sealing system and roll surface. The lowest amount of fines were obtained, when high SCF was set and RR sealing system was applied with smooth rolls. The conclusion of the study of Perez-Gandarillas et al. [36] also revealed, that the reduction of the fine fraction can be achieved the most, when RR and high SCF are applied for roll compaction.

4 Summary

The performance of different types of roll compactors, AlexanderWerk BT120, L.B. Bohle BRC 25 and Gerteis Mini-Pactor, was evaluated in regards to the precision and the deviation from the set value of hydraulic pressure/specific compaction force and gap width depending on the roll compaction design and used model materials. No relationship was found between the type of material and the precision and the deviation from the set value of hydraulic pressure/specific compaction force and gap width. The roll compaction using the AlexanderWerk BT120 roll compactor without any control of the gap width resulted in high variations of process parameters. As modern AlexanderWerk roll compactors have gap control, less variation of process parameters might occur. Furthermore, the manufacturing using smooth rolls caused problems, and thus a part of the design of experiments could not be conducted. In contrast, the obtained data set showed small deviations from the set values and high precision of the specific compaction force and gap width, when the roll compaction process was performed using the BRC 25 and the Mini-Pactor roll compactors. The comparison showed that the presence and the appropriate adjustment of a PI-control loop for gap control improves the agreement with the set values and precision of the roll compaction process. The presence of a gap control in addition to compaction force control is state of the art.

The impact of material properties, process parameters and roll compaction design on roll compaction was investigated through the evaluation of the ribbon relative density. Various types of roll compactors were investigated using two model materials showing different deformation behavior. The most significant process parameter was the hydraulic pressure/specific compaction force independently from the implemented roll compaction design, type of roll compactor or model material. The gap width was found to be a significant factor as well, when smooth rolls were used for compaction, however, problems with sticking influenced the investigation of the impact of the gap width on the ribbon relative density. The sealing system had a major effect on the ribbon relative density compared to the type of roll surface. The compaction of mannitol powder led to the densest ribbons due to its sphere morphology and collapse under compaction resulting in high relative density. The fraction of microcrystalline cellulose had an adverse effect on the

ribbon relative density, as the microcrystalline cellulose ribbons underwent elastic recovery after ejection from the nip zone.

Two different techniques of the ribbon relative density measurement were compared to each other; the GeoPyc powder pycnometry, as conventional method and the X-ray micro-computed tomography, as a more established and complex method. Based on the data set of GVs obtained by X-ray micro-computed tomography, novel approaches were established for the calculation of the ribbon relative density using different software, called ROTHIST, UHIST, UHIST20 and UHIST50. The ROTHIST software enabled to investigate the density distribution in a ribbon across the width, while the UHIST software considered the whole volume of the ribbon in higher spatial resolution, than it is achievable by powder pycnometry. Although, the X-ray μCT tool might provide more accurate relative density results than the powder pycnometry, it is easier, faster and more cost-effective to measure the relative density of ribbons by GeoPyc.

Theoretical principles of the process transfer were shown, in which the ribbon relative density-based transfer of roll compaction was successfully accomplished applying the calculated conversion factors between the AlexanderWerk BT120 and Mini-Pactor roll compactors, and the BRC 25 and Mini-Pactor roll compactors.

One of the main drawbacks of roll compaction/dry granulation is the production of high amount of fines resulting in bimodal granule size distribution. It was shown, that the amount of fines is a function of the set hydraulic pressure/specific compaction force, gap width, the type of material and the used type of roll surface for the AlexanderWerk BT120 roll compactor and for the BRC 25 roll compactor. In case of both compactors, the highest amount of fines and the smallest median particle size was obtained, when mixture ribbons were milled, while the largest median particle size was obtained from the mannitol granules. For the AlexanderWerk BT120 roll compactor, the hydraulic pressure and gap width were found to be the most significant factors for ribbon relative density, d50 and amount of fine fraction, when smooth rolls were used, while only hydraulic pressure had a significant effect on the ribbon relative density and amount of fines, when knurled rolls were used. This observation proved that the ribbon relative density and the type of material govern the granule size distribution through the effect of roll compaction design and process parameters. The less amount of fines were achieved by milling mannitol ribbons compacted with knurled rolls. The median particle size was impacted the most by the set

specific compaction force, gap width and the used sealing system, but not by the applied roll surface during roll compaction.

The design of roll compactors had an influence on the ribbon and granule properties, but the influence of the process parameters and material attributes were found to be more important and can overrule the equipment design effects.

5 Experimental part

5.1 Materials

Microcrystalline cellulose (Avicel PH 101, FMC BioPolymer, USA, (MCC 101) possessing plastic-elastic material behaviour [49], spray-dried mannitol (Pearlitol 200 SD, Roquette, France) as brittle-ductile substance [115] and a 50:50% mixture of mannitol and MCC 101 were roll compacted. During the experimental work with the different roll compactors, different lots of raw materials were used. Table 11 shows the utilized lot numbers of raw materials used in each experimental study. During roll compaction, lubrication was avoided, as it has a high impact on the nip angle of roll compaction [41, 116-118] and also on the granule and tablet properties. Nevertheless, in acetone (analytical grade) dispersed magnesium stearate (5 mg/mL) (Parteck® LUB MST, Merck Millipore, Germany) was applied on the knurled roll surface, when MCC 101 was compacted setting 48 bar HP and 1.5 mm GW using AlexanderWerk BT120 roll compactor, as the material stuck to the roll surface and hence MCC 101 was jammed between the rolls. The lubrication of the roll surface enabled the powder grabbing resulting in ribbons [119]. During the investigation of material deformation behaviour using the Styl'One Evolution compaction simulator (Medel'Pharm, France), the flat faces punches were lubricated with magnesium stearate (Parteck® LUB, Merck Millipore, Germany) using an eye shadow applicator. As the moisture sensitivity of the roll compaction process [23, 24] has already been published and MCC 101 is known to be hygroscopic material [120], the material was kept in climate room at 20-22 ℃ and 40-46% of relative humidity before and or during processing. Nevertheless, the processing of the model materials was not always possible in conditioned laboratories. The manufacturing condition of each roll compaction study is described in the later relevant sections.

Table 11. Different lots of raw materials used during experimental work.

Materials	Alexander Werk BT120	Hosokawa Alpine Pharmapaktor C250	L.B. Bohle BRC 25	Gerteis Mini-Pactor	Styl'One Evolution
MCC 101	61304C	P114827702	P114827702	-	P114827702
Mannitol	E058G	E430G	E430G	E288G, E430G, E925G, E988G	E430G
Magnesium stearate	K4201756 311	-	-	-	K4201756311

5.2 Methods

5.2.1 Design of experiments

Multilevel full factorial experimental plans were established targeting to understand the effect of the process parameters [28], the type of the roll compactor, process design and the fraction of MCC on the ribbon RD. Modde 9.0 (Umetrics, Sweden) was used to create multilevel full factorial experimental plans and to evaluate of the obtained datasets. The experiments were randomized to reduce the effect of experimental failure and to avoid systematic errors. Each roll compactor and used roll compaction design was tested according to an individual experimental setting, however, the parameter settings were kept as similar as possible to enable the comparison between the machines. The SCF and HP were examined at 5 factor levels, while the GW was investigated at 2 factor levels, the RS was kept constant or set to 2 rpm and 4 rpm. The studied parameter settings and roll compaction designs are presented in Table 12.

Table 12. Roll compaction design and parameter setting** using AlexanderWerk BT120, Hosokawa Alpine Pharmapaktor C250, L.B. Bohle 25 and Gerteis Mini-Pactor roll compactors.

Process parameters and roll compaction design	AlexanderWerk BT120	L.B. Bohle BRC 25	Gerteis Mini-Pactor	Hosokawa Alpine Pharmapaktor C250
sealing system	SS	RR	SS/RR	SS
roll surface	smooth / knurled	smooth/knurled***/fine grooved***/coarse grooved***	smooth / knurled	smooth
RS [rpm]	3	2 / 4	2 / 4	2
GW [mm]	1.5 / 3.0*	1.5 / 3.0	1.5 / 3.0	1.5 / 3.0
HP [bar]	18 / 24 / 36 / 48 / 60			
SCF [kN/cm]		2 / 4 / 6 / 8 / 10	2 / 4 / 6 / 8 / 10	2 / 4 / 6 / 8 / 10
fraction of MCC	100 %, 50 %, 0 %	100 %, 50 %, 0 %	0%	100 %, 50 %, 0 %

*2.3 mm for smooth rolls

**Beside the presented parameter settings, also higher SCF values were set, when the control performance of the BRC 25, Mini-Pactor was evaluated. These further settings are described in sections 5.2.2.4 and 5.2.2.5.

***only used for the evaluation of the roll compaction control performance

As qualitative factors, the effect of the roll surface and the sealing system was investigated in case of Mini-Pactor. The type of material was also included in the full factorial experimental plan as quantitative factor, when BRC 25, Pharmapaktor C250 and AlexanderWerk BT120 were used. 100 % as MCC, 50 % as the mixture and 0% as mannitol were adjusted as levels of the fraction of MCC in the models. Multiple linear regression was utilized in order to model the relationship between the independent variables (process parameters, roll compaction design and proportion of MCC) and the selected response variables, RD and GSD. The confidence level was determined at 95%.

5.2.2 Methods of roll compaction

5.2.2.1 Overview

Different types of roll compactors were implemented in order to investigate their control performance and the effect of the process variables, compaction designs (type of roll surface and sealing system) and type of material (brittle and plastic deformation behavior) on the roll compaction process and ribbon and granules quality. In the following sections, the various roll compactors are introduced in detail. The working ranges of the different roll compactors are exhibited in Table 13.

Table 13. Working ranges respecting the SCF, HP, CF, GW and RS.

Process parameters	AlexanderWerk BT120	Hosokawa Alpine Pharmapaktor C250	L.B. Bohle BRC 25	Gerteis Mini-Pactor
SCF [kN/cm]	-	-	0.5-20.0	2.0-20.0
CF [kN]	-	100	-	-
HP [bar]	18-143	-	-	-
GW [mm]	1.0-5.0	1.0-3.0*	0.5-6.0	1.0-6.0
RS [rpm]	2.8-12.1	2-4*	1-30	1-30

*No information about the working ranges of the GW and RS was obtained or found in the literature. The exhibited ranges are the settings that were used during the conducted experimental work.

5.2.2.2 AlexanderWerk BT120

The model of AlexanderWerk BT120 roll compactor (AlexanderWerk, Germany, constructed in 2008) possesses one horizontal feeding screw and vertical positioned rolls. The rolls have 25 mm width and 120 mm diameter. A pair of smooth and a pair of knurled rolls were implemented and SS assembly was used to seal the rolls. The process parameters and used roll compaction designs are introduced in Table 12. These experimental runs were evaluated for the control performance study. The HP was adjusted by the hydraulic system. There is no control system to adjust the set GW, thus the combination of the set screw speed and RS determined the GW development. When a higher screw speed was set while keeping the roll speed constant, a higher GW was achieved. Working with the AlexanderWerk BT120 the RS was kept constant at 3 rpm, so the GW was determined solely by the screw speed. The laboratory temperature was held between 19-21 ºC and the relative humidity varied between 50 and 85%.

5.2.2.3 Hosokawa Pharmapaktor C250

The Pharmapaktor C250 roll compactor (Hosokawa Alpine, Germany, constructed in 2010) was used to produce MCC, mannitol and mixture ribbons using smooth roll surface. It has two horizontal feeding screws and one vertical tamping screw, which convey the powder to the horizontal positioned rolls. The rolls are sealed by a SS assembly and have 30 mm roll width and 250 mm diameter. The CF was set during roll compaction, which is then presented as SCF in the full factorial experimental plan, dividing the value of the CF by the RW (3 cm). The DoE set process parameters and roll compaction designs are shown in Table 12. The GW was adjusted to the set CF through the set speed of the screws and the RS. In order to reach a constant GW and CF, the screw speeds were changed by the operator till the desired parameters were obtained. All experiments were conducted in an uncontrolled laboratory environment concerning temperature and relative humidity.

5.2.2.4 L.B. Bohle BRC 25

The roll compactor BRC 25 (L.B. Bohle, Germany, year 2015), possesses one horizontal feeding screw and one vertical tamping screw. The ratio between the feeding and tamping auger speeds was set at 1:4, so the tamping auger speed was 4 times faster than the feeding auger speed. The powder conveyed into the compaction area is densified between two horizontal positioned rolls of 250 mm diameter and 25 mm width. Powder leakage is inhibited by a RR sealing assembly. Different types of roll surfaces, e.g. smooth, knurled, fine grooved and coarse grooved were investigated. The parameter settings and the implemented roll compaction design are presented in Table 12. For the control performance study, the SCF was set between 10-17 kN/cm at the beginning and the end of the DoE accomplishment, in order to keep the randomized order of the experimental runs. The SCF is set by a spindle motor [121]. The control parameters for the force control are not accessible for the user. The GW depends on the throughput of the tamping auger at a certain roll speed. The GW is controlled by a PI control loop by adapting the tamping auger speed. The PI parameters of the GW control loop, which can be changed by the user, were set at P: 10 and I: 20 s. The laboratory temperature was varied between 20.0-22.2 ℃ and relative humidity between 49.3-66.6 %.

5.2.2.5 Gerteis Mini-Pactor

The Gerteis Mini-Pactor (Gerteis Maschinen+Prozessengineering, Switzerland, year 1999) has a horizontally positioned feeding screw and an inclined tamping screw and roll pair of 250 mm diameter and 25 mm width at an angle of 30^{o} corresponding to the horizontal plane. The screw speeds were coupled with each other in a ratio of 1:2, thus the tamping auger speed was twice faster compared to the feeding auger. All roll compaction runs for the control performance evaluation of the Mini-Pactor were performed using SS assembly with knurled roll surface pattern. Using mannitol, the process parameters and roll compaction designs for conducting the DoE-s are listed in Table 12.

The Mini-Pactor has different production modes regarding the control and maintenance of those parameters that are essential to obtain ribbons with the desired quality attributes. According to the set value in kN/cm, the hydraulic system controls the HP to adapt the CF exerted on the slave roll. The control parameters for the force control are not accessible for the user. To produce ribbons with appropriate properties (strength, RD), it is also necessary to control the GW. For this purpose, a control loop of the GW is implemented, when the automatic mode is used. During roll compaction under the automatic mode conditions, the set value of the GW is achieved due to the speed adjustment of the screws in the manner of a PI control algorithm. In this study, the PI parameters of the GW control were set at P: 12.0, I: 15 s. The experiments were executed in a climate room (temperature: 21.1 - 21.7℃ and relative humidity: 43.7 - 46.3 %).

5.2.2.6 Establishment of the conversion factors

The establishment of a conversion factor introduces a principal methodology to transfer the roll compaction process, between machines from different suppliers. The c_f is an extent, with which the appropriate roll pressure can be adjusted to achieve comparable ribbon RD values obtained by another roll compactor using different measure of the roll pressure. Using the most type of roll compactors, the SCF (kN/cm) or CF (kN) are utilized as measures to exert a certain CF on the roll surface. The SCF is the CF which is exerted on 1 cm RW. Other roll compactors have the attribute to set HP in bar or in MPa. The ribbon RD results of mannitol ribbons obtained by AlexanderWerk BT120, BRC 25 and Mini-Pactor compactors were used to establish c_f-s according to Equation 5 and Equation 6.

$$HP[bar] = \frac{SCF\ \left[\frac{kN}{cm}\right] * RW[cm]}{c_f\ [m^2]}$$ Equation 5

$$SCF_{Mini-Pactor}[kN] = SCF_{BRC25}\ [kN] * c_f \qquad [m^2]$$ Equation 6

The conversion factors were calculated considering those ribbon RD-s, which were achieved using the same roll compaction design (roll surface and sealing system) and setting the same GW. The different set RS, 2 rpm in case of Mini-Pactor and 3 rpm in case of AlexanderWerk BT120 is neglected, because of its insignificant effect on the ribbon RD in the respective models, when a brittle material is compacted [81]. The RD of ribbons produced by the Mini-Pactor were presented against the CF, while the RD of ribbons manufactured by the AlexanderWerk BT120 roll compactor were plotted against the set HP multiplied by the c_f and the calculation of the c_f was accomplished according to Equation 5. The process transfer between the BRC 25 and Mini-Pactor was performed based on Equation 6. Several c_f-s between 0.5-2.0 m^2 with an increment of 0.1 m^2 were substituted in Equation 5 and in Equation 6. The c_f was taken that resulted in the highest overlapping of both curves.

5.2.3 Granulation method

The collected ribbons produced by the different roll compactors were milled separately from the roll compaction step to avoid the influence of the bypassed powder on the GSD. Further information about sample collection is given in section 5.2.4.1. The ribbons were milled by the Gerteis star granulator (Gerteis Maschinen + Processengineering AG, Switzerland) using 1 mm mesh size. The granulation method was kept constant in order to exclude the effect of different granulator type or settings on the GSD. The granulation speed was set at 40 U/min, 120º clockwise and 60 U/min, 180º counterclockwise. The amount of fines, which was not fallen from the granulator wall into the collection bag, was always swept and collected to the rest of the milled granules at the end of each granulation run. The granulator was hoovered after every batch in order to avoid the mixing between two batches following each other.

5.2.4 General methods

5.2.4.1 Sampling methods

After compacting the ribbons, 200-300 g of ribbons were milled into granules. When SS system was used to produce the ribbons, uncompacted powder was less and well distinct from the ribbon pieces compared to those ribbon samples, which were manufactured using rim-rolls. Due to this, the uncompacted material that was collected with the ribbons was separated using a sieve with 125 µm mesh size, when SS assembly was used. Roll compaction using RR resulted in smaller pieces of ribbons and high amount of fines, thus the differentiation between real uncompacted material and small parts of ribbons was not possible through sieving. Because of this, the RR ribbons were milled with the uncompacted powder passed by the rolls during roll compaction. The collection of ribbon pieces from the entire part of ribbon was aimed to measure their RD using GeoPyc powder pycnometer and X-ray µCT. During the sampling of ribbons compacted using RR sealing system, only smaller ribbon pieces were obtained, however some whole ribbon pieces (length= 5-10 mm) were found, too. The collection of representative samples included bigger and smaller pieces and when it was available also whole ribbons were collected. In contrast, the SS ribbons were usually obtained as longer pieces (length= 10- 250 mm), which enables the sampling over the entire body of the ribbons. Samples were chosen and measured by X-ray µCT, when SS assembly was utilized during roll compaction, while the RR ribbons were not in an intact form, therefore the characterization of these samples by X-ray µCT was excluded from this study.

5.2.4.2 Process data recording and evaluation

From the runs of a design of experiments selected experiments were evaluated. The time after a change in the process parameters until reaching steady state conditions again is determined as settling time in order to evaluate the reaction time of the system to a sudden change. The steps in the DoE-s are artificially high and can be interpreted as worst case conditions. The evaluation of the process performance relied on the deviations from the set value and precision of the HP or SCF and GW. The average and the standard deviation during steady-state process conditions were calculated. The steady-state process condition begins when all actual values of the process parameters achieved the specification of the set value. The specification of the SCF is the set value SCF $\pm$ 0.1 kN/cm and for the GW set value $\pm$ 0.1 mm, when the Mini-Pactor and BRC 25 roll compactors were used. In

case of the HP the specification is defined at the set value ± 2 bar, while ± 0.1 mm was decided for the GW specification.

In Figure 57, the determination of the settling time and steady-state process conditions is introduced using an example from the BRC 25 roll compactor. The SCF was increased from 4 kN/cm to 8 kN/cm. After 27 s, 7.90 kN/cm as actual value of the SCF was reached. From this point on, the mean and the standard deviation were calculated and considered as deviation from the set value and precision (8.10 ± 0.05 kN/cm). A constant GW (1.49 ± 0.04 mm) was obtained after 37 s. Due to the control system of BRC 25 roll compactor, the settling time of the SCF is shorter compared to the GW.

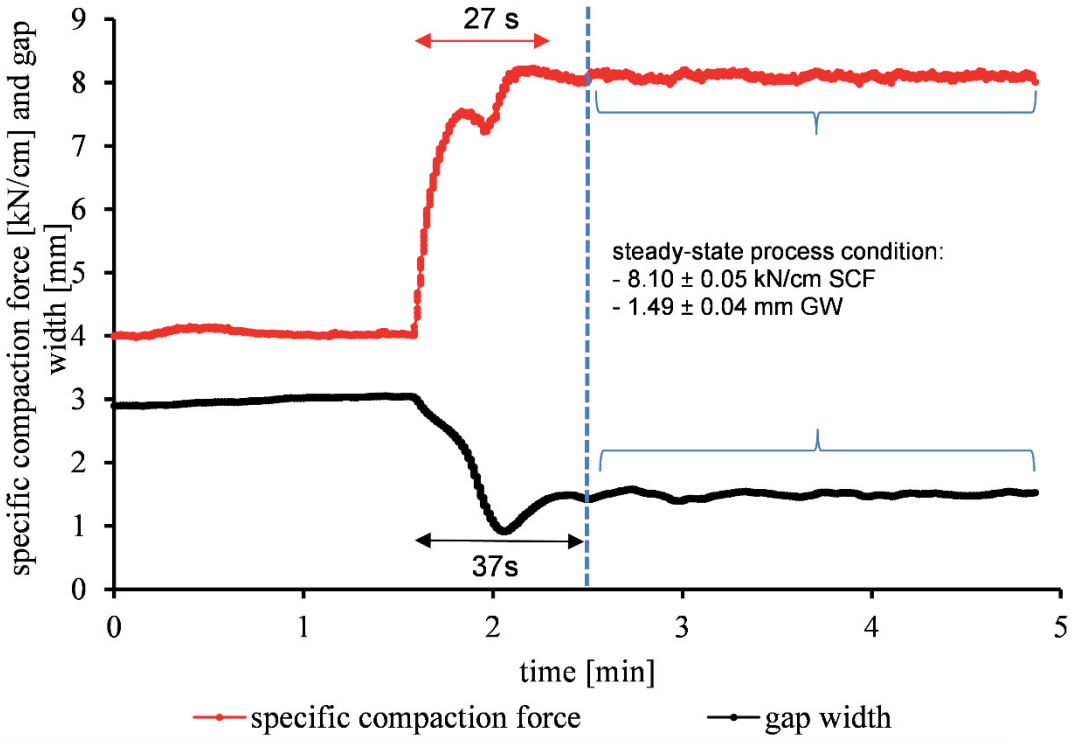

Figure 57. Example for evaluation of settling time and steady-state process condition during roll compaction of mannitol using BRC 25 with knurled rolls.

The endurance of the production of the individual batches differs from each other, thus the stated means and standard deviations refer to different time intervals. In case of Mini-Pactor and BRC 25 roll compactor the production times were set between 1-2 minutes, while in case of AlexanderWerk BT120 roll compactor this time interval varied between 2.5-11 minutes. Furthermore, the data recording frequency was different between the roll compactors. The frequency of the data documentation is introduced in Table 14.

Table 14. Data recording frequency of the different types of roll compactors.

Roll compactor	Roll surface	Data recording frequency
AlexanderWerk BT120	knurled	0.1 Hz
	smooth	0.1 – 0.5 Hz
L.B. Bohle BRC 25	knurled, fine grooved, coarse grooved	0.125 Hz
	smooth	0.09 – 0.1 Hz
Gerteis Mini-Pactor	knurled	1 Hz

5.3 Powder characterization methods

5.3.1 Helium density

The helium density *or* the apparent particle density of the raw materials was measured by helium pycnometry (AccuPyc, Micromeritics GmbH, USA). A 3.5 cm^3 chamber was used during the measurements, which was calibrated using a metal ball before measuring the raw materials. Then, the raw materials were weighted into the 3.5 cm^3 chamber using an analytical balance (CP 224S, Sartorius AG, Germany). The helium density of the raw materials were defined three times and during each measuring cycle the helium density was measured ten times. Afterwards, the average and the standard deviation were calculated.

5.3.2 Scanning electron microscopy

The morphology of MCC and mannitol was studied using Phenom G2 pro scanning electron microscope (Phenom-World BV, Netherlands). The images were made at various magnifications using 5-10 kV acceleration voltage.

5.4 Ribbon relative density characterization methods

The diagram of the evaluation methods is presented in Figure 58. The ribbon RD has been characterized by GeoPyc powder pycnometry and X-ray μCT. Using the GeoPyc, the envelope density of an object is measured using a free-flowing powder. Using the X-ray μCT, 3D image of an object is obtained. The individual volume elements (cubes) of this image are named voxels and have a single property: intensity or grey value (GV). The GV

of the individual voxels corresponds to the density. The analysis of the µCT data was done with two programs: ROTHIST and UHIST. With ROTHIST, the 3 slices (images) of the ribbon were analyzed and with the UHIST the whole volume was considered. Details are given in section 5.4.2.

The three slices of ROTHIST are close to each other (approximately 3-5 mm), which allows to measure a local RD. This can lead to a density distribution over one dimension of the ribbon, e.g. the ribbon width. UHIST provides a mean value for RD, which is representative since it is based on larger volume.

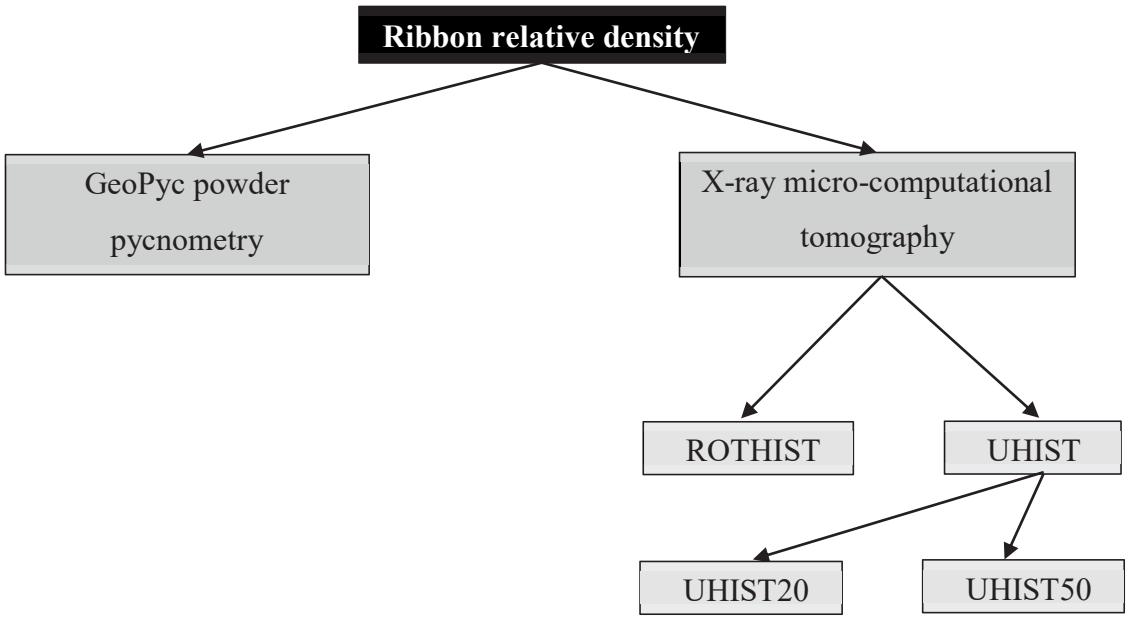

Figure 58. Overview of utilized methods for ribbon RD determination.

5.4.1 Relative density determination by GeoPyc powder pycnometry

The ribbon envelope density or apparent density was measured by a GeoPyc powder pycnometer (GeoPyc 1360 Envelope Density Analyzer, Micromeritics GmbH, USA). A 25.4 mm internal diameter chamber was used for the analysis. 51 N consolidation force was used in order to properly consolidate the samples with the DryFlo, but not to destroy the ribbon pieces. As conversion factor, 0.5153 cm^3/mm was set. 3.5-4.5 g ribbon samples were broken into smaller pieces, when it was necessary, dedusted and weighted using an analytical balance (Sartorius CP224S, Sartorius AG, Germany) before each measurement. At least 3 samples were taken from each ribbon batch and the mean and standard deviation were calculated. During the sampling of the ribbon pieces measured, the whole ribbon

width was considered, when it was available in one piece. The ribbon RD was calculated from the ratio of envelope density of the ribbons and the helium density of the powders according to Equation 7. The envelope density was calculated from the ratio of the weighed mass of ribbons and the measured volume of the ribbons according to Equation 8.

$$RD = \left(\frac{\rho_{env}}{\rho_{He}}\right) * 100$$ Equation 7

$$\rho_{env} = \frac{m_{ribbon}}{V_{ribbon}}$$ Equation 8

5.4.2 Relative density determination by X-ray µCT

The density distribution of mannitol ribbons was analyzed using X-ray µCT tomography (µCT) (CT-ALPHA, Procon X-Ray, Germany) [89]. During measurements, the sample was rotating while the X-ray source and detector were kept at the same position. The scans are transmission data collected by illuminating the object from 1600 projection angles at a resolution of 30-35 µm per voxel, at an acceleration voltage of 80 kV and current of 80 µA. The obtained scans were used for the reconstruction of the 3D structure of the object using the software VG Studio (Volume Graphics, Germany). The visualization and preparation of the cross sections of the subject of interest were executed using Avizo Fire 9.0 (FEI, USA).

The cross sections are grey scale images consisting of a certain amount of voxels. The voxels have a certain GV, which indicates the density. In order to determine the density distribution based on the obtained GV-s, the GVs had to be calibrated. For the calibration of the GV-s, mannitol tablets with different RD were produced [52]. For this purpose, 250 mg of mannitol powder was weighed using an analytical balance (Sartorius Extend ED224S, Sartorius AG, Germany) and pressed into tablets using a hydraulic tablet press (Hydraulische Presse, Perkin-Elmer, Germany) without any lubrication. The RD of the calibration tablets was calculated from the ratio of the envelope density and helium density of mannitol. The envelope density was calculated from the diameter, thickness and height of the tablets, which were measured using a digital caliper (Mitutoyo Absolute Digimatic, Mitutoyo, USA). The helium density of mannitol powder was determined by helium

pycnometry (AccuPyc, Micromeritics GmbH, USA) as described in section 5.3.1. Two sets of calibration tablets were produced, because the usage of the first set of calibration tablets for the measurement of the Mini-Pactor ribbons led to their damage. The tablet RD of the first calibration tablet set was obtained between 60.0 and 88.4 %, while the RD of the calibration tablets from the second set was between 53.9 – 92.9 %. The second set of calibrations tablets was used for the measurement of the AlexanderWerk ribbons. The calibration tablets and ribbon samples were fixed into a piece of foam (Oasis Floral Products, USA), which was fixed on the sample holder during all measurements. Each µCT measurement was performed with the presence of the calibration tablets and, the GV calibration was performed for every µCT scan. An example of the foam filled with samples is presented in Figure 59 a), and a 3D µCT image of Mini-Pactor ribbons and calibration tablets reconstructed from the recorded projections is exhibited in Figure 59 b).

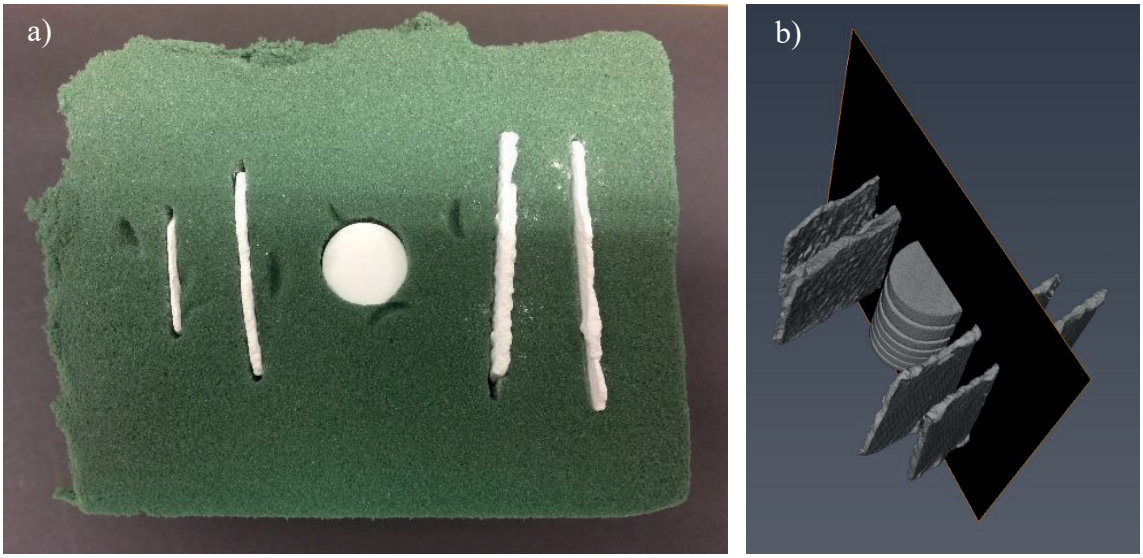

Figure 59. a), b). Mini-Pactor ribbons and calibration tablet samples placed in the foam (a) and a 3D reconstruction of ribbons and tablets (b), selecting a cross section across the ribbon and tablet width.

Two ribbon samples from batches manufactured by the Mini-Pactor using 2 kN/cm, 10 kN/cm SCF and SS system and by the AlexanderWerk BT120 using 18 bar and 60 bar HP were included in the investigation.

5.4.2.1 Calculation of the relative density using ROTHIST

The images of the prepared cross sections of tablets and ribbons were taken for the analysis of the GV-s across the ribbon width using the ROTHIST software. One example of the visualized cross sections is presented in Figure 60 a), while the selection of the area for evaluation from the cross section of a tablet is presented in Figure 60 b) and the same is presented in Figure 60 c) for a ribbon.

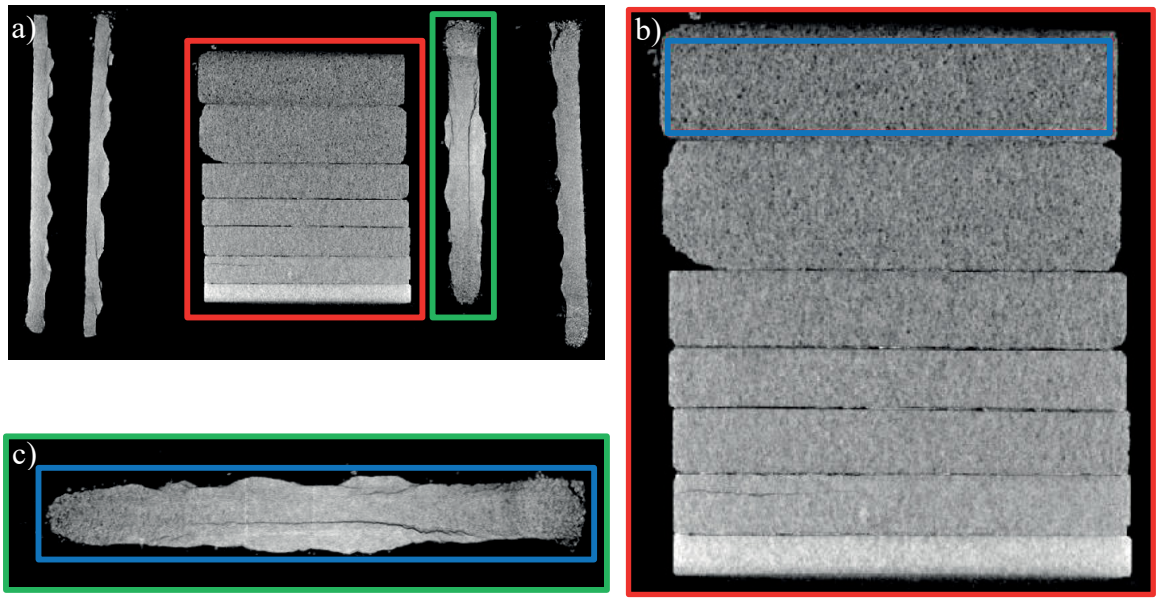

Figure 60. a), b) c). Cross sections of tablets and ribbons after reconstruction of the projections and visualization (a) and the selection of the area for evaluation from the cross section of a calibration tablet (b) and from the cross section of a ribbon (c).

To establish the correlation between the GV-s and RD, a selected image depicting the calibration tablet cross sections was opened with ROTHIST and the individual tablet samples were marked to define the area from which the GV-s were calculated (area bracketed with blue in Figure 60 b)). Each tablet was evaluated at two different cross sections. Therefore, for each measurement, two calibration equations were calculated, as two images (cross sections) of the calibration tablets were evaluated in the described way. Approximately 1-2 mm distance was between the selected cross sections. The threshold for GV was set at 10 in the software, which means the GV-s less or equal to 10 were ignored. Low GV (black and dark grey colours) represents the foam or the air. The other GV-s (grey and white) in the image depict the ribbons or tablets. The obtained mean GV-s of tablets were averaged and plotted against the tablet RD yielding the calibration equation. The GV-s were calibrated between 122 and 231. Figure 61 exhibits an example of such a calibration.

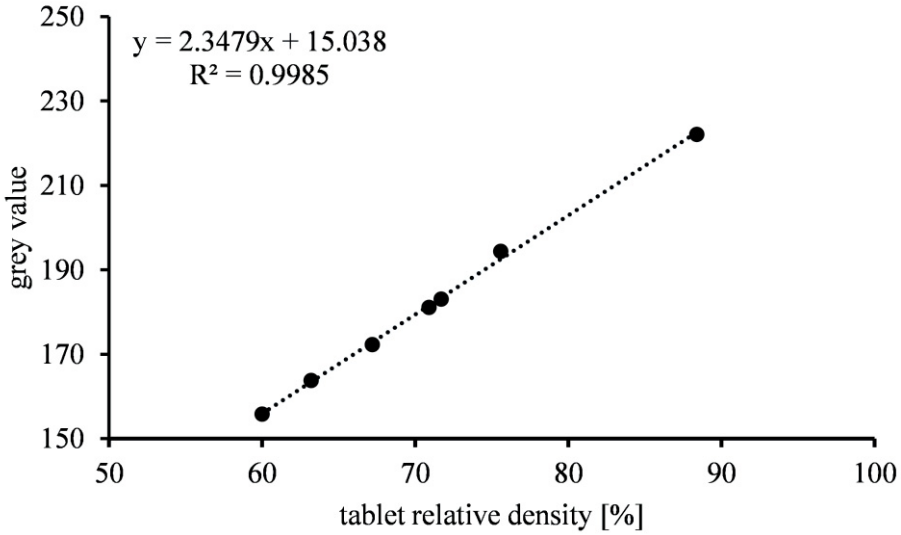

Figure 61. Correlation between the GV and the tablet RD.

As ribbons have non-uniform shape across the width, the area containing the ribbon of interest was selected according to the illustration in Figure 60 c) bracketed with blue. This was performed for each ribbon, at three different cross sections.

The ROTHIST software differentiated the selected area into several layers and so the average GV of each layer in the selected area was recorded. Since the selected area also included the foam, the first and the last 2.5% of the layers in the selected area were discarded from the evaluation in case of each ribbon, as presented in Figure 62.

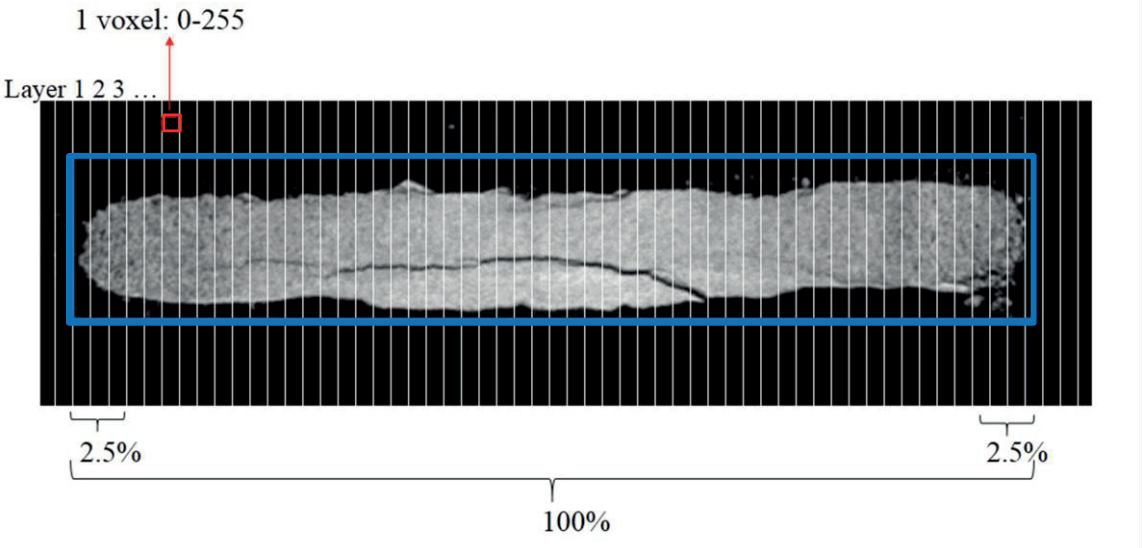

Figure 62. Negotiation of the first and the last 2.5% of the layers in a cross section of a ribbon.

In this way, the systematic failure of the investigation method was reduced by excluding the majority of the foam. The other 95% of the layers were used to calculate the average GV. Each vertical layer resulted into an average GV, which were averaged again. Both calibration equations were used for the calculation of the ribbon RD from the average GV. Equation 9 shows an example for the calculation of the ribbon RD.

$$\mathrm{RD} = \frac{\mathrm{GV_{ribbon}} - 15.038}{2.3479} \qquad \text{Equation 9}$$

The RD values obtained using both calibration equations were averaged resulting in the mean RD value of one cross section. Batch RD was obtained by measuring and averaging two ribbons at three different cross sections.

5.4.2.2 Calculation of the relative density using UHIST

The GV extraction considering the whole ribbon piece was accomplished by using the UHIST software. The frequency of 2^{16} different GV-s (from 0 to 65535) were captured considering the whole selected volume of interest. In order to present the frequency distribution of GV-s more clearly, the 65536 GVs were grouped into 256 GV-s and were used for the calibration equation and RD calculation of the ribbons.

Herefore, all the layers were imported into the UHIST software, in which the individual tablets or ribbon pieces were marked from the top to the bottom covering the volume of the investigated object. The layers in between were evaluated by the software. An example for the selection of the top and the bottom layer in tablets is presented in Figure 63 a) and b).

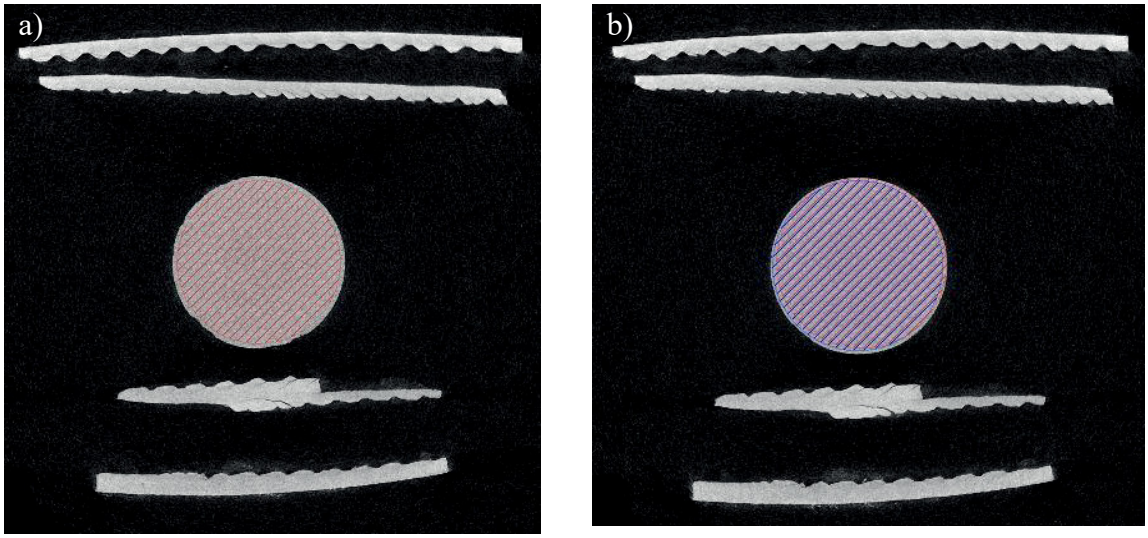

Figure 63. a), b). Selection of layer (a) at the top of the tablet and at the bottom of the tablet (b).

The calibration was performed by correlating the mean GV-s of tablets to the tablet RD values. In this case, the mean GV was calculated from the frequency distributions of GV-s using Equation 10.

$$\text{mean GV} = \frac{\text{sum}(\text{GV}_\text{i} * \text{number of voxels with GV}_i)}{\text{total number of voxels}}$$

Equation 10

In case of ribbons, the selection of the volume of interest to be analyzed was performed in the same way as for the tablets, ensuring that the whole ribbon was included in the selected volume. Figure 64 a) shows the selection of the top layer of the ribbon and Figure 64 b) represents the selected bottom layer.

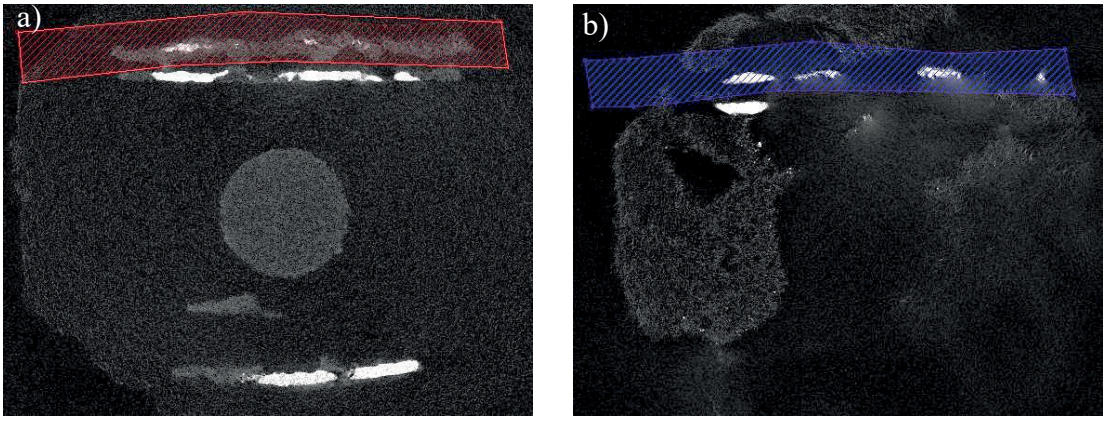

Figure 64. a), b). Selection of the first layer (a) and the last layer (b) of the ribbon.

After layer selection, the number of individual GV-s of all the voxels were counted by the UHIST software for all layers. Figure 65 shows an exemplary frequency distribution of the GVs of the analyzed volume of a ribbon.

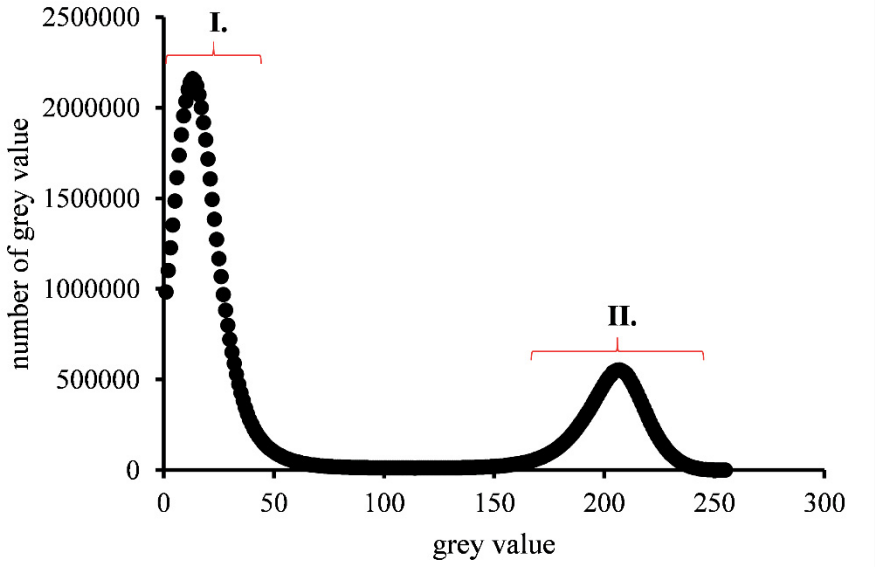

Figure 65. Frequency distribution of GV-s for the whole ribbon.

The presented curve in Figure 65 has two peaks; the first peak at the GV-s below 50 (I.) exhibits the air and the foam, in which the ribbons and tablets were placed and measured. The ribbon itself is displayed by the second peak at GV-s around 200 (II.).

In order to define the ribbon RD, the mean and the SD of the peak II were evaluated. Thus, a Gaussian curve was fitted to peak II. The Gaussian function is shown in Equation 11, in which *a* is a constant, *b* is the mean GV and *c* is the SD of GV-s.

$$f(GV) = a * e^{-\frac{(x-b)^2}{2c^2}} \qquad \text{Equation 11}$$

The accuracy of the Gaussian fit to the original data was measured by the residual sum of square (rss). The fitting of the parameters *a*, *b* and *c* was performed using Excel Solver. The mean GV (*b*) was converted into ribbon RD using the calibration equation according to Equation 12. The SD of RD was calculated using the SD of the GV and the slope coefficient *k* of the calibration curve according to Equation 13.

$$RD_{mean} = \frac{(GV_{mean} - n)}{k} \qquad \text{Equation 12}$$

$$SD(RD_{mean}) = \frac{SD(GV_{mean})}{k} \qquad \text{Equation 13}$$

The whole evaluation was performed on two pieces of ribbons from each batch. The RD values of both ribbons were averaged resulting in the RD value of the manufactured ribbon batch.

5.4.2.3 Calculation of the ribbon relative density using UHIST and averaging 20 and 50 layers

In the previous subsection described evaluation method was expanded in order to investigate the distribution of RD across the ribbon width. The ribbon pieces were divided into groups of 20 and 50 layers. The mean RD as well as the SD of RD were calculated for each group as for the whole ribbon.

5.4.3 Compression study

The deformation behaviour of MCC 101 and mannitol was studied using the Styl'One Evolution compaction simulator (Medel' Pharm, France). 351 ± 1.5 mg of powder were weighed in by hand and filled into the die. Prior to each compression cycle, the flat-faced punches of 11.28 mm diameter were lubricated with magnesium stearate (Parteck LUB MST, Merck Millipore, Germany). To obtain in-die compression profiles, the applied force as well as the corresponding punch displacement were detected at a frequency of 2000 Hz. For each material ten tablets were produced at a mean compression pressure of 250.6 ± 2.3 MPa. The data was analysed following Gharabei [122] and Heckel [123] and the yield pressure determined.

To also respect the elastic recovery of the tablets, furthermore an out-of-die compression analysis was performed. For both materials, tablets (n=10) were compressed at five different levels between 50 and 250 MPa. The RD was calculated from the mass and the outer dimensions of the tablets, which were determined 48 hours after manufacturing using a SmartTest50 (Dr. Schleuniger Pharmatron, Switzerland).

5.4.4 Granule size distribution determination by dynamic image analysis

The granules were divided in representative samples in a size of 15 g using a rotary sample divider (Probenteiler PT, Retsch Technology, Germany). The particle size distribution of the raw materials and granules was determined by dynamic image analysis using

CamSizer XT® (Retsch Technology, Germany) according to a developed method of Wagner et al. [124]. The X-Jet module was used to disperse the particles and granules from each other. The CamSizer XT has two digital cameras, one (CCD-Basic) records the bigger particles, while the other camera (CCD-Zoom) determines the smaller, fine particles in the same time. The cameras are able to detect and measure particles from 3 µm to 3 mm. The dispersing pressure was set at 0.3 bar to avoid the breakage of the granules during the measurements, while 2.5 bar dispersing pressure was set, when raw materials were examined in order to detect each single particle as the eventual agglomerates are destroyed. The speed of the conveying trough was reduced in order to achieve a slow and continuous flow of the particles into the measuring space. From the divided samples at least 2 samples were measured and the mean and standard deviation were calculated. The serious of the mesh sizes following each other were chosen using $\sqrt{2}$ as multiplication factor. The particle size was defined calculating the x_{c_min} value of the particles. The x_{c_min} is the shortest chord of the measured set of maximum chords of a particle projection. Based on the x_{c_min} values, d10, d50, d90, fine fraction <90 µm and coarse fraction >710 µm were determined as characteristics of granules.

6 Annex

Table 15. Experimental setup of DoE conducted by AlexanderWerk BT120 compacting mannitol, mixture and MCC using smooth and knurled rolls.

Experiment name	HP [bar]	GW [mm]
N1	18	1.5
N2	24	1.5
N3	36	1.5
N4	48	1.5
N5	60	2.3*/3.0
N6	18	2.3*/3.0
N7	24	2.3*/3.0
N8	36	2.3*/3.0
N9	48	2.3*/3.0
N10	60	2.3*/3.0
N11	36	1.9*/2.3
N12	36	1.9*/2.3
N13	36	1.9*/2.3

*characteristic GW of roll compaction using a pair of smooth rolls

Table 16. Experimental setup of DoE conducted by BRC25 roll compactor in case of smooth rolls compacting mannitol, mixture and MCC and Mini-Pactor in case of all roll compaction design compacting mannitol.

Experiment name	SCF [kN/cm]	GW [mm]	RS [rpm]
N1	2	1.5	2
N2	4	1.5	2
N3	6	1.5	2
N4	8	1.5	2
N5	10	1.5	2
N6	2	3.0	2
N7	4	3.0	2
N8	6	3.0	2
N9	8	3.0	2
N10	10	3.0	2
N11	2	1.5	4
N12	4	1.5	4
N13	6	1.5	4
N14	8	1.5	4
N15	10	1.5	4
N16	2	3.0	4
N17	4	3.0	4
N18	6	3.0	4
N19	8	3.0	4
N20	10	3.0	4
N21	6	2.3	3
N22	6	2.3	3
N23	6	2.3	3

Table 17. RD ranges obtained by manufacturing with different types of roll compactors and model materials.

Roll compactor	Design	GW [mm]	RS [rpm]	RD of MCC [%]	RD of mixture [%]	RD of mannitol [%]
AlexanderWerk BT120*	SS sm	1.5	3.0	65.9-84.9	77.1-87.4	76.2-90.9
		2.3		66.6-79.5	72.8-74.0	79.7-86.1
	SS kn	1.5		55.8-77.0	65.4-86.6	75.6-86.0
		3.0		57.3-80.0	67.8-83.6	74.9-87.5
Hosokawa Pharmapaktor C250	SS sm	1.5	2.0	51.4-79.0	61.0-81.1	66.8-82.7
		3.0		49.1-77.0	57.4-78.6	67.9-80.1
L.B. Bohle BRC 25	RR sm	1.5	2.0	47.0-68.6	52.0-70.3	63.1-82.5
			4.0	47.0-67.9	51.5-71.0	57.1-77.6
		3.0	2.0	44.8-67.3	49.5-66.8	62.2-75.9
			4.0	44.0-68.0	48.3-69.0	62.0-75.5

*The range of SCF was set between 2-10 kN/cm except in case of AlexanderWerk BT120, where the HP was adjusted between 18-60 bar.

Table 18. RD ranges of mannitol ribbons manufactured by Gerteis Mini-Pactor (n≥3).

	GW [mm]	RS [rpm]	RR sm	RR kn	SS sm	SS kn
Gerteis Mini-Pactor	1.5	2.0	57.9-75.3	61.7-76.8	63.2-82.4	65.9-77.6
		4.0	59.6-72.7	60.1-75.3	60.6-80.4	63.5-75.0
	3.0	2.0	59.7-71.7	60.1-73.4	63.8-79.4	61.8-78.4
		4.0	59.5-76.5	57.7-74.0	62.7-79.7	62.4-75.1

Table 19. d50 values of mannitol granules obtained by applying different roll compaction designs compacting with the Gerteis Mini-Pactor (n≥ 2).

Parameter settings			Roll compaction designs			
SCF [kN/cm]	GW [mm]	RS [rpm]	RR sm	RR kn	SS sm	SS kn
2	1.5	2.0	484.0	477.9	409.2	454.0
4			697.7	609.0	565.2	599.7
6			662.3	656.1	617.9	656.8
8			689.8	692.9	692.7	675.2
10			685.8	654.9	595.1	650.5
2	3.0	2.0	76.1	75.0	55.9	91.6
4			189.6	97.1	76.5	160.2
6			240.3	264.8	130.1	134.9
8			290.6	238.4	186.7	139.1
10			286.6	221.7	225.3	122.7
2	1.5	4.0	56.3	40.8	37.8	94.7
4			124.8	78.3	76.4	109.9
6			223.6	147.2	126.4	153.3
8			235.4	318.6	165.3	169.9
10			220.6	284.3	200.3	176.5
2	3.0	4.0	60.6	41.7	114.6	94.7
4			119.1	53.7	102.0	105.3
6			231.4	125.8	112.8	117.1
8			225.8	182.5	181.8	119.9
10			261.5	252.6	179.3	129.9

7 Acknowledgements

This work was supported by the IPROCOM Marie Curie initial training network, funded through the People Programme (Marie Curie Actions) of the European Union's Seventh Framework Programme FP7/2007-2013/ under REA grant agreement No. 316555.

8 Bibliography

1. European Commision, *The development of in silico process models for roll compaction, Description of work part A*. Description of IPROCOM Consortium. 2012.

2. Miller, R.W., *Handbook of Pharmaceutical Granulation*, in *Handbook of Pharmaceutical Granulation Technology*, D.M. Parikh, Editor. 2005, CRC Press, Boca Raton, FL. USA. p. 159-190.

3. Pietsch, W., *Agglomeration processes*. 2002. Wiley-VCH Verlag GmbH, Weinheim, Deutschland.

4. Pietsch, W., *An interdisciplinary approach to size enlargement by agglomeration.* Powder Technology, 2003. **130**(1–3): p. 8-13.

5. Yang, J., et al., *Dry particle coating for improving the flowability of cohesive powders.* Powder Technology, 2005. **158**(1): p. 21-33.

6. Hausman, D.S., *Comparison of low shear, high shear, and fluid bed granulation during low dose tablet process development.* Drug Development and Industrial Pharmacy, 2004. **30**(3): p. 259-266.

7. Parrott, E.L., *Densification of powders by concavo-convex roller compactor.* Journal of Pharmaceutical Sciences, 1981. **70**(3): p. 288-291.

8. Rumpf, H., *Grundlagen und Methoden des Granulierens.* Chemie-Ingenieur-Technik, 1958. **30**(3): p. 144-158.

9. Kleinebudde, P., *Roll compaction/dry granulation: pharmaceutical applications.* European Journal of Pharmaceutics and Biopharmaceutics, 2004. **58**(2): p. 317-326.

10. Parikh, D.M., *Handbook of Pharmaceutical Granulation Technology*. 2005. Taylor & Francis Group, LLC.

11. Jeon, I. and Betz G., *Roll compaction as a dry granulation method for paracetamol.* Journal of Drug Delivery Science and Technology, 2011. **21**(3): p. 257-262.

12. Vervaet, C. and Remon J.P., *Continuous granulation in the pharmaceutical industry.* Chemical Engineering Science, 2005. **60**(14): p. 3949-3957.

13. Passerini, N., et al., *Melt granulation of pharmaceutical powders: A comparison of high-shear mixer and fluidised bed processes.* International Journal of Pharmaceutics, 2010. **391**(1): p. 177-186.

14. Wahl, P.R., et al., *Inline monitoring and a PAT strategy for pharmaceutical hot melt extrusion.* International Journal of Pharmaceutics, 2013. **455**(1): p. 159-168.

15. Jaminet F. and Hess H., *Untersuchung über Kompaktierung und Trockengranulierung.* Pharmaceutica Acta Helvetiae, 1966. **41**: p. 39-58.

16. Teng, Y., Qiu Z., and Wen H., *Systematical approach of formulation and process development using roller compaction.* European Journal of Pharmaceutics and Biopharmaceutics, 2009. **73**(2): p. 219-229.

17. Sprockel, O.L. and Stamato H. J., *Design and scale-up of dry granulation processes*, in *chemical engineering in the pharmaceutical Industry: R&D to manufacturing*. 2010. John Wiley & Sons, Inc. p. 727-755. New Jersey, USA.

18. Guigon, P. and Simon O., *Roll press design—influence of force feed systems on compaction.* Powder Technology, 2003. **130**(1–3): p. 41-48.

19. Hsu, S.-H., Reklaitis G., and Venkatasubramanian V., *Modeling and control of roller compaction for pharmaceutical manufacturing. Part I: process dynamics and control framework.* Journal of Pharmaceutical Innovation, 2010. **5**(1-2): p. 14-23.

20. Allesø, M., R. Holm, and Holm P., *Roller compaction scale-up using roll width as scale factor and laser-based determined ribbon porosity as critical material attribute.* European Journal of Pharmaceutical Sciences, 2016. **87**: p. 69-78.

21. Perez-Gandarillas, L., *Dry granulation process and compaction behavior of granulated powders*. 2016. Doctoral thesis. Génie mécanique, mécanique des matériaux. École Nationale Supérieure des Mines d'Albi Carmaux. Albi, France.

22. Gupta, A., et al., *Effect of the variation in the ambient moisture on the compaction behavior of powder undergoing roller-compaction and on the characteristics of tablets*

produced from the post-milled granules. Journal of Pharmaceutical Sciences, 2005. **94**(10): p. 2314-2326.

23. Gupta, A., et al., *Nondestructive measurements of the compact strength and the particle-size distribution after milling of roller compacted powders by near-infrared spectroscopy.* Journal of Pharmaceutical Sciences, 2004. **93**(4): p. 1047-1053.

24. Gupta, A., et al., *Real-time near-infrared monitoring of content uniformity, moisture content, compact density, tensile strength, and young's modulus of roller compacted powder blends.* Journal of Pharmaceutical Sciences, 2005. **94**(7): p. 1589-1597.

25. Sahut-Conreur. *Micro-Compactor*. 2013.

26. Sheskey, P.J. and Hendren J., *The effects of roll compaction equipment variables, granulation technique, and HPMC polymer level on a controlled-release matrix model drug formulation*, in Pharmaceutical Technology Europe. 1999. **23**: p. 90-106.

27. Freund-Vector Corporation. *Roller compactor*. 2018.

28. Csordas, K. and Kleinebudde P., *Evaluation of the performance of different types of roll compactors.* Powder Technology, 2018. **337**: p. 84-91.

29. Csordas, K., Wiedey R., and Kleinebudde P., *Impact of roll compaction design, process parameters, and material deformation behaviour on ribbon relative density.* Drug Development and Industrial Pharmacy, 2018. **44**(8): p. 1295-1306.

30. Souihi, N., et al., *Roll compaction process modeling: Transfer between equipment and impact of process parameters.* International Journal of Pharmaceutics, 2015. **484**(1–2): p. 192-206.

31. Daugherity, D.P. and Chu H.J., *Investigation of serrated roll surface differences on ribbon thickness during roller compaction.* Pharmaceutical Development and Technology, 2007. **12**(6): p. 603-608.

32. Rambali, B., et al., *Influence of the roll compactor parameter settings and the compression pressure on the buccal bio-adhesive tablet properties.* International Journal of Pharmaceutics, 2001. **220**(1–2): p. 129-140.

33. Funakoshi, Y., Asogawa T., and Satake E., *The use of a novel roller compactor with a concavo-convex roller pair to obtain uniform compacting pressure.* Drug Development and Industrial Pharmacy, 1977. **3**(6): p. 555-573.

34. Wiedey, R. and Kleinebudde P., *The density distribution in ribbons from roll compaction.* Chemie Ingenieur Technik, 2017. **89**(8): p. 1017-1024.

35. Mazor, A., et al., *Effect of roll compactor sealing system designs: A finite element analysis.* Powder Technology, 2016. **289**: p. 21-30.

36. Perez-Gandarillas, L., et al., *Effect of roll-compaction and milling conditions on granules and tablet properties.* European Journal of Pharmaceutics and Biopharmaceutics, 2016. **106**: p. 38-49.

37. Mirtič, A. and Reynolds G.K., *Determination of breakage rate and breakage mode of roller compacted pharmaceutical materials.* Powder Technology, 2016. **298**: p. 99-105.

38. Inghelbrecht, S. and Remon J.P., *Reducing dust and improving granule and tablet quality in the roller compaction process.* International Journal of Pharmaceutics, 1998. **171**(2): p. 195-206.

39. Sun, C.C. and Kleinebudde P., *Mini review: Mechanisms to the loss of tabletability by dry granulation.* European Journal of Pharmaceutics and Biopharmaceutics, 2016. **106**(106): p. 9-14.

40. Gereg, W.G. and Cappola L.M., *Roller compaction feasibility for new drug candidates. Laboratory to production scale.* Pharmaceutical Technology, 2002. **26**: p. 14-23.

41. Miguélez-Morán, A.M., Wu C.Y., and Seville J.P.K., *The effect of lubrication on density distributions of roller compacted ribbons.* International Journal of Pharmaceutics, 2008. **362**(1): p. 52-59.

42. Bindhumadhavan, G., et al., *Roll compaction of a pharmaceutical excipient: Experimental validation of rolling theory for granular solids.* Chemical Engineering Science, 2005. **60**(14): p. 3891-3897.

43. Johanson, J.R., *A rolling theory for granular solids.* Journal of Applied Mechanics, 1965. **32**(4): p. 842-848.

44. Kleinebudde, P., *Trockengranulieren - Grundlagen I.*, APV Seminar. 2015.

45. Dehont, F., et al., *Granulation of Pharmaceutical Powders by Compaction an Experimental Study.* Drug Development and Industrial Pharmacy, 1994. **20**(1): p. 65-74.

46. Nordström, J., Klevan I., and Alderborn G., *A protocol for the classification of powder compression characteristics.* European Journal of Pharmaceutics and Biopharmaceutics, 2012. **80**(1): p. 209-216.

47. Heng, P.W.S., et al., *Roller compaction of crude plant material: influence of process variables, polyvinylpyrrolidone, and co-milling.* Pharmaceutical Development and Technology, 2004. **9**(2): p. 135-144.

48. Inghelbrecht, S. and Remon J.P., *The roller compaction of different types of lactose.* International Journal of Pharmaceutics, 1998. **166**(2): p. 135-144.

49. David, S.T. and Augsburger L.L., *Plastic flow during compression of directly compressible fillers and its effect on tablet strength.* Journal of Pharmaceutical Sciences, 1977. **66**(2): p. 155-159.

50. Roberts, R.J. and Rowe R.C., *The effect of punch velocity on the compaction of a variety of materials.* Journal of Pharmacy and Pharmacology, 1985. **37**(6): p. 377-84.

51. Rees, J.E. and Rue P.J., *Time-dependent deformation of some direct compression excipients.* Journal of Pharmacy and Pharmacolology, 1978. **30**(10): p. 601-7.

52. Miguélez-Morán, A.M., et al., *Characterisation of density distributions in roller-compacted ribbons using micro-indentation and X-ray micro-computed tomography.* European Journal of Pharmaceutics and Biopharmaceutics, 2009. **72**(1): p. 173-182.

53. Reynolds, G., et al., *Practical application of roller compaction process modeling.* Computers and Chemical Engineering, 2010. **34**(7): p. 1049-1057.

54. Freitag, F. and Kleinebudde P., *How do roll compaction/dry granulation affect the tableting behaviour of inorganic materials? Comparison of four magnesium carbonates.* European Journal of Pharmaceutical Sciences, 2003. **19**(4): p. 281-289.

55. Falzone, A.M., Peck G.E., and McCabe G.P., *Effects of changes in roller compactor parameters on granulations produced by compaction.* Drug Development and Industrial Pharmacy, 1992. **18**(4): p. 469-489.

56. Singh, R., Ierapetritou M., and Ramachandran R., *An engineering study on the enhanced control and operation of continuous manufacturing of pharmaceutical tablets via roller compaction.* International Journal of Pharmaceutics, 2012. **438**(1–2): p. 307-326.

57. Nordstrom, J. and Alderborn G., *The granule porosity controls the loss of compactibility for both dry- and wet-processed cellulose granules but at different rate.* Journal of Pharmaceutical Sciences, 2015. **104**(6): p. 2029-39.

58. Khorasani, M., et al., *Process optimization of dry granulation based tableting line: Extracting physical material characteristics from granules, ribbons and tablets using near-IR (NIR) spectroscopic measurement.* Powder Technology, 2016. **300**: p. 120-125.

59. Zinchuk, A.V., Mullarney M.P., and Hancock B.C., *Simulation of roller compaction using a laboratory scale compaction simulator.* International Journal of Pharmaceutics, 2004. **269**(2): p. 403-415.

60. Katashinskii, V.P., *Analytical determination of specific pressure during the rolling of metal powders.* Soviet Powder Metallurgy and Metal Ceramics, 1966. **5**(10): p. 765-772.

61. Loginov, Y.N., Bourkine S.P., and Babailov N.A., *Cinematics and volume deformations during roll-press briquetting.* Journal of Materials Processing Technology, 2001. **118**(1): p. 151-157.

62. Dec, R.T., Zavaliangos A., and Cunningham J.C., *Comparison of various modeling methods for analysis of powder compaction in roller press.* Powder Technology, 2003. **130**(1): p. 265-271.

63. Muliadi, A.R., Litster J.D., and Wassgren C.R., *Modeling the powder roll compaction process: Comparison of 2-D finite element method and the rolling theory for granular solids (Johanson's model).* Powder Technology, 2012. **221**: p. 90-100.

64. Muliadi, A.R., Litster J.D., and Wassgren C.R., *Validation of 3-D finite element analysis for predicting the density distribution of roll compacted pharmaceutical powder.* Powder Technology, 2013. **237**(0): p. 386-399.

65. Liu, Y. and Wassgren C., *Modifications to Johanson's roll compaction model for improved relative density predictions.* Powder Technology, 2016. **297**: p. 294-302.

66. Mansa, R.F., et al., *Using intelligent software to predict the effects of formulation and processing parameters on roller compaction.* Powder Technology, 2008. **181**(2): p. 217-225.

67. Turkoglu, M., et al., *Modeling of a roller-compaction process using neural networks and genetic algorithms.* European Journal of Pharmaceutics and Biopharmaceutics, 1999. **48**(3): p. 239-245.

68. Nesarikar, V.V., et al., *Roller compaction process development and scale up using Johanson model calibrated with instrumented roll data.* International Journal of Pharmaceutics, 2012. **436**(1–2): p. 486-507.

69. Michrafy, A., et al., *Experimental and numerical analyses of homogeneity over strip width in roll compaction.* Powder Technology, 2011. **206**(1): p. 154-160.

70. Lim, H., et al., *Assessment of the critical factors affecting the porosity of roller compacted ribbons and the feasibility of using NIR chemical imaging to evaluate the porosity distribution.* International Journal of Pharmaceutics, 2011. **410**(1–2): p. 1-8.

71. Reimer, H.L. and Kleinebudde P., *Hybrid modeling of roll compaction processes with the Styl'One Evolution.* Powder Technology, 2019. **341**: p. 66-74.

72. Peter, S., Lammens R.F., and Steffens K.-J., *Roller compaction/Dry granulation: Use of the thin layer model for predicting densities and forces during roller compaction.* Powder Technology, 2010. **199**(2): p. 165-175.

73. Acevedo, D., et al., *Evaluation of three approaches for real-time monitoring of roller compaction with near-infrared spectroscopy.* Journal of American Association of Pharmaceutical Scientists, 2012. **13**(3): p. 1005-12.

74. Wöll, F. and Kleinebudde P., *Charakterisierung der Porosität von Schülpen: Stanzmethode und NIRS-Methode.* Chemie Ingenieur Technik, 2003. **75**(11): p. 1756-1759.

75. Herting, M.G. and Kleinebudde P., *Roll compaction/dry granulation: Effect of raw material particle size on granule and tablet properties.* International Journal of Pharmaceutics, 2007. **338**(1–2): p. 110-118.

76. Gamble, J.F., et al., *Roller compaction: Application of an in-gap ribbon porosity calculation for the optimization of downstream granule flow and compactability characteristics.* Pharmaceutical Development and Technology, 2010. **15**(3): p. 223-229.

77. Khorasani, M., et al., *Visualization and prediction of porosity in roller compacted ribbons with near-infrared chemical imaging (NIR-CI).* Journal of Pharmaceutical and Biomedical Analysis, 2015. **109**: p. 11-17.

78. El-Saleh, F. and Kleinebudde P., *Mercury-free determination of apparent density and porosity of pellets by powder pycnometry.* Pharmaceutical Technology Europe, 1998. **10**(11): p: 18-26.

79. Dumarey, M., et al., *Combining experimental design and orthogonal projections to latent structures to study the influence of microcrystalline cellulose properties on roll compaction.* International Journal of Pharmaceutics, 2011. **416**(1): p. 110-119.

80. Hilden, J., Earle G., and Lilly E., *Prediction of roller compacted ribbon solid fraction for quality by design development.* Powder Technology, 2011. **213**(1–3): p. 1-13.

81. Souihi, N., et al., *Design space estimation of the roller compaction process.* Industrial & Engineering Chemistry Research, 2013. **52**(35): p. 12408-12419.

82. Schiano, S., *Dry granulation using roll compaction process: powder characterization and process undestanding*, Doctoral thesis. Chemical and Process Engineering Faculty of Engineering and Physical Sciences. 2017, University of Surrey, UK.

83. Rowe, J.M., et al., *Mechanistic insights into the scale-up of the roller compaction process: A practical and dimensionless approach.* Journal of Pharmaceutical Sciences, 2013. **102**(10): p. 3586-3595.

84. Pérez Gago, A., Reynolds G., and Kleinebudde P., *Impact of roll compactor scale on ribbon density.* Powder Technology, 2017. **337**: p. 92-103.

85. Nesarikar, V.V., et al., *Instrumented roll technology for the design space development of roller compaction process.* International Journal of Pharmaceutics, 2012. **426**(1–2): p. 116-131.

86. Iyer, R.M., et al., *A novel approach to determine solid fraction using a laser-based direct volume measurement device.* Pharmaceutical Development and Technology, 2014. **19**(5): p. 577-582.

87. Zhang, J., et al., *The application of terahertz pulsed imaging in characterising density distribution of roll-compacted ribbons.* European Journal of Pharmaceutics and Biopharmaceutics, 2016. **106**: p. 20-25.

88. Souihi, N., et al., *Near-infrared chemical imaging (NIR-CI) on roll compacted ribbons and tablets – multivariate mapping of physical and chemical properties.* International Journal of Pharmaceutics, 2015. **483**(1-2): p. 200-11.

89. Zeitler, J.A. and Gladden L.F., *In-vitro tomography and non-destructive imaging at depth of pharmaceutical solid dosage forms.* European Journal of Pharmaceutics and Biopharmaceutics, 2009. **71**(1): p. 2-22.

90. Fu, X., et al., *Application of X-ray microtomography and image processing to the investigation of a compacted granular system.* Particle & Particle Systems Characterization, 2006. **23**(3-4): p. 229-236.

91. Fu, X., et al., *Investigation of particle packing in model pharmaceutical powders using X-ray microtomography and discrete element method.* Powder Technology, 2006. **167**(3): p. 134-140.

92. Farber, L., Tardos G., and Michaels J.N., *Use of X-ray tomography to study the porosity and morphology of granules.* Powder Technology, 2003. **132**(1): p. 57-63.

93. Sinka, I.C., et al., *Measurement of density variations in tablets using X-ray computed tomography.* International Journal of Pharmaceutics, 2004. **271**(1–2): p. 215-224.

94. Busignies, V., et al., *Quantitative measurements of localized density variations in cylindrical tablets using X-ray microtomography.* European Journal of Pharmaceutics and Biopharmaceutics, 2006. **64**(1): p. 38-50.

95. Akseli, I., et al., *A quantitative correlation of the effect of density distributions in roller-compacted ribbons on the mechanical properties of tablets using ultrasonics and X-ray tomography.* AAPS PharmSciTech, 2011. **12**(3): p. 834-53.

96. Wiedey, R. and Kleinebudde P., *Infrared thermography — A new approach for in-line density measurement of ribbons produced from roll compaction.* Powder Technology, 2018. **337**: p. 17-24.

97. Shlieout, G., Lammens R.F., and Kleinebudde P., *Dry granulation with a roller compactor Part I: The functional units and operation modes*. Pharmaceutical Technology Europe. 2000. **12**: p. 24-35.

98. Shlieout, G., Lammens R.F., and Kleinebudde P., *Dry granulation with a roller compactor part II: Evaluating the operation modes*. Pharmaceutical Technology Europe. 2002. **14**(9): p. 32-39.

99. Singh, R., Ierapetritou, M.R., and Ramachandran R., *An engineering study on the enhanced control and operation of continuous manufacturing of pharmaceutical tablets via roller compaction.* International Journal of Pharmaceutics, 2012. **438**(1-2): p. 307-26.

100. Singh, R., Ierapetritou M.R., and Ramachandran R., *System-wide hybrid MPC–PID control of a continuous pharmaceutical tablet manufacturing process via direct compaction.* European Journal of Pharmaceutics and Biopharmaceutics, 2013. **85**(3, Part B): p. 1164-1182.

101. Rehrl, J., et al., *Optimized continuous pharmaceutical manufacturing via model-predictive control.* International Journal of Pharmaceutics, 2016. **510**(1): p. 100-115.

102. Amidon, G.E. and Hought M.E., *The effect of moisture on the mechanical and powder flow properties of microcrystalline cellulose.* Pharmaceutical Research, 1995. **12**(6): p. 923-929.

103. Rowe C, R., Sheskey P.J., and Quinn M.E., *Handbook of Pharmaceutical Excipients*. 6th ed. 2009. Pharmaceutical Press and American Pharmacists Association. London, UK and Washington, USA.

104. Herting, M., *Introduction of roll compaction / dry granulation*. 2016. TTC Seminar, Präsentation über Walzenkompaktierung.

105. Al-Asady, R.B., et al., *Roller compactor: Determining the nip angle and powder compaction progress by indentation of the pre-compacted body.* Powder Technology, 2016. **300**: p. 107-119.

106. Simon, O. and Guigon P., *Correlation between powder-packing properties and roll press compact heterogeneity.* Powder Technology, 2003. **130**(1–3): p. 257-264.

107. Al-Asady, R.B., et al., *Roller compactor: the effect of mechanical properties of primary particles.* International Journal of Pharmaceutics, 2015. **496**(1): p. 124-136.

108. Khorasani, M., et al., *Near-infrared chemical imaging (NIR-CI) as a process monitoring solution for a production line of roll compaction and tableting.* European Journal of Pharmaceutics and Biopharmaceutics, 2015. **93**: p. 293-302.

109. Lecompte, T., et al., *Dry granulation of organic powders—dependence of pressure 2D-distribution on different process parameters.* Chemical Engineering Science, 2005. **60**(14): p. 3933-3940.

110. Freitag, F., *Walzenkompaktieren und Trockengranulieren zur Verbesserung des Tablettierverhaltens anorganischer Hilfsstoffe am Beispiel von Magnesiumcarbonat und Calciumcarbonat*. 2004. Doctoral thesis. Mathematisch-Naturwissenschaftlich-Technischen Fakultät, Martin-Luther-Universität Halle-Wittenberg, Deutschland. p. 22.

111. Souihi, N., et al., *A quality by design approach to investigate the effect of mannitol and dicalcium phosphate qualities on roll compaction.* International Journal of Pharmaceutics, 2013. **447**(1–2): p. 47-61.

112. Thoorens, G., et al., *Microcrystalline cellulose, a direct compression binder in a quality by design environment—A review.* International Journal of Pharmaceutics, 2014. **473**(1–2): p. 64-72.

113. Perez Gago, A., *Roll compaction scale up: impact of material, effect of scale and modelling of process transfer*. 2016. Doctoral Thesis. Institut of Pharmaceutics and Biopharmaceutics, Heinrich-Heine-University Düsseldorf, Deutschland.

114. Mangal, H. and Kleinebudde P., *Is the adjustment of the impeller speed a reliable attempt to influence granule size in continuous dry granulation?* Advanced Powder Technology, 2018. **29**(6): p. 1339-1347.

115. Tarlier, N., et al., *Compaction behavior and deformation mechanism of directly compressible textured mannitol in a rotary tablet press simulator.* International Journal of Pharmaceutics, 2015. **495**(1): p. 410-419.

116. Yu, S., et al., *The effects of lubrication on roll compaction, ribbon milling and tabletting.* Chemical Engineering Science, 2013. **86**(Supplement C): p. 9-18.

117. He, X., Secreast P.J., and Amidon G.E., *Mechanistic study of the effect of roller compaction and lubricant on tablet mechanical strength.* Journal of Pharmaceutical Sciences, 2007. **96**(5): p. 1342-55.

118. Mosig, J. and Kleinebudde P., *Evaluation of lubrication methods: How to generate a comparable lubrication for dry granules and powder material for tableting processes.* Powder Technology, 2014. **266**(Supplement C): p. 156-166.

119. Dawes, J., et al., *An investigation into the impact of magnesium stearate on powder feeding during roller compaction.* Drug Development and Industrial Pharmacy, 2012. **38**(1): p. 111-122.

120. Doelker, E., *Comparative compaction properties of various microcrystalline cellulose types and generic products.* Drug Development and Industrial Pharmacy, 1993. **19**(17-18): p. 2399-2471.

121. L.B. Bohle Maschienen + Verfahren GmbH, *Description of the L.B. Bohle BRC 25 roll compactor.* https://www.lbbohle.de/maschinen-verfahren/granulation/brc 2016 15.08.2016].

122. Gharaibeh, F.S. and Aburub A., *Use of first derivative of displacement vs. force profiles determine deformation behavior of compressed powders.* AAPS PharmSciTech, 2013. **14**: p. 398-401.

123. Heckel, R.W., *Density-pressure relationship in powder compaction.* Transactions of the Metallurgical Society of AIME, 1961. **221**: p. 671-675.

124. Wagner, C.M., Pein M., and Breitkreutz J., *Roll compaction of granulated mannitol grades and the unprocessed crystalline delta-polymorph.* Powder Technology, 2015. **270**, Part B(0): p. 470-475.

9 List of publications

In sections 3.1 and 3.2 described data have already been published in journals and are included in this thesis. The results of granule size distribution and GeoPyc ribbon relative density measurements also have been published in conferences or meetings. The practical work, evaluation of data and manuscript preparations have mostly been performed by Kitti Csordás, which work was supervised by Prof. Dr. Dr. h.c. Peter Kleinebudde. The article "Impact of Roll Compaction Design, Process Parameters, and Material Deformation Behaviour on Ribbon Relative Density", especially the description of the material deformation behaviour could be established due to the cooperation with Dr. Rok Šibanc, Hannah Lou Reimer and Dr. Raphael Wiedey. Dr. Rok Šibanc contributed the softwares UHIST and ROTHIST for grey value evaluation during the X-ray micro-computed tomography study.

Scientific articles

K. Csordás, P. Kleinebudde, *Evaluation of the performance of different types of roll compactors,* Powder Technology. 2017. **337**, p: 84-91.

- Own contribution: 70%
- Description of the own contribution: K. Csordás has taken part in designing the study concept and conducted the practical work. She has evaluated the obtained data set. P. Kleinebudde has taken part in the preparation of the design concept of this study. The supervision of this work and correction of the manuscript were done by P. Kleinebudde.

K. Csordás, R. Wiedey, P. Kleinebudde, *Impact of roll compaction design, process parameters, and material deformation behaviour on ribbon relative density,* Drug Development and Industrial Pharmacy. 2018. **44** (8), p: 1295-1306.

- Own contribution: 60%
- Description of the own contribution: K. Csordás has taken part in designing the study concept, conducted the practical work and evaluated the obtained data set. The "in-die" compression analysis was conducted by K. Csordás and R. Wiedey, while the "out-of-die" compression analysis and Figures 12 a) and b) were prepared by R. Wiedey. P. Kleinebudde has taken part in the preparation of the

design concept of this study. The supervision of this work and correction of the manuscript were done by P. Kleinebudde.

Conference presentations

K. Csordás, A. Perez Gago, P. Kleinebudde, Roll compaction: the impact of system design and scale-up, Partec International Congress on Particle Technology, Nürnberg, 19th-21st April, 2016

Conference posters

K. Csordás, P. Kleinebudde, Effect of material properties and process parameters on roll compaction and ribbon properties, 8th Polish-German Symposium on Pharmaceutical Sciences, Kiel, 29th-30th May, 2015

K. Csordás, P. Kleinebudde, Roll compaction of spray-dried mannitol using different compaction designs and process parameters, 7th International Granulation Workshop, Sheffield, 1st-3rd July, 2015

K. Csordás, P. Kleinebudde, The effect of material properties and process parameters on roll compacted ribbons, Deutsche Pharmazeutische Gesellschaft Jahrestagung, Düsseldorf, 23rd-25th September, 2015

K. Csordás, P. Kleinebudde, Roll compaction of spray-dried mannitol using different roll compactors and process parameters, AAPS Annual Meeting, Orlando, Florida, USA, 25th-29th October, 2015

K. Csordás, P. Kleinebudde, Effect of material properties and process parameters on ribbon porosity and granule size distribution, 10th World Meeting on Pharmaceutics, Biopharmaceutics and Pharmaceutical Technology, Glasgow, United Kingdom, 4th-7th April, 2016

10 Danksagung

Ich möchte mich bei meinem Doktorvater, Herrn Prof. Dr. Dr. h.c. Peter Kleinebudde für die freundliche Aufnahme in seinen Arbeitskreis und für die Aufnahme in das IPROCOM Konsortium bedanken. Besonderes danke ich Ihnen, dass Sie immer ein offenes Ohr für meine Fragen über mein Dissertationsthema, und andere interessante Fragestellungen gehabt haben. Sie haben mir ermöglicht eine andere Welt der pharmazeutischen Technologie für mich zu entdecken. Die tolle Kongressreisen im Rahmen von IROCOM und auch die internationalen Konferenzen waren besonders schöne Erlebnisse während meiner Promotion. Vielen Dank für all diese Werte und Erfahrungen, die ich sammeln durfte.

Herrn. Professor Dr. Jörg Breitkreutz danke ich für die Übernahme des Koreferats und für die vielen interessanten Gesprächen, die mein Blick in vielen verschiedenen Richtungen erweitert hat. Auch Ihnen möchte ich mich für die Möglichkeit der zahlreichen Konferenzbesuche bedanken.

Herrn Dr. Klaus Knop möchte ich mich für seine Hilfsbereitschaft und für die vielen interessanten Diskussionen bedanken, die mich stets während der Promotion begleitet haben. Vielen Dank für die freundliche Einführung in die Welt des Praktikums während der Betreuung der Arzneiformenlehre.

Frau Professor Dr. Klára Pintye-Hódi und Dr. Géza Regdon Jr. möchte ich mich für die Ermutigung für das Promovieren im Ausland bedanken. Ohne die Unterstützung von Ihnen hätte ich nicht in Düsseldorf promoviert.

Der Firma L. B. Bohle Maschinen + Verfahren GmbH und dessen Mitarbeiter, Dr. Hubertus Rehbaum, Andreas Altmeyer, Andreas Teske und Daniel Bexte danke ich für die Möglichkeit und für die freundliche Unterstützung, dass meine Versuchsreihen mit dem Walzenkompaktor BRC25 durchgeführt werden durften.

Hosokawa Alpine AG danke ich für die Bereitstellung des Pharmapaktor C250 für die Durchführung ein Teil meiner Versuchsreihen.

I would like to thank to all the IPROCOM members, who inspired me from the beginning of this work. I would like to thank to Professor Dr. Charley Wu, who led the IPROCOM project and made it possible for many of the IPROCOM fellows to work in this international consortium. Especially, I would like to thank to Professor Dr. Gavin Reynolds and to Dr. Andreja Mirtič, who supported my work at AstraZeneca in Macclesfield. Thank you for your suggestions and time for interesting discussions.

Herrn Dr. Rok Šibanc danke ich für seine Hilfe und Unterstützung bei der Auswertung der X-Ray µCT Daten. Ohne die von ihm entwickelten Softwares könnte diese Arbeit nicht in der Form erstellt werden, wie es geworden ist.

Herrn Dr. Raphael Wiedey danke ich für die Einführung der Messungen mittels X-ray µCT. Frau Dr. Johanna Anlahr und Dr. Carl Moritz Wagner für die Vorstellung und Hilfe bei Aufbau der Gerteis Mini-Pactor am Anfang meiner Promotionszeit.

Bei allen Institutsmitarbeiter mochte ich mich für die freundliche Aufnahme in diesem Institut bedanken.

Bei meinen Bürokolleginnen, Christin, Elisabeth, Hannah Lou, Kasama, Oscar und Yasmin bedanke ich mich herzlich für die viele lustige Momente, die diese unvergessliche Zeit am Institut noch besonderer gemacht haben. Weitere unvergessliche Feierabende danke ich Carmen, Fritzie, Josi, Isabell, Sandra, Shirin und Yasmin.

Für die stete und liebevolle Unterstützung möchte ich mich bei meinen Freundinnen und Freunden, Elisabeth, Johanna, Lilla, Niki, Shirin, Rok, Raphael und Yasmin bedanken.

A családomnak, Anyukámnak, Ritának, Mamának szeretném szívből megköszönni, hogy elengedtek, és otthonról támogattak, támogatnak, bátorítanak, mind a mai napig, hogy megvalósuljon életem egyik legnagyobb álma. Köszönöm, hogy mindig mellettem álltok. Anett és Imi köszönöm a ti támogatásotokat is, ami ugyancsak mindig körbevesz. Niki, köszönöm, hogy mindig a pozitív szemléletmódot erősíted meg bennem. Végül, de nem utolsó sorban szeretném a vőlegényemnek, Sanyinak, a türelmét, bátorító szavait, törődését és vígasztalását megköszönni, amely nélkül ez a munka nem valósulhatott volna meg.

Danke schön! Thank you! Köszönöm!

Düsseldorf, Dezember 2018 Kitti Csordás

11 Erklärung

Hiermit versichere ich gemäß PO § 5 Absatz 1b; § 6 Absatz 5 der Promotionsordnung der Mathematisch-Naturwissenschaftlichen Fakultät der Heinrich-Heine-Universität Düsseldorf des Eides Statt, dass die Dissertation von mir selbstständig und ohne unzulässige fremde Hilfe unter Beachtung der „Grundsätze zur Sicherung guter wissenschaftlicher Praxis an der Heinrich-Heine-Universität Düsseldorf“ erstellt worden ist und dass ich diese in der vorgelegten oder in ähnlicher Form noch bei keiner anderen Institution eingereicht habe.

Düsseldorf, 18.12. 2018 Kitti Csordás